Active Control of Narrow Tilting Vehicle Dynamics

Robertson, James

Award date:
2014

Awarding institution:
University of Bath

Active Control of Narrow Tilting Vehicle Dynamics

James William Robertson

A thesis submitted for the degree of Doctor of Philosophy

Department of Mechanical Engineering
University of Bath

February 2014

Abstract

Narrow tilting vehicles offer an opportunity to tackle both traffic congestion and carbon emissions having a small footprint, low weight and small frontal area. Their narrow width requires that they tilt into corners in order to maintain stability; this may be achieved by means of an automated tilt control system.

A three-wheeled tilting vehicle prototype, known as the Compact Low Emission VEhicle for uRban transport (CLEVER), was constructed at the University of Bath in 2006. The vehicle was equipped with a direct tilt control system in which a pair of hydraulic actuators applied a moment between the cabin and a non-tilting base. This tilt control system provided satisfactory steady state performance but limited transient stability. High tilt rate demands associated with rapid steering inputs would lead to large tilting moments being applied to the non-tilting rear engine module; this, combined with the engine module's own propensity to roll out of the bend, could cause the inside wheel to lift and the vehicle to capsize.

This thesis details the implementation of a Steering Direct Tilt Control (SDTC) system, whereby the front wheel steer angle is used to generate some of the tilting moment, on the prototype CLEVER Vehicle. Simulation and experimental results are presented which show a 40% reduction in load transfer across the rear axle during a transient ramp steer manoeuvre. The influence of the SDTC system, and associated steer angle alteration, on the vehicle trajectory is considered. A human driver is found to be capable of adapting their steer inputs such that they can follow their chosen path.

Finally, a feed-forward control strategy is shown to reduce the load transfer across the rear axle by an additional 30% in transient situations, but only if the steer input signal is sufficiently free of noise.

Acknowledgements

Thanks go to Dr J. Darling and Prof A. Plummer for their supervision and guidance.

Thanks also go to Dr J. H. Berote for the supply of simulation models of the CLEVER Vehicle and for his assistance in the early stages of my research.

Finally, I would like to thank my family for their continued support throughout the process.

Contents

Nomenclature

Uppercase Letters

Symbol	Description	Unit
A_p	Hydraulic actuator piston area	(m^2)
B	'Magic Formula' stiffness factor	-
C	'Magic Formula' shape factor	-
$C_\alpha / C_{F\alpha}$	Tyre lateral slip (or cornering) stiffness	-
C_k	Tyre longitudinal slip stiffness	-
C_s	Tyre lateral slip stiffness coefficient	-
$C_\gamma / C_{F\gamma}$	Tyre camber stiffness	-
D	'Magic Formula' peak factor	-
E	'Magic Formula' curvature factor	-
F_{xy}	Tyre resultant force (of x and y components)	(N)
F_y	Tyre lateral force	(N)
F_{yf}	Front tyre lateral force	(N)
F_{yr}	Rear tyre lateral force (left and right combined)	(N)
$F_{y\gamma}$	Tyre camber thrust	(N)
F_{yss}	Tyre lateral force at steady state	(N)
F_z	Tyre vertical load	(N)
F_{zf}	Front tyre vertical load	(N)
F_{zl}	Left tyre vertical load	(N)
F_{zr}	Right tyre vertical load	(N)
F_{z0}	Rear tyre vertical load at rest with cabin upright	(N)
I_z	Yaw inertia about vehicle centre of gravity	($kg \cdot m^2$)
K_{as}	Active steering gain	-
K_d	Derivative gain	-
K_{ff}	Feed-forward gain	-
K_i	Integral gain	-
K_p	Proportional gain	-
K_v	Hydraulic valve constant	-

K_δ	Steer angle gain (Karnopp and Fang)	-
L	Wheelbase	(m)
M	Moment	(Nm)
M_c	Roll moment capacity	(Nm)
M_{DTC}	Moment produced by DTC actuators	(Nm)
M_f	Yaw moment produced by front tyre	(Nm)
M_r	Yaw moment produced by rear tyre / roll moment reserve	(Nm)
P_r	Rated pressure drop across one side of hydraulic valve	(Pa)
P_s	Hydraulic supply pressure	(Pa)
Q	Hydraulic flow rate	(mm^3/s)
Q_a	Hydraulic flow rate to annulus side of actuator	(mm^3/s)
Q_p	Hydraulic flow rate to piston side of actuator	(mm^3/s)
Q_r	Rated flow rate of hydraulic valve	(mm^3/s)
R	Corner radius	(m)
R_{sb}	Gear ratio of steering box	-
S_H	'Magic Formula' horizontal shift	-
S_V	'Magic Formula' Vertical shift	-
T	Track width	(m)
T_d	Driver steering torque output	(Nm)
U	Vehicle speed	(m/s)
U_p	Hydraulic actuator piston velocity	(m/s)
V	Vehicle centre of gravity velocity, tyre velocity	(m/s)
V_f	Velocity of front tyre	(m/s)
V_r	Velocity of rear tyre	(m/s)
V_{rod}	Hydraulic actuator rod velocity	(m/s)
V_x	Tyre longitudinal velocity component	(m/s)
V_y	Tyre lateral velocity component	(m/s)
V_0	Vehicle centre of gravity velocity with no tyre slip	(m/s)
X	Position in the X direction (global)	(m)
Y	Position in the Y direction (global)	(m)
Z	Position in the Z direction (global)	(m)

Lowercase Letters

Symbol	Description	Unit
a	Distance between CofG and front axle	(m)
a_c	Longitudinal position of cabin centre of gravity	(m)
b	Distance between CofG and rear axle	(m)
g	Gravitational force	(N/kg)
h	Centre of gravity height above axis when upright	(m)
h_c	Cabin centre of gravity height above ground when upright	(m)
h_r	Height of rear module centre of gravity above ground plane	(m)
h_{tb}	Height of CLEVER Vehicle tilt bearing above ground plane	(m)
k	Longitudinal slip ratio of tyre	-
l	Wheelbase	(m)
l_c	Longitudinal position of tilt bearing	(m)
m	Total vehicle mass	(kg)
m_c	Mass of cabin (including driver)	(kg)
m_r	Mass of rear module	(kg)
r_{sa}	Radius of steering arm	(m)
r_e	Effective rolling radius of tyre	(m)
r_t	Radius of tyre cross section	(m)
t	Track width	(m)
v	Side slip velocity of the centre of gravity	(m/s)
x	Position in the x direction (vehicle fixed)	(m)
y	Position in the y direction (vehicle fixed)	(m)
y_c	Lateral displacement of cabin centre of gravity	(m)
y_f	Lateral displacement of front tyre contact patch	(m)
$\ddot{y}$	Lateral acceleration	(m/s^2)
z	Position in the z direction (vehicle fixed)	(m)
z_c	Vertical position of cabin centre of gravity	(m)

Greek Letters

Symbol	Description	Unit
Δ	Kinematic steer angle	(rad)
ΔF_z	Vertical wheel load variation (from static value)	(N)
ΔP_v	Hydraulic pressure loss across valve	(bar)
α	Slip angle	(rad)
α_{eq}	'Magic Formula' equivalent slip angle	(rad)
α_f	Slip angle of front wheel	(rad)
α_r	Slip angle of rear wheel	(rad)
β	Centre of gravity side slip angle / Effective bulk modulus of hydraulic fluid	(rad / Pa)
γ	Camber angle of front wheel	(rad)
δ_a	Ackerman steer angle	(rad)
δ_{as}	Active steering angle	(rad)
δ_d	Driver's demand steer angle at front wheel	(rad)
δ_{das}	Active steering demand angle	(rad)
δ_{dff}	Steer demand angle including feed-forward element	(rad)
δ_e	Active steering angle error	(rad)
δ_f	Steer angle of front wheel	(rad)
δ_r	Steer angle of rear wheel(s)	(rad)
ε	Castor angle	(rad)
θ	Tilt angle	(rad)
θ_d	Demand tilt angle	(rad)
θ_{dff}	Demand tilt angle including feed-forward element	(rad)
θ_e	Tilt angle error	(rad)
θ_{eff}	Effective tilt angle / Tilt angle error including feed-forward element	(rad)
μ	Pitch angle	(rad)
μ_r	Coefficient of friction between tyre and road surface	-
ξ	Tilt axis inclination from ground plane	(rad)
σ	Tyre relaxation length	(m)
σ_α	Tyre relaxation length - slip	(m)

σ_γ	Tyre relaxation length - camber	(m)
ψ	Yaw angle	(rad)
ω	Angular velocity	(rad/s)
ω_d	Angular velocity of driver's steer input at steering wheel	(rad/s)

Chapter 1. Introduction

1.1. Active Control of Narrow Tilting Vehicle Dynamics

The dynamic behaviour of road vehicles is increasingly being controlled by electronic systems which aim to improve safety, ride comfort, and the driving experience [1]. This research aims to further the understanding of how electronic systems can be used to control the dynamics of a specific group of vehicles, Narrow Tilting Vehicles (NTVs), and to overcome some of their inherent dynamic limitations. Particular attention will be given to control of the tilting mechanisms and active steering systems that many of these vehicles employ.

1.2. Narrow Tilting Vehicles – Raison d'être

Narrow Tilting Vehicle (NTV) is a term generally applied to vehicles with the following characteristics: Compact dimensions - width especially, low weight, and an ability to tilt into corners to aid stability. Such vehicles are conceived for use over short distances, primarily in urban environments.

NTVs offer the potential to alleviate two pressing urban transportation problems; traffic congestion and carbon emissions, whilst retaining the degree of personal mobility that modern society takes for granted. Compact dimensions, particularly the narrow body style, enable a greater number of vehicles to occupy a given road space thus reducing traffic congestion. Carbon emissions are reduced as a result of low weight and a small frontal area that leads to a substantial reduction in aerodynamic drag forces [2]. Given their intended use as urban commuter vehicles, NTVs may lend themselves to electric propulsion, thus eliminating tailpipe emissions altogether.

In addition to their environmental credentials, NTVs also offer significant passive safety advantages over alternatives such as motorcycles and scooters [3]. This, combined with increased weather protection, may encourage a greater number of commuters to switch from conventional passenger cars.

1.3. Wheel Configuration and Tilting Mechanism

Although the majority of conventional road cars utilise four wheels, it is noteworthy that a significant proportion of NTVs use just three. One explanation for this difference could be that the dynamic limitations of three wheeled vehicles become less significant in the

context of low speed urban transport and that the cost and weight savings associated with the three-wheeled layout gain importance.

Whilst NTVs have many potential benefits, there remain some fundamental problems associated with their configuration. Whilst considerably safer than alternatives such as motorcycles, their small dimensions do mean that they offer considerably less in the way of impact protection than a conventional passenger car. In addition, their tall, narrow, body styles make them vulnerable to overturning during vigorous manoeuvres.

In order to overcome the tendency to overturn, NTVs are equipped with a tilting mechanism that allows them to lean into bends in much the same way as a motorcycle. NTVs can be classified in one of three broad categories; Passive Tilt Control, Steering Tilt Control (STC) and Direct Tilt Control (DTC).

Passive Tilt Control describes vehicles in which the driver is solely responsible for maintaining the stability of the vehicle through steering inputs and shifts in body weight. This is the system employed by motorcycles and bicycles. It requires considerable skill from the operator, and an additional means of stabilisation at very low speeds or when stationary.

Vehicles equipped with STC relieve the driver of the task of maintaining stability by automatically making steering inputs that balance the vehicle at the desired tilt angle. In order for STC to function, the mechanical link between the driver's steering wheel and the steered wheel(s) must be broken and an active steering system introduced. Whilst STC systems work well at high speeds where modest front wheel steer angles generate large lateral accelerations, at low vehicle speeds, very large steering inputs are required [4]. Thus, as is the case with passive tilt control, an additional stabilisation mechanism is required at very low speeds and when stationary.

As with STC, DTC relieves the driver from the responsibility of maintaining vehicle roll stability. DTC systems generate a tilting moment through the use of actuators linked to the suspension or non-tilting parts of the body rather than through use of the front wheel steer angle. Systems of this type have the considerable advantage that they are effective at low speeds (and whilst stationary) as the magnitude of the tilting moment is independent of vehicle speed. In highly transient conditions the tilting moments generated by DTC systems can be large in magnitude causing variations in tyre vertical loading that can impact upon vehicle stability. In addition, their power consumption can be considerable [5].

Systems that combine both STC and DTC, i.e. systems which use both the front wheel steer angle and direct actuation to control the tilt angle may be referred to as Steering Direct Tilt Control (SDTC). Such systems aim to combine the transient stability and low power consumption associated with STC, with the low speed stability of DTC.

1.4. Tilting Road Vehicles – A History

To date, tilting vehicles have not been produced in large numbers for sale in western markets but various prototypes and small series production vehicles have been produced.

Perhaps the first commercially successful tilting vehicle, the Honda Gyro, can trace its roots back further than any other. In 1965 a patent entitled "Improvements in or Relating to Pedal or Power-Driven Tricycles" [6] containing a tilting tricycle was filed by a Mr G Wallis. This lead to the creation of the BSA Aerial 3; a tilting tricycle that failed to find commercial success. The rights to the design were sold to Honda and in 1982 the Honda Gyro was launched [7].

Figure 1.1: Honda Gyro Canopy delivery vehicles.

The Gyro featured a single front wheel which tilted with the cabin, whist the two rear wheels were attached to a non-tilting engine module. The design found favour as a small urban delivery vehicle in its home market of Japan and as of 2013 was still on sale [8]. However; the Gyro is heavily based upon two wheeled scooter technology and shares little in common with passenger cars. In addition; its tilting mechanism is entirely passive save for a low speed lock that ensures it remains upright when stationary or at very low speeds.

The first serious attempt at an actuated tilting vehicle came from General Motors in the form of the Lean Machine of 1983 [9]. The Lean Machine comprised of a tilting cabin (with single front wheel) and a two-wheeled rear engine module. It featured a fully enclosed cabin with a clear aircraft style 'canopy' and 'streamlined' styling. Management of the Lean Machine's ±55° tilt angle was performed by the driver through foot pedal operated actuators [10] and therefore required significant skill.

An alternative approach to tilting vehicles was presented by Mercedes Benz with their 'F300 Life Jet' concept car unveiled at the 1997 Frankfurt motor show. As with the earlier Lean Machine, this vehicle featured a two seat tandem cabin but other aspects of the vehicles design were radically different. A one piece cabin/engine was tilted by means of an 'Active Tilt Control' (ATC) system [11] acting upon the two front wheels. The single rear wheel transmitted drive and was suspended by a swing arm in much the same way as that of a motorcycle. Despite its direct tilt control ATC system, the Life Jet was nearly as wide as a small conventional car with a front track width of 1560mm [12], this limited its appeal as an urban commuter vehicle considerably.

In 2006 Italian manufacturer Piaggio launched the MP3 [13], a three-wheeled scooter with two front wheels giving greater stability and braking performance than two-wheeled equivalents. The MP3 is offered for sale across Europe and North America and as of March 2013 had sold in excess of 130,000 units [14] at a cost of around €7000 (depending on version). Like the Honda Gyro, the MP3 uses passive tilt control and a low speed lock to keep it upright when stationary and at low speed. Whilst special 'wide track' versions can be driven on a car licence, the driving experience is predominantly similar to that of a motorcycle.

The 2008 Geneva Motor Show saw the unveiling of the Lumeneo Smera, a four-wheeled NTV with electric propulsion and a DTC system capable of producing a maximum tilt angle of 20° [15]. As of 2013 the Smera is available to customers in France through the Lumeneo website or a dealership in Paris at a cost of approximately €25,000; the author could not obtain any reliable production or sales statics.

Nissan unveiled a functioning prototype of their 'Land Glider' at the 2009 Tokyo Motor Show. The vehicle was a four wheeled NTV with a one piece tandem body that used active control of the suspension travel to lean into corners. Powered by an electric motor and battery pack the vehicle could reach a top speed of 100km/h, had a maximum tilt angle of 17°, and a width of just 1100mm [16].

Figure 1.2: Nissan Land Glider at the 2009 Tokyo Motor Show. (© 2006 Tennen-Gas, used under a Creative Commons Attribution-ShareAlike 3.0 license).

To date, the only vehicle with an active tilting mechanism to be offered for sale throughout Europe is the Vandenbrink Carver. This vehicle featured a similar configuration to the GM Lean Machine in that it had a tilting tandem cabin, single front wheel and a non-tilting rear engine module.

Figure 1.3: Vandenbrink Carver vehicle. (© 2006 Mike Roberts, used under a Creative Commons Attribution-ShareAlike 2.0 license).

Management of both the front wheel steer angle and the tilt angle was conducted by a hydro-mechanical system called 'Dynamic Vehicle Control' (DVC). This system used hydraulic valves to apportion flow to the tilt actuators in response to the steering torque input from the driver. The cabin was capable of tilting to a maximum of ±45° and

featured a maximum tilt rate of 82°/s [17]. The high speed tilting response was required to maintain stability during transient conditions. Additionally, the system featured a means to limit the steering torque applied by the driver at high speeds and thus limit the severity of maneuvers to maintain stability. Carver production ceased in 2009 after approximately 200 vehicles had been produced [18].

The aerodynamic and manoeuvrability advantages offered by NTVs may be obtained by narrow non-tilting vehicles provided adequate stability can be assured; such an approach would reduce cost and vehicle weight. The Renault Twizy, launched in 2012, is a four-wheel narrow vehicle which does not tilt into corners; instead it relies upon a high suspension roll stiffness to prevent lateral movement of the centre of gravity, and tyres which produce limited lateral force. No reliable maximum lateral acceleration figures are available for the Twizy, but road testers have noted that the car understeers readily [19]; the high roll stiffness has also contributed to negative reviews of the ride quality. At 1237mm (excluding mirrors) the Twizy is wider than most narrow tilting vehicles, this limits its ability to slip through gaps in traffic.

In addition to the above mentioned examples, various other tilting vehicles have been constructed by individuals and small companies, as well as a number constructed by academic institutions for research purposes.

1.5. The CLEVER Vehicle

The 2006 CLEVER (Compact Low Emission VEhicle for uRban transport) is a three-wheeled NTV born of an EU funded project with nine collaborators from across Europe. The University of Bath were responsible for the chassis design and the dynamics whilst other collaborators, notably BMW, were responsible for aspects such as manufacturing, passive safety and market research.

CLEVER features a two seat tandem layout, a single front wheel, tilting cabin, and a two-wheeled rear engine module. The total vehicle mass is approximately 332kg (excluding driver and bodywork); with a 75kg driver the static weight distribution is 39% front and 61% rear. The rear module does not tilt and accounts for approximately 40% of the laden vehicle mass meaning only 60% can be tilted to balance the vehicle whilst cornering. CLEVER's wheelbase is 2.4m, as long as many conventional city cars, but there are no overhangs. The track width is just 0.84m giving a total vehicle width of 1.00m.

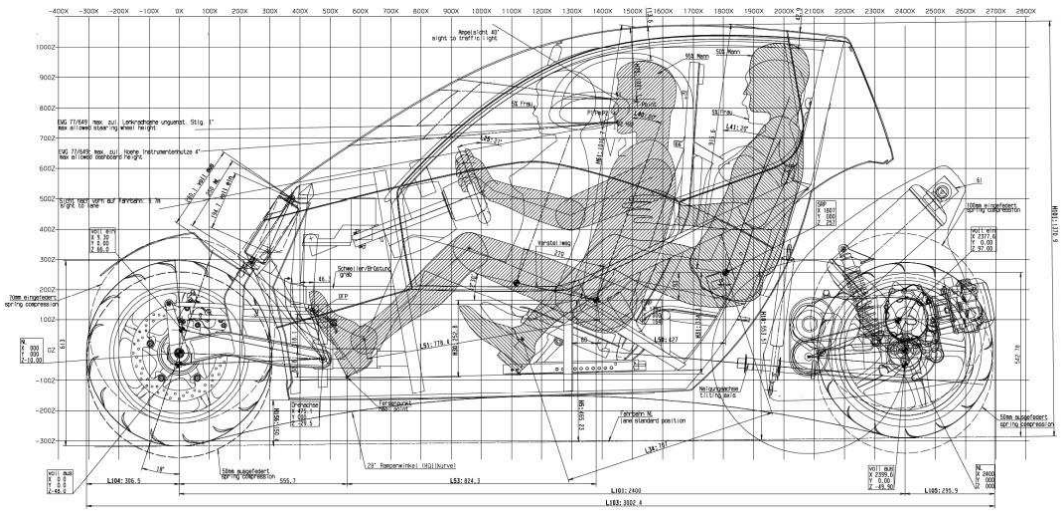

Figure 1.4: Line drawing of the CLEVER Vehicle.

CLEVER employs an electronically controlled and hydraulically actuated DTC system with a maximum tilt angle of ±45° [10]. A pair of single acting hydraulic actuators generate the required tilting moment. The DTC system provides excellent stability whilst stationary and at low speeds, but during vigorous manoeuvres at higher speeds the moment produced can be large enough to lift the inside rear wheel and, in extreme cases, capsize the vehicle.

A total of 5 prototype CLEVER Vehicles were constructed; three were used for crash testing, one remains in service as a research prototype at the University of Bath. The final example, complete with body work and interior, is in the custody of the BMW museum in Munich.

Figure 1.5: One of the five CLEVER Vehicles constructed.

Whilst the CLEVER Vehicle was intended to use a low emission engine burning compresses natural gas, the research prototype at the University of Bath uses a 13kW 176cc single cylinder petrol engine taken from BMW C1 scooter. The original CVT gearbox is retained (albeit modified to provide a power take off to drive the pump for the tilt hydraulics); belt drives are used to transmit power to the two rear wheels. Rear suspension is by way of independent trailing arms, adjustable Öhlins spring/damper units and an anti-roll bar. The front wheel is suspended by a leading four bar linkage with a single Öhlins spring/damper unit and uses a hub-centric steering system. A single track-rod transmits steer inputs to the front wheel from the output arm of a worm-gear steering box. The driver's steer inputs are transmitted to the steering box via a modified wheel and column sourced from a BMW car.

1.6. Research Justification and Objectives

Having established that narrow tilting vehicles offer the potential to dramatically reduce carbon emissions and congestion within urban environments, it would be of value to society if this potential could be realised. Before this can happen, the inherent dynamic limitations of this vehicle type must be overcome to ensure acceptable levels of safety and ease of driving.

As documented in Chapter 2, research to date in the field of narrow tilting vehicle dynamics has highlighted many issues associated with both DTC and STC systems, not least the inability to ensure vehicle roll stability under all operating conditions. Combined SDTC strategies have been proposed which aim to combine the best aspects of DTC and STC systems, but verification of their performance has been limited to the simulation of a small number of scenarios and some very low lateral acceleration experiments.

In addition, it has been noted that the use of a STC or SDTC system will lead to some deviation from the driver's intended path since such systems rely on alterations to the front wheel steer angle to maintain stability; the effect of this deviation on the driver's ability to control the vehicle is unknown. There is also an unexplored possibility that in an effort to follow the intended path, a driver will make steer inputs which cancel out the automated inputs from the active steering system thus removing any stability benefit.

In order to further the development of future narrow tilting vehicles, this research study will use both simulations of the CLEVER Vehicle, and experiments conducted on a prototype vehicle, to:

- Provide experimental verification of the performance of Steering Direct Tilt Control strategies at high lateral accelerations and under transient conditions.
- Investigate the effect of a SDTC strategy on the driver's ability to control the vehicle's path and to examine the interaction between driver and active steering system.
- Explore further refinements to SDTC strategies to improve both transient and steady state stability.

1.7. Thesis Structure

In order to provide a description of the current state of the art, Chapter 2 contains a review of the literature concerning automatic tilt control systems for narrow tilting vehicles and a brief description of current applications of active steering systems. Chapter 3 describes the unique blend of motorcycle and car like dynamic properties associated with NTVs, and how the tilting moment produced by DTC systems can have a negative impact upon vehicle stability.

Chapter 4 details the implementation of an active steering system on the prototype CLEVER Vehicle and the control logic developed to create a combined Steering Direct Tilt Control (SDTC) system. Chapter 5 introduces a multi-body simulation model of the CLEVER Vehicle that is used in later chapters to examine the influence of an active steering system on the vehicle's dynamics and stability.

Chapter 6 contains the results of experiments conducted using the prototype CLEVER Vehicle which provide a direct comparison between the performance of DTC and SDTC systems.

Chapter 7 describes the use of the simulation model introduced in Chapter 5 to investigate the influence of a SDTC strategy on the path followed by the CLEVER Vehicle in response to a series of open-loop steer inputs. Experimental results are also presented to verify the simulation findings and examine the interactions between the human driver and the active steering system.

Simulations are performed to explore further advances to the SDTC system in Chapter 8. When using a synthetic ramp steer input, the use of feed-forward of the tilt angle error rate to the active steering system (but not the DTC system) is found to potentially enhance the vehicle stability considerably. When a real steer signal complete with noise is

used, the necessary filtering leads to the loss of any performance advantage. Further, the influence of increased payload and differing surface friction coefficients are considered.

Finally, Chapter 9 draws a series of conclusions from the data presented within the thesis and suggests further avenues of investigation into the dynamics and control of narrow tilting vehicles.

Chapter 2. A Literature Review on the Dynamics and Control of Narrow Tilting Vehicles

2.1. Automatic Tilt Control Strategies

2.1.1. Single Acting Tilt Control Systems

Much of the early work published on the topic of narrow tilting vehicles was based upon models developed to describe the dynamic behaviour of bicycles and motorcycles. In [20], Karnopp and Hibbard developed a linearised steady state demand tilt angle equation (Equation (2.1)) for tilting vehicles by balancing the moments acting on an inverted pendulum model (Figure 2.1). This equation gave the tilt angle (θ_d) required to achieve a steady state 'balanced cornering condition' (one in which zero net roll torque is acting about the tilt axis) for a given lateral acceleration ($\ddot{y}$).

$$\sum M_A = mgh\sin\theta - m\ddot{y}h\cos\theta = 0 \Rightarrow \tan\theta_d = \frac{\ddot{y}}{g} \Rightarrow \theta_d \approx \frac{\ddot{y}}{g} \qquad (2.1)$$

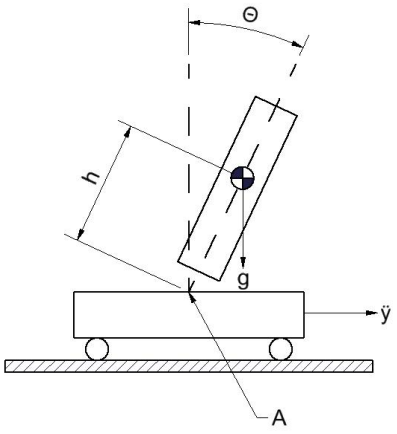

Figure 2.1: Inverted pendulum model.

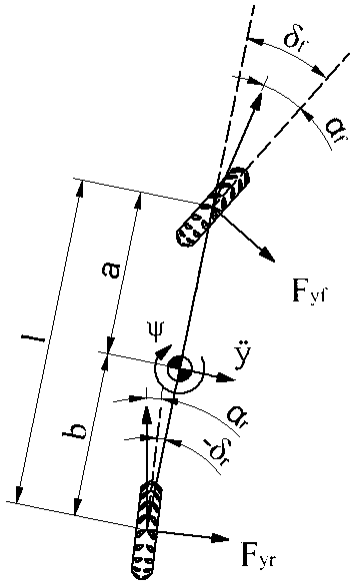

Figure 2.2: Bicycle model.

In [4] Karnopp and Fang used a simple model of the ground plane kinematics of a bicycle (Figure 2.2) to calculate the lateral acceleration of a motorcycle for a given vehicle speed (U), wheelbase (l), and steer angle (δ_f) assuming no tyre slip, Equation (2.2); this was combined with Equation (2.1) to produce Equation (2.3). In order to stabilise the motorcycle, a simple steering control law, Equation (2.4), was introduced in which the front wheel steer angle was a function of a gain (K_d) and the tilt angle error (θ_d-θ).

$$\ddot{y} = \frac{U^2}{l}\delta_f \tag{2.2}$$

$$\theta_d = \frac{U^2}{gl}\delta_f \tag{2.3}$$

$$\delta_f = -K_\delta(\theta_d - \theta) \tag{2.4}$$

Simulations were performed of the motorcycle's responses to a step change in the demand tilt angle, θ_d. With this method, Karnopp and Fang were able to demonstrate that a countersteering action was required in the early stages of a manoeuvre in order to maintain stability. The authors commented that as well as applying to motorcycles, this countersteering action would be applicable to the Steering Tilt Control (STC) system of a Narrow Tilting Vehicle (NTV), or, in the case of a NTV with a Direct Tilt Control (DTC) system, could be used to reduce the torque required to tilt the body.

An alternative tilt control strategy for NTVs, DTC, was demonstrated by Hibbard and Karnopp in 1993 [21]. The authors initially proposed a DTC control logic that used a PD controller (with low gains) acting upon the tilt angle error, with the demand tilt angle being calculated from the vehicle's lateral acceleration; they then used simulations to compare the dynamics of tilting and non-tilting narrow vehicles. The simulations were performed using a multi-body model created specifically for the study of tilting commuter vehicles; the model featured 7 degrees of freedom, a non-zero wheel track, and a non-tilting rear chassis component of finite mass. A simple actuator connected the non-tilting rear chassis component to a tilting cabin component in order to control the tilt angle. In addition, the model featured vertical tyre compliance, suspension dynamics, and remained valid at large tilt angles. Lateral tyre dynamics were deliberately omitted.

Using their model, the authors were able to demonstrate that upon entering a motorway slip road (of radius 78m, lateral acceleration 0.3g), passengers travelling in a vehicle equipped with a low-gain DTC system were subject to a maximum perceived lateral acceleration of 0.13g which then settled to zero at steady state, whilst those in a non-tilting vehicle experienced 0.39g in steady state. Equally, plots of tyre vertical loads were

used to demonstrate that roll stability was significantly improved; during the transient turn-in phase, weight transfer was reduced to approximately 30% of its former value, and once in steady state left and right tyre loads were virtually identical. It was suggested, although no supporting evidence was provided, that yaw stability would be enhanced in the tilting case as a result of the reduced variation in tyre vertical loading. Further simulations showed that during a lane change manoeuvre at 25m/s, peak weight transfer was reduced by 50% in the tilting case, and that the path followed by both the tilting and non-tilting vehicles was virtually identical. The power consumption of the DTC system was demonstrated to be reasonable in the context of a small commuter vehicle.

Whilst the advantages of tilting a narrow vehicle were established, it was clear that the low controller gains lead to considerable lag in the transient tilt angle response. Whilst higher controller gains were shown to improve the tilting response in normal manoeuvres, the authors claimed that in extreme manoeuvres the higher gains were potentially unsafe. An alternative control strategy, utilising low gains and the steer angle rate as an additional control input, was proposed; the improved controller introduced a feed-forward term and was shown to significantly reduce lag in the tilting response. No plots of perceived lateral acceleration or vehicle stability using the revised control strategy were presented.

Finally, Hibbard and Karnopp noted that their model could be used to asses the dynamic performance of various tilting vehicle configurations by altering the magnitude of the tilting and non-tilting masses and their respective inertias. In the event, the non tilting mass was modelled as insignificant in comparison to the total vehicle mass and this potential avenue of investigation was not explored further.

Working at the University of Bath, Drew [10] and Barker [22] designed and constructed a prototype three-wheeled narrow tilting vehicle known as CLEVER (Compact Low Emission VEhicle for uRban transport).

In [10] Drew detailed the development of a DTC system for the vehicle whose design presented a number of additional challenges, for example, a non-tilting rear module of considerable mass and a tilt axis raised above the ground plane. In common with many of the aforementioned control systems, a PID controller acted upon the tilt angle error, whilst the demand tilt angle was calculated from the steer angle and vehicle velocity. Calculations for the maximum moment that could be applied between the tilting cabin and the non-tilting rear module, without causing the rear module to capsize, were presented.

Drew used a simple inverted pendulum model (excluding tyre slip, friction, suspension effects, hydraulic effects, tilt axis height, and the mass of the non-tilting rear module) to simulate the response of the DTC system to a step steer input of 5º at a forward speed of 10m/s. The high tilt acceleration of the cabin following the step input resulted in a large peak in the perceived lateral acceleration. The author suggested that as well as being a source of discomfort, the large perceived acceleration could also signal diminished vehicle roll stability as it is accompanied by a large tilt moment which would result in load transfer from the inside to outside rear wheel. Further simulations were conducted for a ramp steer input of 5º over 0.5s at a forward speed of 14m/s and the resultant tilting moment analysed. The tilting moment applied to the rear module was found to exceed its roll moment capacity; it was suggested that the short duration of this moment may be insufficient to lead to wheel-loft and rollover, but the limitations of the DTC system were apparent.

Barker [22] constructed a more complex simulation model of the CLEVER Vehicle in Simulink featuring yaw dynamics, body roll, DTC system hydraulics and tyre dynamics. The model was used to investigate the influence various chassis parameters on vehicle stability. Introducing an anti-roll bar to increase the rear axle roll stiffness was found to reduce the roll angle of the rear module in response to tilting moments; however, load transfer was slightly increased. Increasing the damping of the rear suspension was found to have only a marginal effect on the roll angle and load transfer, while increasing rear track width led to significant stability benefits but undermined CLEVER's credentials as an urban commuter vehicle.

Barker also used his simulation model to asses the viability of STC strategies. He found that if the tyres were capable of producing sufficient lateral force for 1g of lateral acceleration, the maximum tilting moment a STC system fitted to the CLEVER Vehicle could generate is similar to that produced by the DTC system. Therefore a STC system would not be capable of a faster tilting response. Barker concluded that using a DTC system and limiting the rate at which the driver could apply steering lock (through fitment of a steering damper) may provide a means of ensuring vehicle stability (at the cost of some agility).

The final implementation of a tilt controller upon the CLEVER Vehicle prototype saw the demand tilt angle calculation modified to include an over-lean function to account for the reduced effective tilt angle caused by the raised tilt axis. In steady state testing, an over-lean gain of 1.2 was found to provide the driver with a natural and balanced feel during cornering; accelerometer measurements showed that a driver experienced a small

perceived acceleration in the same direction as the actual lateral acceleration. Transient step-steer input tests confirmed that the DTC system could generate large moments in response to rapid steer inputs, and that vehicle capsize could result. Drew and Barker recognised that further work was required to ensure stability of the vehicle in transient situations and suggested that an additional element of STC be considered in future.

In 2004, Gohl *et al.* [23] published both multi-body simulation and experimental results of a STC system applied to a three wheeled tilting vehicle. Calculation of the front wheel steer angle (δ_f) differed from earlier STC systems in that it contained an additional term (δ_d) which allowed steady state balancing about a non-zero tilt angle thus facilitating trajectory control, Equation (2.5). Note that the STC system of a NTV differs from the steering system of a motorcycle in that there is no direct mechanical connection between the driver's steering wheel and the steered front wheel of the vehicle; hence δ_f can differ from δ_d. A driver model was used to generate the necessary steer demand inputs to track a pre-defined path.

$$\delta_f = -K_\delta(\theta_d - \theta) + \delta_d \tag{2.5}$$

Initially Gohl *et al.* performed simulations to verify that the STC system was capable of maintaining stability whilst following a pre-defined path; experiments were then performed using an un-manned prototype vehicle. Despite some performance limitations of the prototype (notably a slow maximum steer rate) the authors were able to demonstrate that closed loop STC was able to maintain stability for a period in excess of 60s; albeit with larger than expected deviations from the command tilt angle. A plot of the command trajectory and the path actually followed by the prototype vehicle was conspicuous by its absence, but satisfactory performance was claimed.

Whilst many researchers in the field concentrated their efforts on combined SDTC systems, in 2011 Mourad *et al* [24] returned to the study of DTC systems. They opted to directly control the perceived lateral acceleration (as Snell, section 2.1.2), rather than the tilt angle, on the basis that such a system should be valid on banked roads and fewer approximations (associated with calculation of the correct demand tilt angle) are required. A basic 3 DoF bicycle model with simplified linear tyre dynamics was used to simulate the controller performance. The authors considered the use of such a simple vehicle model justifiable so long as the resulting controller had sufficient robustness properties. Simulation results showed that whilst the control strategy resulted in a steady state perceived lateral acceleration of close to zero; this was not the case in transient conditions. In [25], Mourad et al further enhance their controller by using feed forward of

the driver's steer rate (as first proposed by Hibbard and Karnopp [21]); this strategy was found to reduce the perceived lateral acceleration considerably and reduce the torque output of the DTC system by 40%.

2.1.2. Combined SDTC Systems

In their 1997 paper, So and Karnopp [26] compared the performance of STC and DTC systems with the aid of multi-body simulation tools. Both STC and DTC systems were found to follow a demand tilt angle well, and a number of advantages of each system were identified. They presented evidence to show that the acceleration perceived by passengers in a STC equipped vehicle was considerably lower than that perceived by passengers in a DTC equipped vehicle; it was suggested that this would have a significant impact upon the occupants comfort. In addition, the high suspension roll stiffness required to counteract the actuator torque in a DTC equipped vehicle was identified as a further source of discomfort. Equally, STC's inability to maintain stability at low speeds, and whilst stationary, was highlighted.

So and Karnopp proposed that by combining DTC and STC, a system could be created that would overcome the issues associated with each system. They were unable to successfully combine both STC and DTC in a continuous fashion due to conflict between the two control methodologies. In the transient situation of corner entry their STC system introduced a countersteering action; the DTC system, responding to the front wheel angle, then tilted the body out of the turn (see Equation (2.2)) rather than into the forthcoming corner.

To avoid conflict, So and Karnopp implemented an alternative approach of switching between STC and DTC in a speed dependant manner. The system utilised DTC at speeds of up to 8.5m/s at which point it switched to STC; to avoid unnecessary switching DTC would not be re-engaged until speeds dropped below 7.5m/s. Simulations of the control strategy's performance were conducted with a sinusoidal steer input and parabolic vehicle speed to create transient conditions. Satisfactory switching performance was claimed; a plot of the vehicle's lateral acceleration showed no significant disturbance around the switching points.

In [26] So and Karnopp had used a model with the simplifying assumption that no tyre slip occurred, in the same year they published [27] in which their switching STC/DTC model was refined to include a simple linear slip/tyre-force relationship. The introduction of tyre slip, and the associated lag, had a significant impact upon the system response and

lead to discontinuities in the perceived lateral acceleration around the switching points. To improve switching performance, the DTC system was modified to include negative feedback of the tilt angle rate in addition to the pre existing tilt angle error signal. It was also modified to include an integral term in the DTC controller to eliminate steady state errors. Using the refined STC/DTC switching strategy, So and Karnopp produced a plot of the passenger's perceived lateral acceleration; whilst discontinuities around the switching points were minimal, the plot did serve to highlight the significant differences in perceived lateral acceleration under the DTC and STC control regimes. With DTC significant accelerations were felt by occupants, with STC these accelerations were negligible; this may be felt by the driver as an inconsistency of response. No insight into the driver's ability to control the vehicle in the presence of this inconsistent feedback was offered by the authors. Finally, So and Karnoop noted that should a STC equipped vehicle encounter a low friction road surface, it may not be able to generate sufficient lateral accelerations and therefore balancing moments. A controller was proposed that compared the measured lateral acceleration to that generated by a reference model, in the event of a large discrepancy the control would witch from STC to DTC.

Contrary to So and Karnopp's difficulties, in his 1998 paper Snell [28] was able to develop a combined SDTC control system where both elements of the control strategy were active at all times and did not rely on switching in a speed dependant manner. Before proposing his combined control system, Snell demonstrated the behaviour of a DTC system that worked on the principal of minimising the perceived acceleration, rather than tilt angle error. Whilst perceived acceleration was reduced, this refined DTC system was found to demand large tilt moments sufficient to cause the non-tilting rear part of the chassis to overturn. Comparison was also made between the trajectories of vehicles equipped with STC and DTC when subjected to a step lateral acceleration demand. The countersteering action of STC was found to cause a small momentary displacement of the vehicle in the opposite direction to the driver's demand; thus, a smaller net displacement of the vehicle was achieved for a given steer input and vehicle speed.

Snell's combined SDTC approach overcame the conflicting outputs of the two control elements by utilising the driver's steer demand (δ_d), rather than the front wheel steer angle (δ_f), to calculate a command lateral acceleration; both systems could then work simultaneously to achieve this common goal. In addition, Snell introduced a lag into the steer output; this prevented large lateral forces being generated long before the tilt mechanism has reached its demand tilt angle. Note that Snell's model omitted tyre characteristics; in practise a small lag does occur between the introduction of a slip angle

(by steering the wheel) and the generation of lateral forces. The magnitude of this lag is dependant upon the tyre's 'relaxation length' characteristic (see Pacejka [29]).

Noting that STC amounted to tilting a vehicle about its centre of gravity, and that DTC amounted to tilting a vehicle about a fixed tilt axis, Snell also proposed a further control strategy with the ability to effectively tilt about a 'virtual tilt axis' chosen to give the desired mix of STC like and DTC like behaviour. The control laws worked on the principal of minimising the perceived lateral acceleration at the chosen virtual axis. Snell suggested locating the virtual axis just below the height of the driver's inner ear. Any lower and greater accelerations are perceived, any higher and disorientating reverse accelerations are felt. Snell presented simulation results that demonstrated the compromise between accurately following the driver's intended path with a 'DTC like' low virtual tilt axis, and the enhanced stability and lower perceived accelerations of a high 'STC like' tilt axis.

In 2005 Kidane *et al.* [30], following on from the work of Gohl *et al.* [23], developed a combined SDTC system that used different methods to calculate the demand tilt angle for each of the two modes of operation. Their DTC system used the lateral acceleration and an inverted pendulum model (refined to include gyroscopic moments and the lateral acceleration of the cabin due to the tilting motion) to calculate the tilt angle that resulted in a net tilting moment of zero. The demand tilt angle for the STC system was defined independently of the vehicle speed using the driver's steer input (δ_d) and a scaling factor (K_s), as per Equation (2.6). The front wheel steer angle (δ) was then calculated to minimise the tilt angle error as per Equation (2.7).

$$\theta_{dSTC} = K_s \delta_d \tag{2.6}$$

$$\delta = K_p(\theta - \theta_d) + K_d\left(\dot{\theta} - \dot{\theta}_d\right) + \delta_d \tag{2.7}$$

Since the STC tilt angle calculation (Equation (2.6)) omits the vehicle speed, an increase in speed during a turn results in a tilt angle error. In-turn, Equation (2.7) causes a reduction in the front wheel steer angle (δ) and an increase in the turn radius; in this way a constant lateral acceleration is maintained and the vehicle remains properly balanced.

Although scaled to produce the same steady state demand tilt angle, in transient conditions it is possible for the DTC and STC systems to conflict; the countersteering action of the STC system can produce an inverted lateral acceleration to which the DTC system reacts by attempting to tilt the vehicle the wrong way. Integration of the

potentially conflicting DTC and STC systems relied upon speed dependent scaling factors. At low speeds the DTC system was dominant, as speed rose the STC system's influence grew and the DTC system's influence diminished.

In [31] Kidane *et al*. refined their control system so that both the DTC and STC systems used the demand tilt angle calculation given in Equation (2.6), and the front wheel steer angle calculation was modified to incorporate the integral of the tilt error rather than the steer demand, Equation (2.8). As well as resolving the conflicts between the two control systems, this control strategy ensures that should the vehicle parameters change (e.g. additional payload mass is added), zero steady state tilting moment is maintained.

$$\delta = K_p(\theta - \theta_d) + K_d\left(\dot{\theta} - \dot{\theta}_d\right) + K_i\int\left(\theta - \theta_d\right)dt \tag{2.8}$$

Again integration into a single control system was performed with the aid of speed dependant scaling factors which varied the dominance of one or other component. This time, at speeds of up to 5m/s only the DTC control system would be active, at speeds between 5 and 10m/s the influence of the DTC system would diminish as the influence of the STC system increased. Above 10m/s only the STC system functioned.

A series of simulation results were presented to show that a vehicle equipped with the speed varying SDTC system, and a simple driver model, was able to track a circular path very accurately, even when a sinusoidal speed input was used to ensure transition between control systems. Because of the non-speed-dependent demand tilt angle calculation, in order to follow a constant radius in the presence of varying speed, the driver model had to continuously vary the steer input. This steering behaviour is analogous to a vehicle with a significant understeer tendency, as speed increases more steering input is required to maintain a given turn radius. Some experimental verification of the tilt control system performance is presented but it fails to address the question of whether a human driver would be able to maintain control of the vehicle trajectory in light of the need to vary the steer input as the speed changes.

In their 2008 [32] and 2009 [33] papers, Kidane *et al.* retain the use of a common tilt angle demand for both STC and DTC systems; the scaling factors used in their earlier publications to apportion control to the DTC and STC systems, in response to vehicle speed, are absent and both control systems remain active at all times. The authors acknowledge that the omission of speed (U) from the tilt angle demand calculation leads to an excessive understeer tendency. A revised tilt angle equation is proposed with the aim of producing a neutral steer characteristic, Equation (2.9).

$$\theta_d = K_s \delta_d U^2 \tag{2.9}$$

A limited number of low speed experiments were performed using a prototype vehicle, and a control system programmed with both the non-speed-dependent and the speed-dependent tilt angle calculations. Comparison of the results showed that the revised tilt angle equation successfully gave neutral steering behaviour. Whilst stability of the vehicle is implied by the good tilt angle tracking behaviour (remembering that the tilt angle is defined to provide a zero steady state torque and therefore balanced cornering), no explicit results were presented to confirm this. Equally, although the authors claimed their prototype was capable of tilt angles of ±35º and lateral accelerations as high as $7m/s^2$, the low speed nature of the experimental results presented meant that tilt angles of only 14º and accelerations of $2.45m/s^2$ were reached. The performance of the control system in vigorous, transient manoeuvres remained un-verified.

Continuing the earlier work of Drew [10] and Barker [22], in [34] Berote *et al.* developed a comprehensive multibody simulation of the CLEVER Vehicle's lateral dynamics. The model included non-linear tyre dynamics using Pacejka's 'Magic Formula' calculations [29], suspension dynamics, 7 major mass bodies, and hydraulic system dynamics; longitudinal dynamics resulting from aerodynamics drag, driving torque and braking were consciously omitted. Plots of the tilt angle, lateral acceleration, and rear module roll obtained from the simulation model showed a good correlation to results from experiments conducted using the prototype CLEVER Vehicle.

In [35] and [36] Berote used his model to investigate the application of a combined SDTC system to the CLEVER Vehicle in an effort to improve its transient stability. The driver steering input (δ_d), the vehicle wheelbase (L) and the forward speed (U) were used to calculate a lateral acceleration demand and hence demand tilt angle; the over-lean factor of 1.2 introduced by Drew and Barker was retained, Equation (2.10).

$$\theta_d = 1.2 \times \frac{U^2}{gL} \delta_d \tag{2.10}$$

Whilst both DTC and STC systems responded to the tilt angle error simultaneously, Berote noted that the optimal STC behaviour varied as a function of speed with smaller steer inputs required at higher speeds. Simulations of the CLEVER Vehicle's lateral acceleration response to a step steer input were used to derive values for a non-linear speed dependant active steering gain, Figure 2.3.

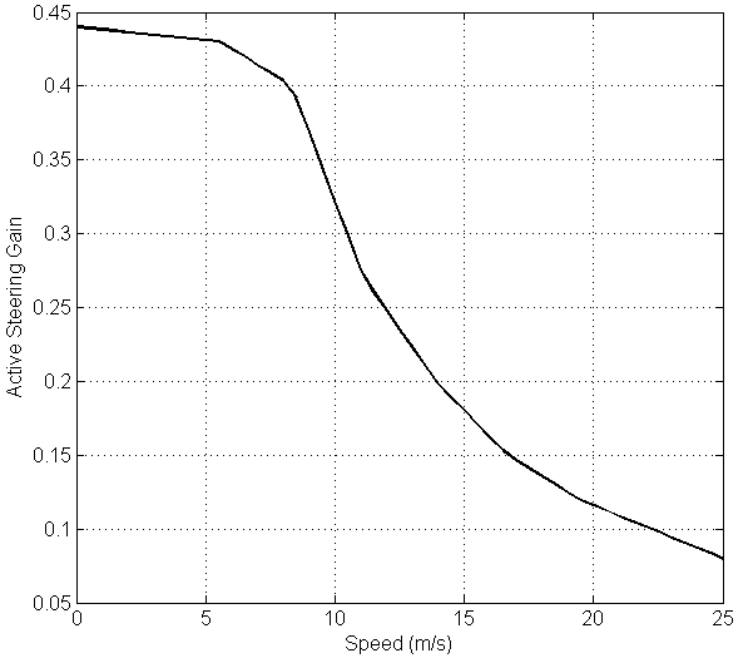

Figure 2.3: Berote's active steering gain curve [34].

Berote used his simulation model to compare the performance of his combined SDTC system to the performance of the DTC system originally used on the CLEVER Vehicle. In the transient conditions that exist upon corner entry and corner exit, the SDTC system showed a better tilting response and improved vehicle stability. Lateral acceleration plots showed that the SDTC system had a much reduced settling time and lower overshoot, whilst plots of the inside wheel load showed that variation was reduced to less than 25% of that present using a DTC strategy. Simulation results were limited to a single step steer input conducted at a forward speed of 30km/h and no experimental verification of the combined SDTC system was offered.

Working at the Vienna University of Technology, Edelmann *et al.* [37] and Edelmann and Plöchl [38], developed a detailed multi-body simulation model of a narrow tilting vehicle. The control system of their NTV used a SDTC system in which the DTC component was active only when the vehicle speed was below 3m/s. A feed-forward of the tilt angle error rate was used to enhance the tilting response. The authors used a simplified version of the model to show that NTVs may be subject to the same well know 'weave', 'wobble' and 'capsize' modes as motorcycles, while they used the full model to investigate the response of the vehicle to ramp steer inputs. In response to severe steer inputs, the control system resulted in an initial countersteering action with an accompanying inverted yaw rate; significant overshoot of the demand tilt angle was observed. Since the control system relied principally on STC, vehicle stability and energy efficiency were claimed to be good; however, the vehicle deviated significantly from the

desired trajectory. Unfortunately, no results were presented to show the influence of the feed-forward loop on the tilting response and no data measured in physical experiments was presented.

In 2012, Furuichi *et al.* published descriptions of a model that allowed the simulation of three-wheeled NTVs running on just two wheels whilst cornering [39] & [40]. The model was then used to verify the performance of a DTC system and two different SDTC systems. The first SDTC system simply used a transfer function, acting on the drivers steer demand, to introduce a lag into the front wheel steer angle output; the second SDTC strategy used another transfer function to introduce a countersteering action.

The simulations indicated that under DTC the inside wheel would lift clear of the ground if the vehicle was subjected to a ramp steer input of approximately 20° when travelling at a speed of 20km/h; an experiment using a prototype vehicle lead to capsize under the same conditions. Both of the SDTC systems were shown to eliminate inside wheel lift-off in both simulation and experiments. Although the authors claim satisfactory agreement, plots show that the simulation model does not replicate the tilt angle performance in transient simulations particularly well. In addition, the experimental results do not quantify the load transfer from inside to outside wheel other than to state whether the vehicle capsized or the inside wheel lifted clear of the ground.

2.1.3. Brink Dynamics DVC

An alternative tilt control strategy for a tilting three-wheeled vehicle (called Dynamic Vehicle Control) was presented by van den Brink (1997) [41] in which tilting was not controlled by an electronic processor but by a hydro-mechanical system. The system worked on the principal that at the 'ideal' tilt angle, for a given speed and corner radius, zero steering torque input is required from the driver. A torsion bar, connected to the steering column, was used to operate a valve which in turn sent flow to a pair of hydraulic tilt actuators. When the vehicle reached a balanced cornering condition the applied steering torque was zero, the hydraulic valve was closed and the current tilt angle maintained. Maximum steering torque was limited to 25Nm (by means of a force feedback actuator termed 'anti-steer') to prevent a situation in which the tilt mechanism could not provide sufficient torque, and therefore tilt angle rate, to balance the vehicle against the lateral acceleration generated by the front wheel steer angle. Note that a mechanical link was maintained between the front wheel and the driver's steering wheel. Comparison was made between the anti-steering torque's tendency to reduce steer angle at high speeds and the onset of understeer in conventional vehicles. It was claimed that as

a result of the DVC system, a prototype vehicle could negotiate a lane change manoeuvre safely at a speed of 100km/h, and felt smooth and natural to drive. In a further paper [42] (1999), van den Brink stated that 'EC Home Type Approval' had been granted for a vehicle equipped with DVC; this vehicle later entered limited production as the Brink Carver. Whilst the type approval undoubtedly adds weight to the author's claim that the vehicle was stable and safe, no quantifiable evidence was published to this effect.

Noting the lack of mathematical proof of the Brink Dynamics DVC system, Pauwelussen published a pair of papers, [43] in 1999 and [44] in 2000, in which he derived the equations of motion of a vehicle thus equipped and performed a limited number of simulations. The results showed that the DVC system was capable of obtaining a steady state tilt angle close to the optimum (for balanced cornering), and that in response to a ramp steer torque input, the tilt angle followed the steering torque satisfactorily. In addition the 'anti-steer' torque was shown to reduce the tilt moment considerably to the benefit of vehicle stability. Evidence, in the form of lateral acceleration and yaw rate plots at a single speed, was presented to show that the driver's intended path was compromised to only a limited extent by the anti-steer function.

In 2004 van den Brink and Kroonen published a further paper [45] including several refinements to the DVC system. Principally the system had been altered to include a STC element which was active at high lateral accelerations, and active rear wheel steering which operated only at high speeds. Improvements to the maximum tilt rate and a substantial reduction in the tilt actuator moment were claimed, but, in common with van den Brink's earlier papers, no simulation or experimental results were offered.

2.2. Active Steering Systems

Whilst the development of an active steering system is required for the implementation of a SDTC system, it is not in itself the primary focus of this thesis. Never the less, a brief literature review of active steering follows. This literature review is included to address the regulatory and practical concerns surrounding the use of active steering on road vehicles.

2.2.1. Regulations Relevant to the use of Active Steering Systems

Revision 2 of UN Regulation 79 [46] contains provision for the use on the public highway of 'Advanced Driver Assistance Steering Systems'. The document further specifies two types of these systems; "Automatically Commanded Steering Functions" - systems that perform path following at low speeds (e.g. self-parking), and 'Corrective

Steering Function' systems - those which perform limited duration changes to the steer angle in order to maintain the desired path or influence the vehicle's dynamic behaviour. A SDTC system utilising active steering would fall into the latter classification.

In the interests of safety, Regulation 79 contains a number of performance specifications for both normal operating conditions and in the event of system failure. The system failure requirements can be summarised as follows; in the event of a failure, an active steering system must alert the driver to the problem, the driver must be able maintain control over the front wheel steer angle without needing to apply excessive steering torque and the road wheel steer angle should not be subject to sudden change. Any SDTC system developed for use on the public highway would have to comply with these requirements.

2.2.2. Existing Applications of Active Steering

Whilst active steering can be found on many agricultural machines and some heavy plant, these systems have very different performance requirements and functions to those of a NTV and are not considered in this document. Of more relevance is the application of active steering in conventional passenger cars. BMW have made an active steering system available (principally as a cost option) since 2004. In 2004, Koehn and Eckrich of the BMW group published a description of the system [47]; given that the system is commercially sensitive, technical detail is limited but the scope of the system's function and the principals of the mechanism through which it is achieved are presented.

In the document, the authors explain that the BMW active steering system has two principal functions; a variable steering ratio and stabilising corrective steering actions. The provision of a variable steering ratio allows the magnitude of the steer inputs required at low speeds (for example whilst parking) to be reduced whilst achieving a given front wheel steer angle; at high speed the steering ratio is increased to promote stability. The corrective steering function uses data from the vehicle's ESP system to detect oversteer. In the event of mild oversteer a countersteering action is applied to the front wheels in order to correct the slide without the need to brake individual wheels as in a conventional ESP system. In more extreme oversteer situations, and during understeer, conventional ESP function is required.

The document also describes how the variable steering ratio and corrective steering actions are facilitated by the addition of a planetary gearbox at the base of the steering column. If the gearbox housing is kept still, a simple mechanical gear train conducts

steering inputs from the input sun gear to the output sun gear via two planetary gears and conventional steering is retained. In addition, a motor and worm drive is able to rotate the gearbox housing, in doing so the position of the output sun gear can be varied relative to the input sun gear thus altering the relationship between steering wheel position and front wheel steer angle.

Although almost no data is provided to support their arguments, Koehn and Eckrich claim that by eliminating braking actions in mild oversteer situations, passenger comfort and driver enjoyment are enhanced and the vehicle can carry more speed through a lane change manoeuvre. It is also claimed that by using the mechanical configuration described, driver-independent steering actions can be performed whilst ensuring that in the event of a motor failure, conventional steering is retained.

The use of a planetary gearbox mounted in the steering column is one way in which an active steering system may be developed to allow implementation of SDTC on a narrow tilting vehicle.

2.2.3. Active Steering to Enhance Roll Stability of Non-Tilting Vehicles

Whilst the active steering systems developed by BMW have concentrated on controlling the yaw behaviour of a vehicle, active steering can also be used to influence the roll behaviour. In [48] Ackermann *et al.* describe the use of an active steering system to mitigate the rollover behaviour of non-tilting vehicles with a high centre of gravity relative to their track width. As a vehicle equipped with the proposed system reaches the point of rollover, and emergency steering control loop is activated. This control loop prioritises rollover avoidance over lane-keeping by reducing the steer angle and thus the curvature of the vehicle path; the system is supplemented by application of the vehicle's brakes to minimise deviation from the intended path.

Many of the working principals applicable to the above rollover prevention strategy are also applicable to the SDTC of narrow tilting vehicles; for example, the reduction of the steering angle in the interests of stability and the need to sacrifice ideal lane-keeping/path following performance. However, in the interests of consistent driver feedback and reduced energy consumption, most active steering systems for narrow tilting vehicles are intended to operate continuously rather than only intervening in emergency situations.

Ackermann *et al*. also state that there are a number ways in which active steering can be implemented in both a fail-safe and cost effective manner. An illustration of an active

steering system is shown where an otherwise conventional steering rack is mounted in laterally compliant bushings, and its position controlled by an actuator.

2.3. Concluding Remarks

Both Steering Tilt Control (STC) and Direct Tilt Control (DTC), when implemented in isolation, have been shown to possess significant limitations which prevent their use in a successful automated tilt control system for a NTV. Whilst STC is energy efficient and, in principal, capable of maintaining stability at high speeds, it cannot perform satisfactorily at low speeds and its performance on low-grip surfaces (such as ice) has been shown to be poor. In contrast, DTC works well whilst the vehicle is stationary or travelling at low speed, and because it does not rely on lateral forces produced by the tyres to generate the roll moment, it is likely to be effective (though its demand tilt angle estimation will be poor) on low friction surfaces. The power consumption of DTC systems is considerable, and in vigorous, transient manoeuvres the tilting moment they produce has a significant detrimental influence on vehicle stability. Switching between STC and DTC strategies in a speed dependant manner leads to un-satisfactory performance around the switching points and inconsistent feedback to the driver.

Combined Steering Direct Tilt Control (SDTC) systems in which STC and DTC work simultaneously to achieve the demand tilt angle have been demonstrated by a number of authors. In the case of Snell [28], a SDTC system was shown to offer improved performance but claims were made solely on the basis of rudimentary simulations omitting or simplifying many significant factors (e.g. tyre dynamics, suspension effects, and yaw behaviour).

Kidane *et al.* [33] demonstrated a combined SDTC system in which the maximum possible lateral acceleration was limited by effectively increasing the steering ratio exponentially with speed; both satisfactory stability and path following were claimed, however it was noted that in order to remain on course, the driver would have to adjust his steering inputs in the presence of variations in the vehicle's speed. Whilst experimental results were offered to supplement the simulation findings, these were limited to a small number of low speed and low lateral acceleration cases. Vehicle stability, and a human driver's ability to follow a path were not sufficiently verified.

Comprehensive simulations of SDTC performance were presented by Berote [36]; however, no experimental verification was offered and the impact of the system upon

path following was not investigated. Experimental verification of Berote's proposed SDTC system forms one of the key objectives of this thesis.

Furuichi *et al*. [39] & [40] did provide some experimental verification of the performance of their SDTC system in a limited number of vigorous manoeuvres; however, the experimental confirmation of vehicle stability was limited to whether wheel lift-off or capsize did or did not occur.

Finally, active steering is permitted for use on the public highway provided certain safety considerations are met. Existing applications of active steering in passenger cars suggest that the packaging and cost considerations of such a system are not insurmountable.

Chapter 3. Narrow Tilting Vehicle Dynamics

This chapter aims to introduce the unique dynamic properties associated with Narrow Tilting Vehicles (NTVs); many of these properties are incorporated into the CLEVER Vehicle simulation model which will be discussed in Chapter 5. The single front wheel of the CLEVER Vehicle is subject to large camber angles and little load variation in much the same way as a motorcycle wheel. The rear wheels, by contrast, remain largely upright, like those of a conventional car, and because the rear axle provides the vehicle with all of its roll stiffness, the rear wheels are subject to large load variations when cornering. In addition, the hydraulic tilt control system introduces moments, and therefore load variations, not seen in either motorcycle or conventional car dynamics; further, the tilting kinematics introduce a rear wheel steer angle. This combination of dynamic properties makes for a complex and intriguing subject.

Figure 3.1 shows the coordinate system used to define the position of the vehicle. X,Y,Z, represent the global coordinate system where as x,y,z, are a vehicle fixed coordinate system with its origin at ground level on the vehicle centreline and directly below the rear axle line.

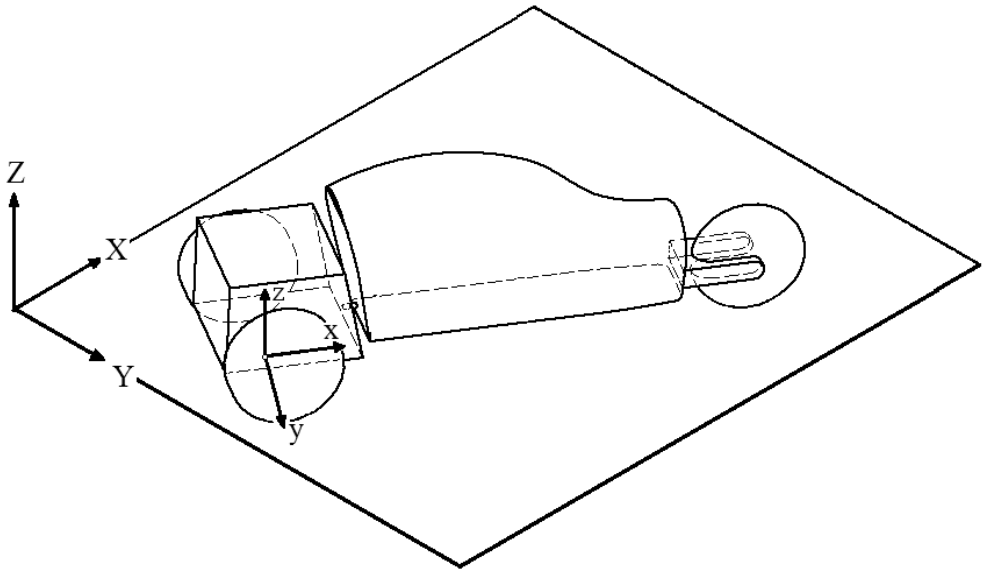

Figure 3.1: Coordinate system.

3.1. Front Wheel Steering Kinematics

When a narrow tilting vehicle is steered, the kinematic steer angle (Δ) (the front wheel steer angle relative to the ground plane) is not simply equal to the angle about the steer

axis through which the wheel is rotated (δ). Rather, the castor angle (ε) pitch angle (μ) and the tilt angle (θ) all have an influence on the kinematic steer angle (Δ) Figure 3.2.

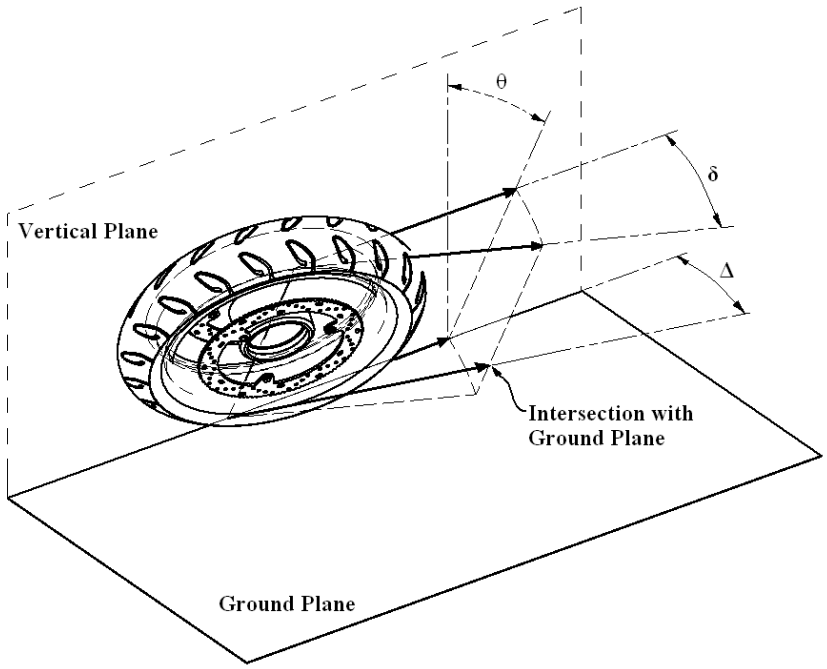

Figure 3.2: The steer angle (δ) and kinematic steer angle (Δ).

Cossalter [49] gives the following equation for the kinematic steer angle:

$$\Delta = \arctan\left(\frac{\sin\delta\cos(\varepsilon+\mu)}{\cos\theta\cos\delta - \sin\theta\sin\delta\sin(\varepsilon+\mu)}\right) \tag{3.1}$$

Ignoring pitch motions, Equation (3.1) becomes:

$$\Delta = \arctan\left(\frac{\sin\delta\cos\varepsilon}{\cos\theta\cos\delta - \sin\theta\sin\delta\sin\varepsilon}\right) \tag{3.2}$$

Using Equation (3.2), and the 17° castor angle of the CLEVER Vehicle's front wheel steer axis, the following steer angle / kinematic steer angle relationships are obtained for a number of tilt angle values (Figure 3.3). At a zero tilt angle, the kinematic steer angle is slightly smaller than the steer angle; however, at larger tilt angles the kinematic steer angle is amplified.

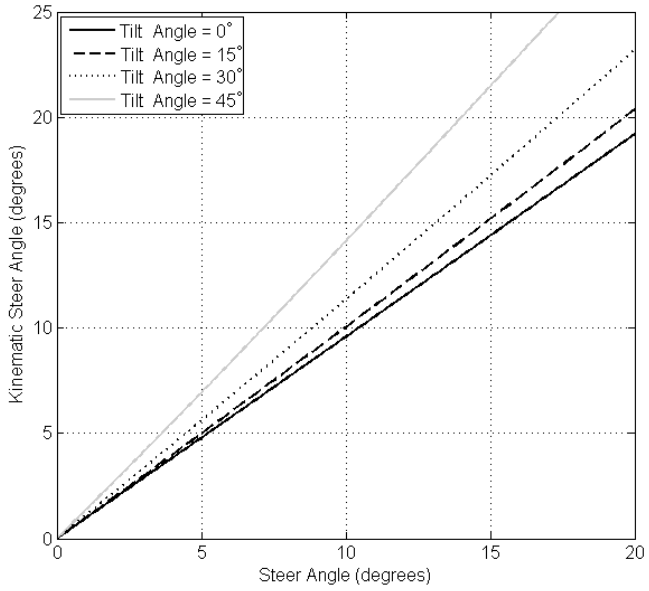

Figure 3.3: Steer angle / kinematic steer angle relationship.

Similarly to the kinematic steer angle, the camber angle (γ) of the front wheel is influenced by the vehicle steering kinematics. Ignoring pitch motions, the camber angle is obtained from Equation (3.3) [49]:

$$\gamma = \arcsin\left(\cos\delta \sin\theta + \cos\theta \sin\delta \cdot \sin\varepsilon\right) \tag{3.3}$$

The kinematic steer angle and camber angle calculations are incorporated into the tyre force calculations within the CLEVER simulation model introduced in Chapter 5.

3.2. Tilt Axis Height

Much of the literature written on the subject of NTVs assumes that the vehicle is tilting about an axis on the ground plane. Whilst this is true for motorcycles and some NTVs that use suspension travel to facilitate tilting, NTVs exist that tilt about a mechanically defined tilt axis at a height (h_o) above (or below) the ground plane.

Cossalter *et al.* 2000 [50] published a study into the effects of tilt axis height on the dynamics of a passively tilting three-wheeled vehicle. A four-bar linkage with adjustable geometry was used to provide a variable tilt axis height both in multi-body simulations and on a prototype vehicle. Simulations showed that a tilt axis raised 150mm above ground level resulted in significant load transfer from the inside wheel to the outside wheel. With the tilt axis on the ground plane load transfer to the outside wheel was reduced. A tilt axis 150mm below ground level produced a higher load on the inside

wheel than the outside wheel. Experimental results were presented that supported the simulation findings.

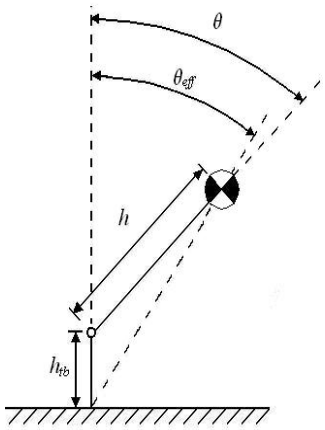

Figure 3.4: Effective tilt angle.

In [51] Barker *et al.* demonstrated that the effect of a tilt axis raised above the ground plane is to reduce the effective tilt angle (θ_{eff}) for a given tilt angle (θ), Figure 3.4. An 'over-lean' function was introduced into the control strategy to compensate for the raised tilt axis but the maximum effective tilt angle remained compromised.

3.3. Tyre Dynamics

The tyre dynamics of narrow tilting vehicles are different to those of both passenger cars and motorcycles. In the case of the CLEVER Vehicle the front tyre is subject to larger camber angles, as commonly experienced on motorcycles, but the rear wheels remain principally upright, as per a conventional car.

Depending on the tilting strategy chosen, and how well it performs, a narrow tilting vehicle may experience large vertical wheel load variations. In motorcycle dynamics, if the resulting longitudinal dynamics are assumed to remain small, lateral accelerations do not lead to variations in the vertical wheel loads; the same is true of the front wheel of CLEVER. However, given the narrow rear track, the zero roll stiffness of the front suspension and the moment generated by the DTC actuators, the rear wheels may be subject to very high load variations. On the limit of stability the inside wheel will carry no vertical loading, whilst the outside wheel is subject to twice the nominal static value.

The tyres used on the CLEVER Vehicle were created specifically for the project and as a result no performance data is known. A generic tyre may be modelled using a simple linear tyre model or a more complex non-linear model such as Pacejka's 'Magic

Formulas' [29]. When applying the Magic Formulas to the CLEVER Vehicle a different formula is used for the front wheel, which experiences large camber angle variations, and the rear wheels, which experience operating conditions closer to those of a car.

This section will introduce a simple linear tyre model; the more complex non-linear Magic Formulas will be discussed in the context of their application to the CLEVER simulation model in Chapter 5.

3.3.1. Linear Tyre Modelling

Slip

Tyres generate lateral force through two principal mechanisms: slip and camber thrust. The slip angle of a tyre may be defined as the negative inverse tangent of the ratio of lateral and longitudinal tyre velocity (Equation (3.4)), Figure 3.5. Using this definition, a positive slip angle results in the generation of a positive lateral force (F_y).

$$\alpha = -\tan^{-1}\left(\frac{V_y}{V_x}\right) \tag{3.4}$$

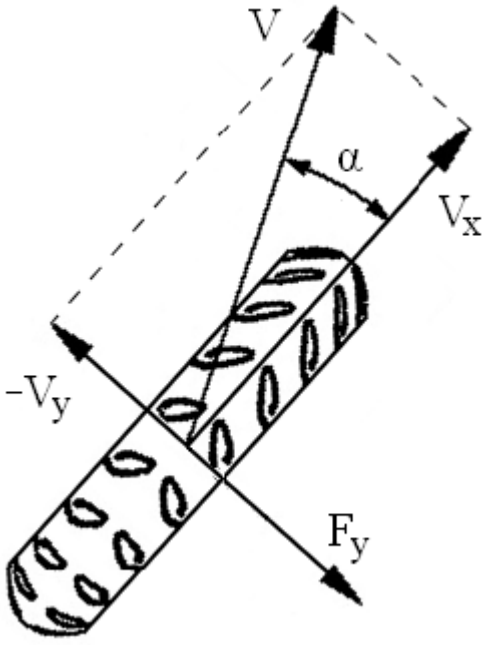

Figure 3.5: Slip angle definition.

The presence of a non-zero slip angle does not necessarily entail a sliding action occurring between the tyre tread and the road surface as the name implies; rather, small slip angles occur as a result of deformation on the tyre carcass.

The lateral force/slip relationship is often simplified to a linear form whereby the force is a function of the slip angle (α) and the tyre lateral slip (or cornering) stiffness (C_α).

$$F_y = \alpha C_\alpha \tag{3.5}$$

The slip stiffness (C_α) can be further defined as the slip stiffness coefficient (C_s) (a measured property of the tyre) multiplied by the vertical load (F_z) carried by the tyre.

$$C_\alpha = C_s F_z \tag{3.6}$$

$$F_y = \alpha C_s F_z \tag{3.7}$$

The linear approximation holds at small slip angles; however, as with many aspects of tyre behaviour, the true lateral force/slip relationship is non-linear. A typical non-linear force/slip relationship for a tyre on dry tarmac is shown in Figure 3.6.

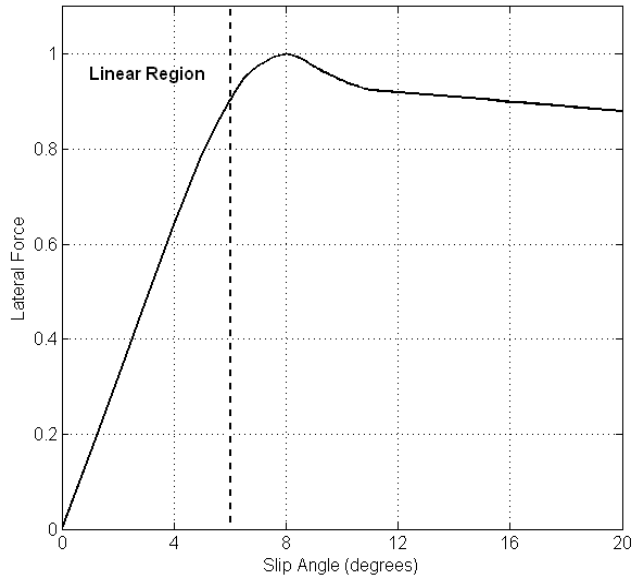

Figure 3.6: Typical lateral tyre force/slip characteristics on dry tarmac.

Camber Thrust

As well as the contribution from the slip angle, lateral tyre force is also generated as a result of camber thrust. Camber angle (γ) is defined as the angle between the wheel plane and an axis normal to the road surface, Figure 3.7. When the camber angle is non-zero, the wheel rotation axis is out of alignment with the ground plane and lateral deformation of the tyre contact patch will occur. Since the tyre has non-zero stiffness, a lateral force is generated towards the intersection of the wheel rotation axis and the ground plane.

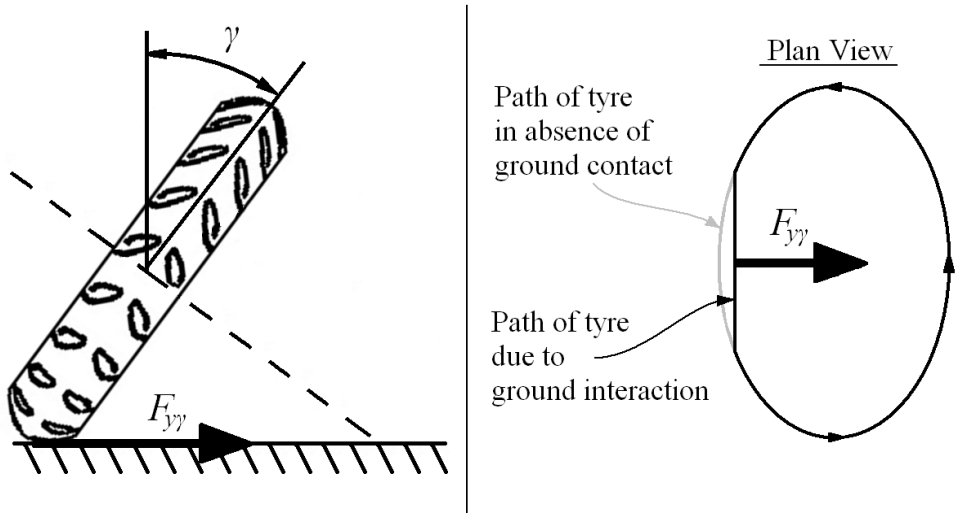

Figure 3.7: Camber thrust mechanism.

As with lateral slip, the force generated by camber thrust can be approximated as a linear relationship with the camber stiffness (C_γ) a function of vertical load (F_z) and the camber stiffness coefficient ($C_{s\gamma}$):

$$F_y = \gamma C_\gamma \tag{3.8}$$

$$C_\gamma = C_{s\gamma} F_z \tag{3.9}$$

Combining the linear models of lateral slip and camber thrust gives a total lateral force equation:

$$F_y = \alpha C_\alpha + \gamma C_\gamma \tag{3.10}$$

Relaxation Length

The simple linear approximations of the lateral tyre force given thus far are only valid under steady state conditions. It has been documented that, under transient conditions, a lag occurs between the application of a slip angle and the generation of lateral forces as the tyre carcass deforms [52].

In order to describe the lag properties of a tyre, a new parameter is introduced; the relaxation length (σ) is defined as the distance covered (x) when the transient lateral force reaches 63% (or 1-e^{-1}) of the steady state value. Whilst the relaxation length has been shown to vary from tyre to tyre, and to be a function of slip angle (α), angular velocity (ω) and vertical load (F_z) [52]; as a rule of thumb, Pacejka states that the relaxation length can be treated as equal to the tyre radius (r) [29].

As is the case when generating forces through slip angle, forces generated through camber thrust do not occur instantaneously. In the camber thrust case, there is both a lagging and non-lagging force element. Depending on the vertical loading and tyre characteristics, the non-lagging element can vary in magnitude and can even occur in the opposite direction to the steady state force [29]. Given the complexity and inconsistency of the non-lagging force, and its typically small magnitude, it is often omitted from calculations [49]. With the non-lagging element disregarded, the relaxation length for camber thrust (σ_γ) is equal to the relation length for slip (σ_α).

$$\sigma = \sigma_\alpha = \sigma_\gamma \tag{3.11}$$

The lateral tyre force equation can be modified to incorporate the relaxation length where F_{yss} is the steady state lateral force:

$$F_y = F_{yss}\left(1 - e^{\frac{x}{\sigma}}\right) \tag{3.12}$$

3.3.2. Longitudinal Tyre Dynamics

As well as generating lateral forces, a tyre must also generate longitudinal forces to facilitate acceleration and braking of the vehicle; these forces are generated as the result of longitudinal slip.

A free rolling tyre with forward speed V_x and nominal angular velocity ω_0 has an effective rolling radius r_e:

$$r_e = \frac{V_x}{\omega_0} \tag{3.13}$$

When transmitting braking or drive torque longitudinal slip occurs ($\omega_0 \neq \omega$) and Equation (3.13) no longer holds. The slip ratio (k) is defined as per equation (3.14).

$$k = -\frac{\omega_0 - \omega}{\omega_0} \tag{3.14}$$

If the vehicle is travelling forwards resulting in a free rolling angular velocity of ω_0 but the actual angular velocity (ω) of a given wheel is 0rad/s (i.e. the wheel is locked), the slip ratio (k) = -1. Since there is (in principal) no limit to the maximum value of ω, when excessive drive torque is applied the value of k can become very large.

As was the case for lateral slip, a linear approximation of the force generated from pure longitudinal slip can be used for small values. The longitudinal slip stiffness C_k is introduced; this parameter is a function of both the tyre properties and the vertical load F_z.

$$F_x = kC_k \tag{3.15}$$

3.3.3. Combined Slip

Under many common operating conditions tyres are generating both lateral and longitudinal forces simultaneously; for instance, when a driver brakes whilst in a corner or accelerates (therefore generating a longitudinal force at the driven wheel(s) contact patch) before fully exiting the corner. The interaction between the longitudinal and lateral forces is often illustrated by the traction circle concept, Figure 3.8. Where both lateral (F_y) and longitudinal (F_x) forces are produced by the tyre, the resultant force vector (F_{xy}) cannot exceed the radius of the traction circle; the radius value being determined by the friction coefficient and the vertical load (F_z).

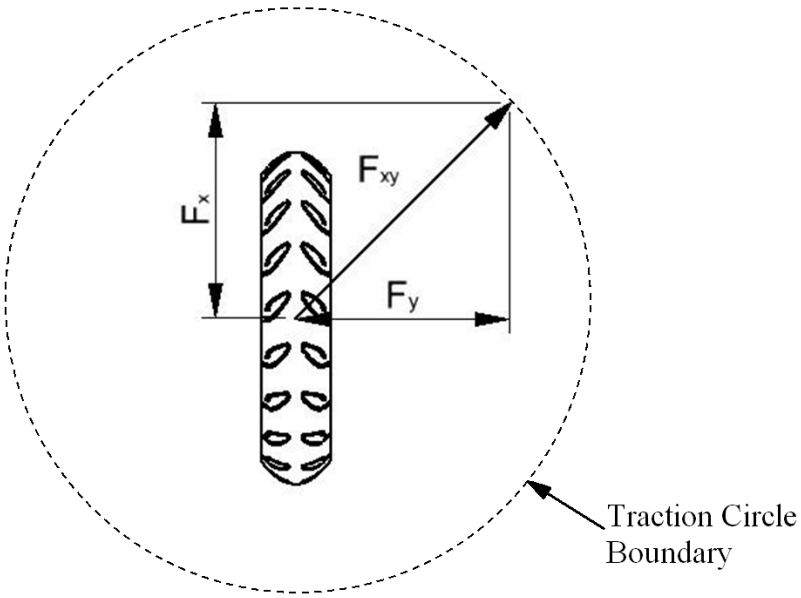

Figure 3.8: Traction circle concept.

Assuming the magnitude of the longitudinal force generated through braking or acceleration is maintained, the maximum lateral force that can be generated simultaneously is less than the maximum lateral force that can be generated by a free-rolling tyre:

$$F_{y\,MAX} = \sqrt{F_{xy\,MAX}{}^2 - F_x{}^2} \tag{3.16}$$

In practise the lateral and longitudinal frictional coefficients of a tyre often differ, this results in a traction ellipse rather than the traction circle shown.

Although longitudinal tyre forces are omitted from the CLEVER Vehicle simulation model, the reduced lateral force capacity of tyres when longitudinal forces are also being produced has particular implications for the behaviour of narrow tilting vehicles. The generation of large longitudinal tyre forces will reduce the lateral force output of a tyre. As a result, the tilt control system's estimation of lateral acceleration and demand tilt angle will be affected, particularly under heavy braking. In addition, NTVs which rely upon STC may not be able to generate sufficient tilt moment from the front wheel steer angle.

3.4. Lateral and Yaw Dynamics

The lateral and yaw dynamics of a narrow tilting vehicle can be studied with the aid of a simple bicycle model, Figure 3.9. By treating the vehicle track width as negligible in comparison to the turn radius, a pair of wheels on a common axle can be represented as a single wheel on the vehicle centre line. The influence of load transfer on the tyre forces is omitted, as are longitudinal tyre forces from driving, rolling resistance and braking.

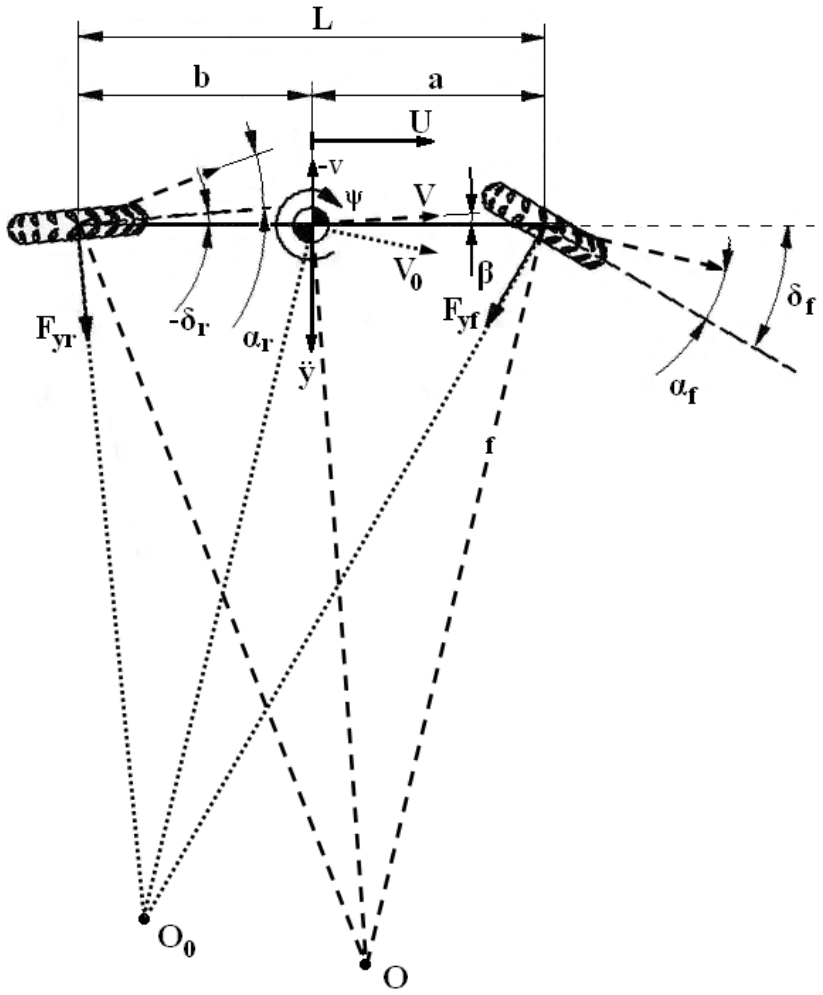

Figure 3.9: Bicycle model.

If no tyre slip were to occur, the centre of gravity of the vehicle represented in Figure 3.9 would follow path V_0 and rotate about the origin O_0; however, in order to generate lateral forces some tyre slip must occur. With the inclusion of tyre slip, the vehicle centre of gravity will move in the V direction and rotate about a point O. There will be a slide slip angle of the centre of gravity (β) which will be negative at small tyre slip angles and will become positive at larger tyre slip angles.

The total force generated in the *y* direction by the tyres is given by:

$$F_y = \left(F_{yf} \cos\delta_f + F_{yr} \cos\delta_r\right) \tag{3.17}$$

Note that at higher steer and slip angles, the tyres will also generate a significant longitudinal force component.

Assuming steer and slip angles remain small; the lateral force calculation can be simplified to:

$$F_y = \left(F_{yf} + F_{yr}\right) \tag{3.18}$$

Except in the steady state case, where the yaw rate remains constant (i.e. there is no yaw acceleration), the front and rear tyre forces will act to generate a net yaw moment about the vehicle's centre of gravity. By neglecting the influence of pneumatic trail, each tyre's contribution to the yaw moment (*M*) can be calculated simply by multiplying the tyre force by the tyre's longitudinal position relative to the centre of gravity:

$$M_f = aF_{yf} \tag{3.19}$$

$$M_r = -bF_{yr} \tag{3.20}$$

The resulting lateral and yaw motion of the centre of gravity is described by:

$$I_z\ddot{\psi} = aF_{yf} - bF_{yr} \tag{3.21}$$

$$m\ddot{y} = F_y \tag{3.22}$$

Where I_z represents the yaw inertia of the vehicle and $\ddot{y}$ the lateral acceleration of the centre of gravity.

Limiting the analysis to steady state conditions, the yaw acceleration, and therefore the yaw moment, become zero.

$$M = aF_{yf} - bF_{yr} = 0 \tag{3.23}$$

To produce a zero yaw moment, the lateral force produced by each of the tyres must be proportional to the vertical load which they are supporting:

$$F_{yf} = F_y\left(\frac{b}{L}\right) \tag{3.24}$$

$$F_{yr} = F_y\left(\frac{a}{L}\right) \tag{3.25}$$

Now that the lateral force required from each tyre to produce steady state handling has been determined, a tyre model or look-up table can be used to establish the steady state slip angle of each wheel.

Where the rear wheel steer angle (δ_r) is dictated by the tilting kinematics, is defined as positive to the right, and remains small, the front wheel steer angle (δ_f) a driver needs to generate in order to effect a turn of radius (R) is given by:

$$\delta_f = \frac{L}{R} + \delta_r + \alpha_f - \alpha_r \tag{3.26}$$

In [51] Barker *et al.* used a simplified linear tyre model to derive the steady state handling characteristics of a narrow tilting vehicle at a range of different lateral accelerations and corner radii. They showed that in the absence of rear wheel steering, the CLEVER Vehicle would have a significant oversteer tendency. Barker et al. derived their steady state handling characteristic equations as follows:

The lateral forces produced by the front and rear axles are found from the centre of gravity position, total vehicle mass and the centre of gravity position:

$$F_{yf} = m_f\ddot{y} = m\left(\frac{b}{L}\right)\ddot{y} \tag{3.27}$$

$$F_{yr} = m_r\ddot{y} = m\left(\frac{a}{L}\right)\ddot{y} \tag{3.28}$$

Substituting Equations (3.27) & (3.28) into the simple linear tyre model, Equation (3.10), and re-arranging gives the front and rear slip angles:

$$\alpha_f = \frac{m_f \ddot{y} - \gamma C_\gamma}{C_{\alpha f}} \tag{3.29}$$

$$\alpha_r = \frac{m_r \ddot{y}}{C_{\alpha r}} \tag{3.30}$$

In the absence of rear wheel steering Equation (3.26) becomes:

$$\delta_f = \frac{L}{R} + \alpha_f - \alpha_r \tag{3.31}$$

Substituting in the slip angle equations (3.29) & (3.30) gives the equation for the steer angle in terms of the tyre properties, the corner radius, mass distribution, wheelbase length and the camber angle (γ).

$$\delta_f = \frac{L}{R} + \left(\frac{m_f \ddot{y} - \gamma C_\gamma}{C_{\alpha f}} \right) - \left(\frac{m_r \ddot{y}}{C_{\alpha r}} \right) \tag{3.32}$$

Assuming steer angles remain small and the camber angle is not influenced by the kinematic effects of Equation (3.3), and by omitting the over-lean function in the CLEVER Vehicle controller, the front wheel camber angle is:

$$\gamma = \theta = \frac{\ddot{y}}{g} \tag{3.33}$$

Barker *et al.* used the parameters given in Table 3.1, to calculate the handling characteristics of the CLEVER Vehicle without rear wheel steering.

Table 3.1: Tyre parameter values [51].

Parameter	**Unit**	**Value**
$C_{\alpha f}$	rad^{-1}	$9.74m_f$
C_{ar}	rad^{-1}	$10.89m_r$
C_γ	rad^{-1}	$0.86m_f$

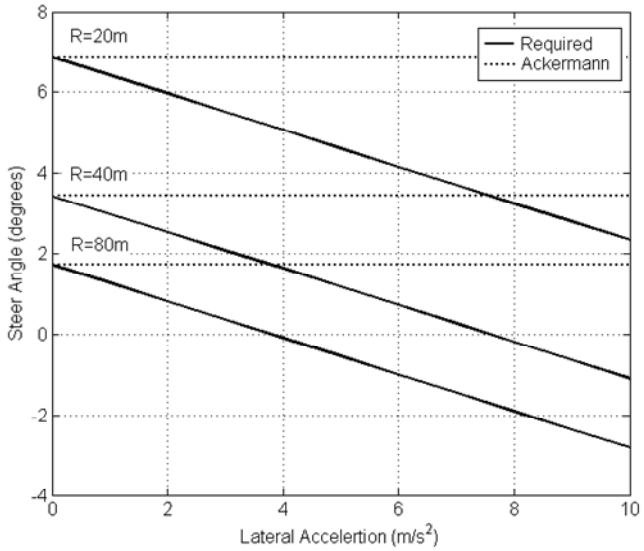

Figure 3.10: Steer response, δ_r=0 [51].

Figure 3.10 is a plot of the front wheel steer angle (δ_f) against lateral acceleration ($\ddot{y}$) at a selection of fixed corner radii. It shows that without rear wheel steering, the CLEVER Vehicle would be subject to a large amount of oversteer with the driver having to apply less steer angle at higher lateral accelerations. Since the front wheel is linked to the tilting cabin mass, at high lateral accelerations large front wheel camber angles produce large amounts of camber thrust. Barker *et al.* were able to determine that a tilt axis inclination (ξ) of 5º would give a near Ackermann (neutral) steering characteristic up to tilt angles of 30º, beyond this some oversteer would remain.

Experimental results recorded using the prototype CLEVER Vehicle showed that with the tilt axis inclination of 5º, the steer angle generated by the driver was close to the ideal Ackermann angle for a range of lateral accelerations.

3.5. Moment Reserve

The concept of a 'moment reserve' was introduced by Berote [35] as a means of quantifying the maximum moment the DTC system could exert without causing wheel lift. The moment reserve can be calculated by considering the moments acting on the CLEVER Vehicle when in a steady state cornering condition, and subtracting this value from the total moment capacity.

Since only a proportion of the CLEVER Vehicle's mass can be tilted, and there are practical limitations on the extent to which the cabin can be 'over-tilted', it is not possible to achieve a zero steady state roll moment when the vehicle is subjected to lateral accelerations. During transient conditions, the rear module may be subjected to an additional roll moment generated by the DTC actuators. If the combined roll moment is larger than the moment capacity of the rear module, wheel lift and possibly capsize, will occur, Figure 3.11.

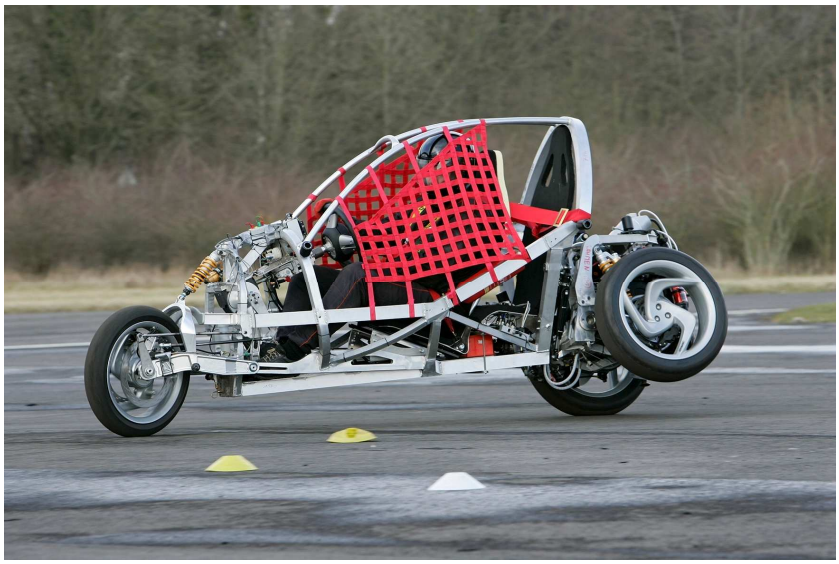

Figure 3.11: CLEVER Vehicle prototype demonstrating lack of roll stability in transient conditions.

The kinematic model show in Figure 3.12 is used to derive equations for the moment reserve; it is simplified by assuming a rigid chassis with no suspension or tyre compliance, by constraining the yaw motion of the rear module, and by ignoring pitch motions coupled to the tilt motion (and therefore variations in tilt bearing height (h_{tb}) and tilt axis inclination (ξ)). In addition, the mass of the rear module is assumed to be directly over the rear axle and the front wheel steer angle (δ_f) is assumed to remain zero.

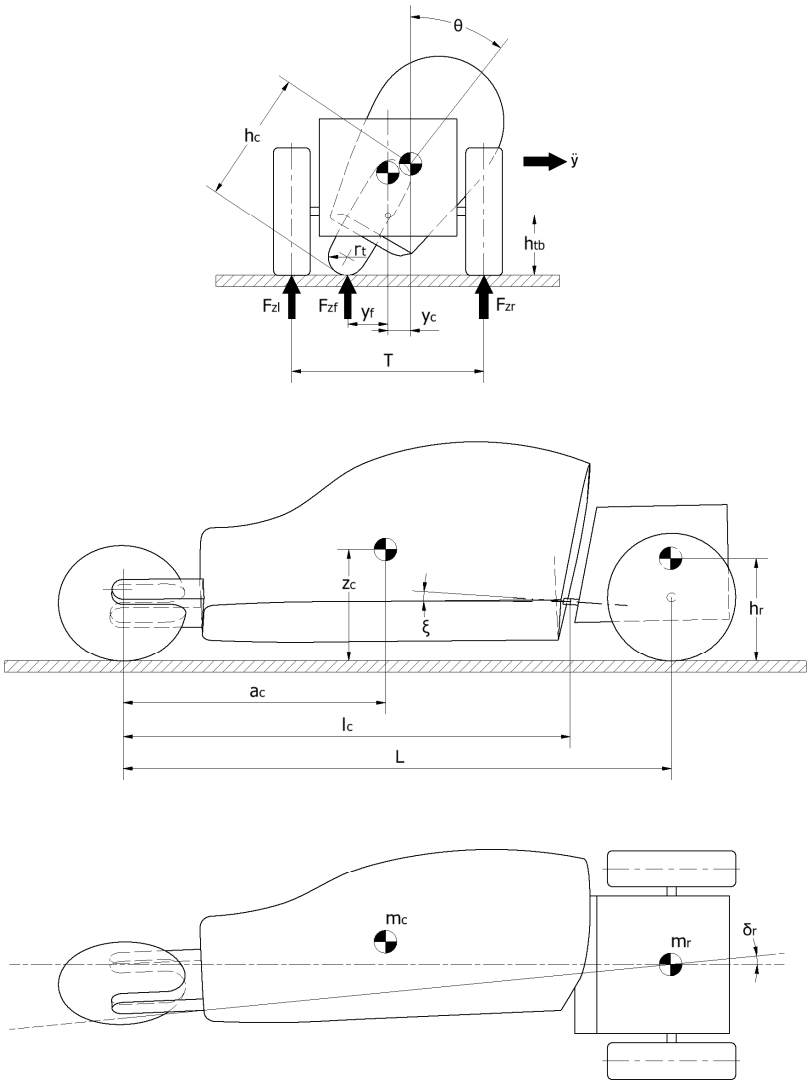

Figure 3.12: CLEVER Vehicle kinematic parameters.

As a consequence of the raised and inclined tilt axis, with the rear module constrained in yaw, a lateral displacement of the front tyre contact patch (y_f) occurs when the cabin tilts. In practise the displacement of the front tyre contact patch manifests itself as a rear wheel steer angle (δ_r).

The lateral displacement of the cabin centre of gravity (y_c) and the lateral displacement of the front tyre contact patch (y_f) are given by:

$$y_c = \sin\theta\left[h_c - h_{tb} - \xi(l_c - a_c)\right] \tag{3.34}$$

$$y_f = \sin\theta\left[h_{tb} - r_t + \xi l_c\right] \tag{3.35}$$

And the rear wheel steer angle (δ_r) is given by:

$$\delta_r = \arcsin\left(\frac{\sin\theta\left[h_{tb} - r_t + \xi l_c\right]}{L}\right) \tag{3.36}$$

The vertical height of the cabin centre of gravity also changes as a result of the tilting motion:

$$z_c = \cos\theta\left[h_c - \left(h_{tb}\frac{a_c}{l_c}\right)\right] + h_{tb}\frac{a_c}{l_c} \tag{3.37}$$

The tilt angle of the cabin (θ) is given by the following expression (incorporating the 20% over-lean factor used in the CLEVER Vehicle controller):

$$\theta = 1.2 \times \left(\frac{\ddot{y}}{g}\right) \tag{3.38}$$

Taking moments about the centre of the rear track (on the ground plane) gives a roll moment of:

$$M = (m_c g y_c) + (F_{zf} y_f) - (m_c \ddot{y} z_c) - (m_r \ddot{y} h_r) \tag{3.39}$$

The total roll moment capacity (M_c) of the rear engine module is taken to be the maximum moment that can be applied to the rear engine module without a rear wheel lifting clear of the ground (F_z>0). Assuming an even static load distribution between the two rear wheels, M_c can expressed as a function of the rear tyre vertical loads (F_{zl} & F_{zr}) and the track width (T):

$$M_c = \pm(F_{zl} + F_{zr})\frac{T}{2} \tag{3.40}$$

The steady state moment reserve M_r in either direction is therefore given by:

$$M_r = [\pm(F_{zl} + F_{zr})\frac{T}{2}] + [(m_c g y_{ce}) + (F_{zf} y_f) - (m_c \ddot{y} z_c) - (m_r \ddot{y} h_r)] \tag{3.41}$$

Table 3.2: Moment reserve parameter values.

Symbol	Description	Unit	Value
a_c	Longitudinal position of cabin mass from front axle	m	1.158
F_{zf}	Vertical load supported by front wheel at rest	N	1242
F_{zl}	Vertical load supported by left rear wheel at rest with cabin upright	N	1280
F_{zr}	Vertical load supported by right rear wheel at rest with cabin upright	N	1280
g	Acceleration due to gravity	m/s^2	9.81
h_c	Height of cabin mass CG from ground plane in upright position	m	0.59
h_r	Height of rear module mass CG from ground plane	m	0.54
h_{tb}	Height of tilt bearing from ground plane	m	0.271
L	Wheelbase length	m	2.4
l_c	Longitudinal position of tilt bearing from front axle	m	1.953
m	Total vehicle mass	kg	412
m_c	Cabin mass (including driver and un-sprung mass)	kg	250
m_r	Rear engine module mass (including un-sprung mass)	kg	162
r_t	Radius of tyre cross section	m	0.07
T	Track width	m	0.84
ξ	Tilt axis inclination from horizontal plane	rad	0.0873

Using the parameter values for the CLEVER Vehicle given in Table 3.2, the steady state moment reserve can be plotted against the lateral acceleration to give an indication of the maximum moment that the DTC system can apply without causing wheel lift-off, Figure 3.13. The data plotted in Figure 3.13 is likely to be an overestimate of the moment reserve as it excludes the influence of the rear module roll angle (which if included would act to reduce the effective tilt angle). In transient conditions there is also likely to be a tilt angle error so the moment reserve available will be lowered further.

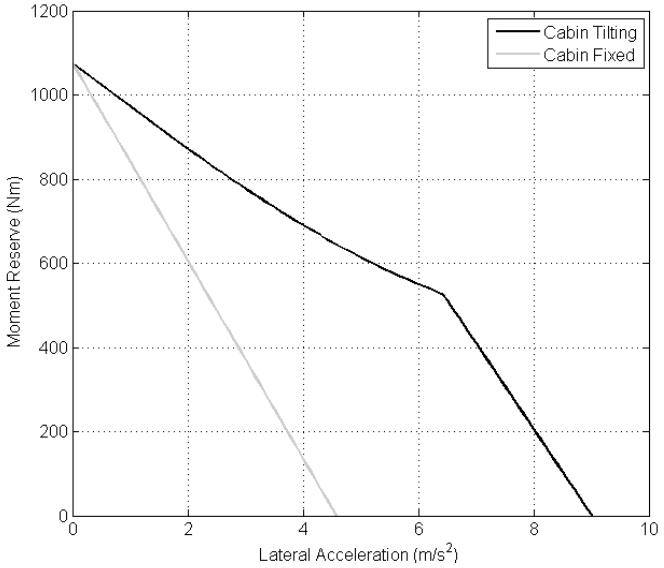

Figure 3.13: Steady state moment reserve.

Whilst, according to Figure 3.13, the CLEVER Vehicle can safely reach lateral accelerations of 9m/s^2 in steady state, wheel lift off has been observed from the prototype at lateral accelerations of less than 4m/s^2 under transient conditions. In highly transient situations large tilt angle errors are generated; these tilt angle errors act to both reduce the stabilising influence of the cabin mass (and therefore reduce the available moment reserve), and also to prompt the generation of tilting moments from the DTC actuators. Thanks to the simultaneous reduction in the moment reserve and the application of the tilting moment, the moment reserve may be exceeded and wheel lift can occur.

Whilst the DTC actuator moment is limited by a 2Hz low pass filter on the tilt angle error signal within the controller (see Section 4.3.5), a strategy of lowering it further is not considered viable as slowing the cabin tilt response would increase the tilt angle error, and in turn, lower the available moment reserve still further. Alternatively, controlling the front wheel steer angle with an active steering system could make two contributions to improving stability; firstly, the generation of lateral accelerations in response to a driver's steer inputs could be delayed giving time for the tilting action to occur before the moment reserve is depleted. Secondly, a momentary countersteering action could be generated creating a reverse lateral acceleration and generating a tilting moment that assists the DTC actuators.

3.5.1. Load Transfer

Since the single front wheel of the CLEVER Vehicle has zero roll stiffness, the net roll moment leads to load transfer across the rear axle.

The magnitude of the steady state load transfer (ΔF_z) can be calculated by dividing the roll moment due to lateral acceleration (M) and the roll moment introduced by the DTC actuators (M_{DTC}), by the rear tack width (T):

$$\Delta F_z = \frac{M + M_{DTC}}{T} \tag{3.42}$$

$$\Delta F_z = \frac{\left[(m_c g y_c) + (F_{zf} y_f) - (m_c \ddot{y} z_c) - (m_r \ddot{y} h_r)\right] + M_{DTC}}{T} \tag{3.43}$$

As well as roll stability, load transfer across the rear axle will influence the tyre lateral force generation and therefore the yaw behaviour of the vehicle.

When tyre forces are assumed to be linear, load transfer from the inside wheel to the outside wheel (ΔF_z) has no impact upon the total lateral force (F_y) generated by an axle. The increased vertical load ($F_{zo}+\Delta F_z$), and resulting lateral force produced by the outside wheel, being cancelled by the reduced load ($F_{zi}-\Delta F_z$) and lateral force from the inside wheel:

$$F_y = \alpha C_s (F_{zi} - \Delta F_z) + \alpha C_s (F_{zo} + \Delta F_z) \tag{3.44}$$

As with many aspects of tyre behaviour, the true load/lateral force relationship is non-linear. Increases in tyre vertical load do not result in an increase of proportional magnitude in the lateral force. A load/force relationship for a generic tyre running at a nominal slip angle (α) is illustrated in Figure 3.14.

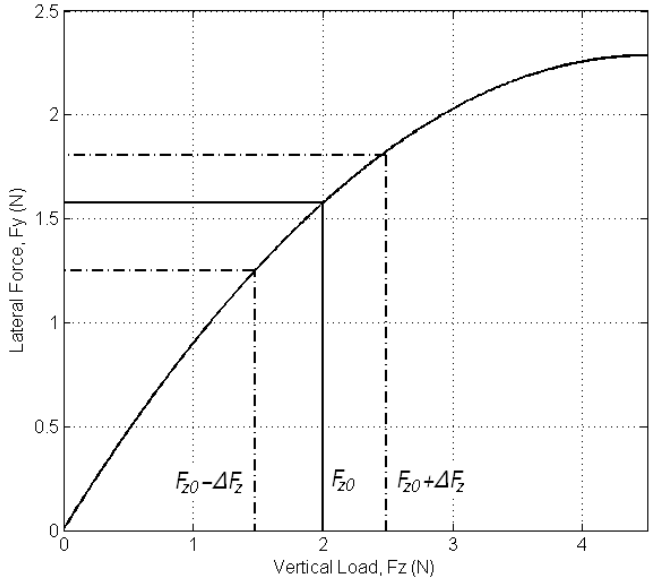

Figure 3.14: Typical load/lateral force curve. Adapted from [53].

In the example illustrated in Figure 3.14, with no load transfer each of the rear wheels is supporting a nominal load (F_{z0}) of 2kN and generating approximately 1.6kN of lateral force, giving a total lateral force for the axle of 3.2kN. In the presence of a load transfer (ΔF_z) of 500N, the inside wheel is supporting a load of 1.5kN and the outside wheel 2.5kN. The inside and outside wheels are producing lateral forces of 1.25kN and 1.8kN respectively giving a total lateral force for the axle of 3.05kN. In this way, load transfer reduces the total lateral force produced by a pair of tyres on a common axle.

Whilst the tilting action of the CLEVER Vehicle cabin mass considerably reduces the load transfer across the rear axle at steady state, under transient conditions the tilt angle error and the moment produced by the DTC actuators can combine to produce very large load transfers. These load transfers have the potential to cause un-predictable yaw responses as the total lateral force produced by the rear axle varies. It is therefore in the interests of improved yaw stability to develop a tilt control system that minimises the load transfer by reduction of both the tilt angle error and the DTC moment.

3.6. Concluding Remarks

This chapter has introduced the unique dynamic properties of narrow tilting vehicles, many of which are incorporated into the CLEVER Vehicle simulation model presented in Chapter 5.

In this chapter a simple linear tyre model has been introduced for the calculation of lateral forces resulting from both slip and camber angles, the generation of longitudinal forces and their influence on the lateral force generation have been examined. A non-linear tyre model using Pacejka's 'Magic Formulas' will be introduced in Chapter 5.

The kinematic effects of the tilting action on both the front and rear wheel steer angles have been demonstrated and the bicycle model has been introduced to enable study of the steady state handling characteristics. The CLEVER Vehicle configuration has been shown to lead to an oversteer handling characteristic; a tilt axis inclination, and the resulting rear wheel steering action, are used to produce the desired neutral response.

By considering the moments acting on the vehicle during steady state cornering, the 'moment reserve' has been calculated providing a measure of the maximum DTC moment that can be safely applied. The CLEVER Vehicle design should allow steady state cornering at lateral accelerations approaching 1g; however, in transient situations the tilt angle error will lower the available moment reserve considerably.

Finally, the influence of load transfer, resulting from both the lateral acceleration and the DTC system moment, on the vehicle handling characteristic has been discussed.

Chapter 4. Implementation of a Steering Direct Tilt Control System on a Prototype Narrow Tilting Vehicle

This chapter records the development and installation of a Steering Direct Tilt Control (SDTC) system on the prototype CLEVER Vehicle. The SDTC system supplements the pre-existing Direct Tilt Control (DTC) actuators with an active steering system; the active steering system is required to de-couple the driver's steer inputs from the front wheel steer angle and thus to facilitate automated control of the steer angle. As well as the active steering system's mechanical components, new controller hardware and software were also required.

4.1. Active Steering Actuation

4.1.1. Original Non-Active Steering System

When constructed in 2006, the prototype CLEVER Vehicle was equipped with an un-assisted mechanical steering system as shown in Figure 4.1. The system principally consists of a steering column connecting the driver's steering wheel to a reduction gearbox (the Steering Box), a lever arm (the Steering Arm) which converts the rotary gearbox output to a (near) linear motion, and a connecting rod (the Steering Rod) which conveys motion to the front wheel hub assembly. The hub assembly features 'hub-centre' steering whereby the hub assembly incorporates an internal steering axis. This provides for 30° of front wheel steer angle in each direction.

The relationship between the magnitude of the input at the driver's steering wheel and the magnitude of the corresponding front wheel steer angle is known as the steering ratio. As a result of geometric effects, the steering ratio of the CLEVER Vehicle is non-constant; a 3D CAD model of the steering system was used to produce the steering ratio curve, Figure 4.2. For the purposes of designing and controlling the active steering system, the steering ratio is assumed to remain constant at 12:1.

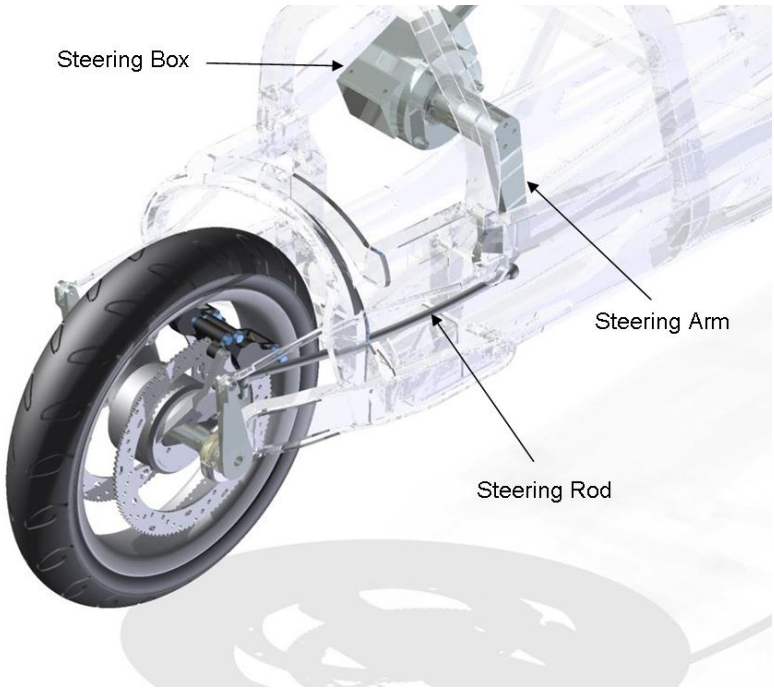

Figure 4.1: CLEVER Vehicle original non-active steering system.

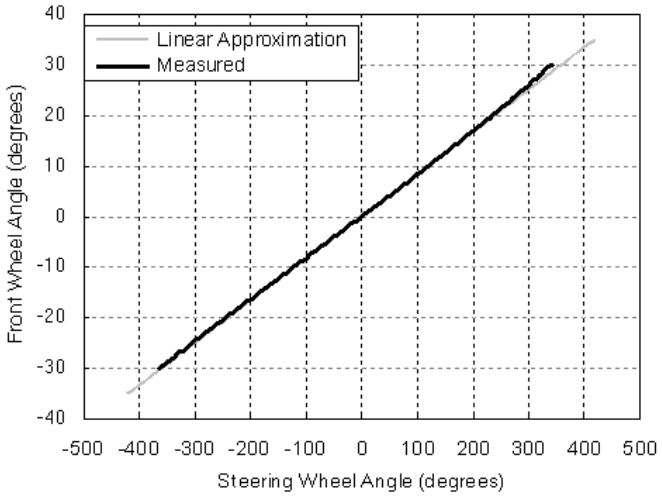

Figure 4.2: CLEVER Vehicle steering ratio.

4.1.2. Active Steering Mechanical Implementation

In order to facilitate the use of a SDTC strategy, a hydraulic 'in-series' active steering system was developed for the prototype CLEVER Vehicle, Figure 4.3. The term 'in-series' is used in this context to describe an active steering system that, rather than sever the driver's mechanical connection to the front wheel completely, contains a means of modifying that connection to influence the front wheel angle. This type of system has the advantage that, when the active steering system is idle, normal steering feel is retained and no artificial steering feedback need be created.

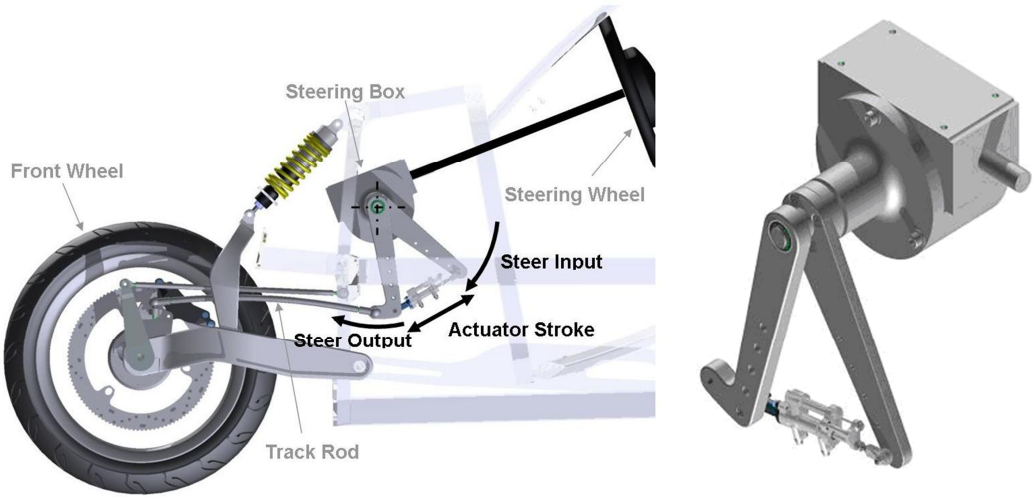

Figure 4.3: CLEVER Vehicle active steering installation.

Note that UN Regulation R79 Revision 2 [46] stipulates that any active steering system used on the road must maintain a number of performance criteria in a failure condition. However, no attempt was made to comply with these requirements when designing the active steering system for the CLEVER Vehicle on the basis that it is a research prototype and shall not be used on the public highway.

Active Steering Actuator Selection

Using the 3D CAD model of the CLEVER Vehicle, it was ascertained that in order to achieve a full ±30º active steering angle, the stroke of the steering actuator must be 130.7mm or greater. Packaging such an actuator in-series on the existing CLEVER Vehicle was not a practical proposition and a more compact actuator was sought. Fortunately, a small Moog EX085X134 actuator with integrated LVDT was available for immediate use; the specifications of the actuator are given in Table 4.1:

Table 4.1: Actuator specifications.

Parameter	Value	Unit
Stroke	25.4	(mm)
Bore Diameter	11	(mm)
Rod Diameter	6	(mm)
Piston / Annulus Area	67 / 67	(mm^2)
Rated Pressure	210	(Bar)

The actuator's stroke length of just 25.4mm limits the active steering angle (δ_{as}) to ±5.8° (this is then restricted further in software to ±5.6° to prevent top/bottom out). Whilst the limited active steer angle may initially appear insufficient to facilitate SDTC of the

CLEVER Vehicle, it should be remembered that instability afflicts the CLEVER Vehicle at higher speeds where the steer angle required to generate a given lateral acceleration is small. Furthermore, the in-series active steering system was designed with a variety of actuator mounting positions at varying radii from the steering box output shaft; this facilitates an increase in the maximum active steering angle at the expense of mechanical advantage.

As well as the limited stroke length, the chosen actuator's small area limits the maximum force it can produce. In order to access whether it is sufficient, the actuator force was compared to the estimated force requirement.

Whilst an estimate of the actuator force requirement may in principal be obtained from simulation, the CLEVER Vehicle simulation model does not include computation of the necessary tyre self-centring forces. An alternative method is to assume that the driver is capable of exerting sufficient torque at the steering wheel to control the vehicle under all circumstances. The force a driver can induce in the steering rod is then approximated using Equation (4.1):

$$F = \frac{T_d \times R_{sb}}{r_{sa}} \tag{4.1}$$

Where R_{sb} is the ratio of the steering box and has a value of 21.8:1 and r_{sa} is the length of the steering arm (230mm).

Whilst a driver of average mass (75kg) can exert a peak steering torque of around 60Nm on a 254mm steering wheel [54], typical steering weights for road vehicles are in the range of 4-8Nm [54]. Whilst the steering on the CLEVER Vehicle is notably light (thanks in part to the low weight and narrow front tyre), so probably closer to the 4Nm value, using the higher 8Nm value results in a force in the steering rod of:

$$F = \frac{8 \times 21.8}{0.23} = 758N \tag{4.2}$$

Since the active steering actuator is mounted at the same radius from the steering box as the steering rod, it should be able to produce a force in excess of 758N in order to control the front wheel steer angle.

An approximate estimate of the actuator stall force can be determined as follows:

$$F = A_p \times P_s \tag{4.3}$$

Where P_s is the system supply pressure of 160bar; combined with the piston area of 67mm^2, this gives an initial stall force estimate of 1072N, this is in excess of the requirement.

4.1.3. Active Steering Valve Selection

In a situation where a driver initiates an emergency avoidance manoeuvre, the active steering actuator must be able to achieve velocities sufficient to both cancel out the driver's input and provide a counter steering action. In common with other hydraulic systems, the velocity at which the active steering actuator can extend or retract is a function of the flow rate through the valve and actuator piston and annulus areas. An appropriate valve must be selected to provide the necessary flow rate.

An estimate of the minimum active steering actuator velocity (U_p) necessary to cancel out the driver's steer inputs is provided by:

$$U_p = \frac{\omega_d}{R_{sb}} \times r_{sa} \tag{4.4}$$

Where ω_d is the driver's steer demand rate, R_{sb} is the reduction ratio in the steering box and r_{sa} is the radius of the steering arm.

Work by Berote [35] has shown that the maximum steer demand rate possible from a human driver of the CLEVER Vehicle is ω_d=6.98rad/s (or 400°/s). Given values of R_{sb}=21.8:1 and r_{sa}=230mm, the minimum actuator velocity to cancel out a driver's steer inputs must be U_p=74mm/s.

The flow rate required is given by:

$$Q = U_p \times A_p \tag{4.5}$$

Where A_p=67mm^2, the flow rate (Q) is 4960mm^3/s or 0.30l/min.

A second estimate of the actuator velocity was obtained from simulations of an emergency lane change manoeuvre performed at a speed of 10m/s, Figure 4.4. The maximum active steering rate (ω_{as}) during the manoeuvre was 11°/s; given that a front wheel steer angle range of 60° requires a 130.7mm actuator stroke, 11°/s corresponds to an actuator speed of 24mm/s. Note that, whilst harsh, this manoeuvre does not necessarily constitute the worse case scenario.

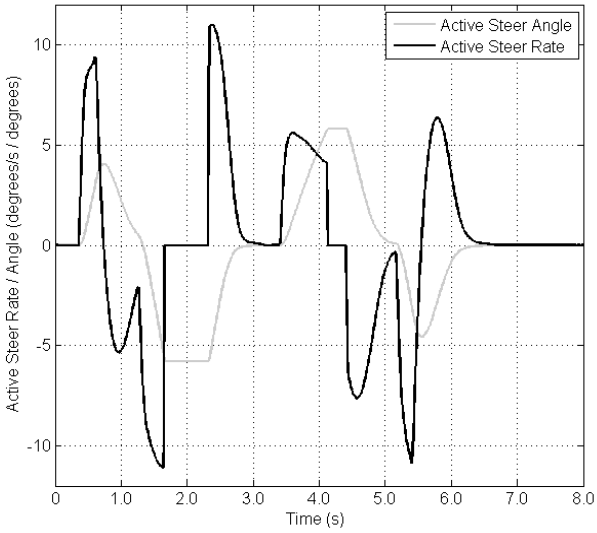

Figure 4.4: Simulated active steer rate and angle.

Using Equation (4.5), an actuator velocity of 24mm/s gives a flow rate requirement of Q=1605mm^3/s or 0.096l/min.

To facilitate fine control of the actuator position, the valve should not be too large; a Bendix servovalve with a quoted flow rate of 0.8l/min (at ΔP_v=70bar) was sourced. Whilst the specified flow rate of the selected valve is larger than the active steering flow requirement, a 70bar pressure drop would lead to an un-acceptable reduction in the actuator force output. Using a larger valve size considerably reduces the pressure losses.

4.1.4. Actuator Force Including Pressure Drop

The pressure loss across a valve (ΔP_v) can be calculated using the valve orifice equation:

$$\Delta P_v = P_r \left(\frac{Q_p}{Q_r} \right)^2 + P_r \left(\frac{Q_a}{Q_r} \right)^2 \tag{4.6}$$

Where P_r is the rated pressure drop across each side of the valve, Q_p the flow rate to/from the piston side of the actuator, Q_a the flow rate to/from the annulus side of the actuator and Q_r the rated flow rate of the valve.

Using the higher actuator velocity estimate of 74mm/s and the corresponding flow rate demand of 0.297l/min calculated above, the pressure drop (ΔP_v) across both sides of the valve combined is 9.65bar:

$$\Delta P_v = 35\left(\frac{0.297}{0.8}\right)^2 + 35\left(\frac{0.297}{0.8}\right)^2 = 9.65bar \tag{4.7}$$

Taking into account the pressure losses across both sides of the valve, the actuator force is given by:

$$F = A_p \times (P_s - \Delta P_v) \tag{4.8}$$

$$F = 67 \times (160 - 9.65) \times 10^5 \times 10^{-6} = 1007N \tag{4.9}$$

The maximum actuator force at an extension speed of 74mm/s is found to be 1007N; this is higher than the estimated 758N requirement.

In practise, when conducting tests of the prototype CLEVER Vehicle, negligible deviation of the active steering from the demand position has been recorded. Since position control is maintained, the actuator force output is considered sufficient.

4.2. Controller Hardware Implementation

4.2.1. Previous DTC Controller Hardware

When the CLEVER Vehicle was originally developed in 2006 it was fitted with a 'TD40' 40MHz 16-bit AMD 186 controller manufactured by TERN Technologies. The controller was programmed in C-code and fitted with a keyboard and LCD display for user interface. A separate signal conditioning unit was used to convert the voltage ranges of the 6 analog inputs (Tilt Angle, Vehicle Speed, Steer Angle, Lateral Acceleration, Yaw Rate and Hydraulic System Pressure) to 0 to 5V before sampling, and the 2 analog output signals (Tilt Valve Demand and Hydraulic System Un-loading Valve) from the 0 to 4.095V produced by the TD40 to -10 to +10V and 0 to +10V respectively. The signal

conditioning unit also applied a hardware low pass filters with a 15Hz cut off frequency to all analog input channels and supplied a regulated voltage output to the various sensors.

The TD40 controller was very limited in its processing power; this placed many constrictions on the complexity of the software that could be developed for the CLEVER Vehicle [10]. Additionally, the limited number of input channels and lack of on-board data recording capability meant that separate data-loggers were required to store information. Programming the controller in C-code required special skills and was time consuming; as a result, alterations to the controller were difficult to perform. Finally, through several years of use, the LCD screen attached to the controller had been damaged and no-longer functioned.

4.2.2. New SDTC Controller Hardware

In order to facilitate the fitment of the active steering system, a new controller was required. As well as improved processing power, other requirements included a larger number of input and output channels, easy programming and a data storage capability.

Selection of the appropriate hardware was driven by the decision to use 'xPC Target Embedded Option' to create the software for the controller. xPC Target Embedded Option is an additional toolbox for MATLAB which allows controller code to be generated in an automated fashion from Simulink models. In order to execute the code generated by xPC Target Embedded, a controller with 'PC like' architecture and an available PCI slot was required. A mobile 'In-Car PC' with 2.2GHz Intel Core 2 Duo CPU, removable solid state Compact Flash hard drive and 12V power input was selected for its relative cost effectiveness, semi-rugged construction and high processing power, Figure 4.5. Control software can be loaded onto the Compact Flash card from a PC with a MATLAB xPC installation. Equally data logged to the Compact Flash card can be read directly into MATLAB. A National Instruments PCI-6229 input/output card with 4 analog outputs (±10V), 16 differential analog inputs and 48 bi-directional digital channels occupies the controller's PCI slot.

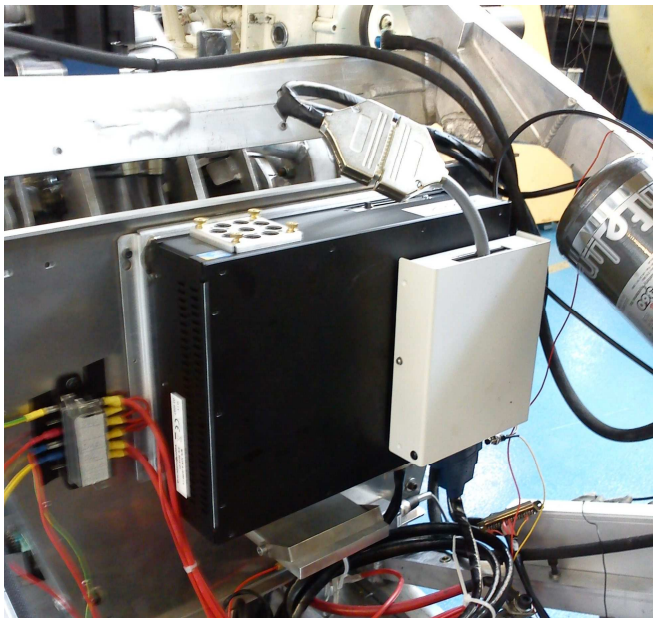

Figure 4.5: xPC Embedded controller installation on CLEVER prototype.

Reflecting its higher performance, the new controller's larger physical size meant it could not be mounted on the dashboard area as per the previous TD40. Instead CLEVER's rear seat was removed and replaced with a 3mm thick laser cut aluminium controller mounting plate. The altered position of the controller necessitated re-wiring of the complete vehicle instrumentation and control system. The loss of the original controller's LCD display also necessitated the development of a new dashboard interface with a series of LED indicators and mode control switches. Whilst re-wiring, the opportunity was taken to route all sensor signals previously recorded by the separate data loggers into the controller for storage on its 2GB Compact Flash hard drive. The DL1 data logger previously installed on the CLEVER Vehicle prototype was retained in order to provide a GPS signal and a lateral acceleration signal from its integrated accelerometer. A fuse box was added to protect the instrumentation and controller from short-circuits and a new 9V voltage regulator installed to supply the instrumentation with a constant voltage regardless of battery charge level.

4.2.3. Vehicle Instrumentation

The CLEVER Vehicle is fitted with numerous sensors, those listed below in **bold** are used in the control system, whilst the remaining sensors are logged for post-test analysis:

- **Vehicle speed** – optical sensor on serrated front wheel brake disc, frequency to voltage converter.
- **Drivers steer demand** – contactless linear position sensor with integrated electronics.
- **Tilt angle** – contactless linear position sensor with integrated electronics.

- **Active steering actuator position** – Linear Variable Differential Transformer (LVDT), signal conditioner card.
- Left and right rear suspension positions – linear position sensors.
- Hydraulic system pressure – pressure transducer.

Upon fitment of the SDTC system, many of the pre-existing sensors on the CLEVER Vehicle prototype had to be replaced. Due to the un-clean operating environment, and constant excitation around a single point, 'dead spots' had been worn into no less than three linear voltage dividers used to measure both suspension and tilt position. When used to sense the tilt position, the dead spots cause the output voltage to drop dramatically thus giving false information to the controller and causing a sudden tilting motion. To overcome this difficulty, a contactless tilt position sensor with integrated electronics (model number PLS0956-SV-200-R5) was sourced from Active Sensors, Christchurch, UK. A similar sensor of shorter stroke (PLS0956-SV-100-R5) was sourced to replace the worn steer position sensor.

Due to budgetary constraints, the worn linear voltage dividers were retained for use on the rear suspension. Re-mounting the sensors in a different position moved the dead-spots out of the normal operating range and resulted in acceptable signals.

Sensor Calibration

All of the above listed sensors required calibration before operation of the CLEVER Vehicle. Whilst some of the sensors were calibrated in the controller software simply by adding or subtracting an off-set from the analog voltage input, and then multiplying by an appropriate gain, some were found to exhibit non-linear behaviour and required the use of more complex calibration methods.

Calibration of the optical speed sensor was performed by comparing its output to the DL1 data logger's GPS speed signal. Figure 4.6 shows the speed signal from the optical sensor plotted with the GPS data. The GPS data is subject to some noise created by the differentiation of the (inevitably imperfect) position data. Equally, at $t \approx 52s$ the front wheel of the CLEVER Vehicle partially locked under braking causing a sudden drop in the recorded speed.

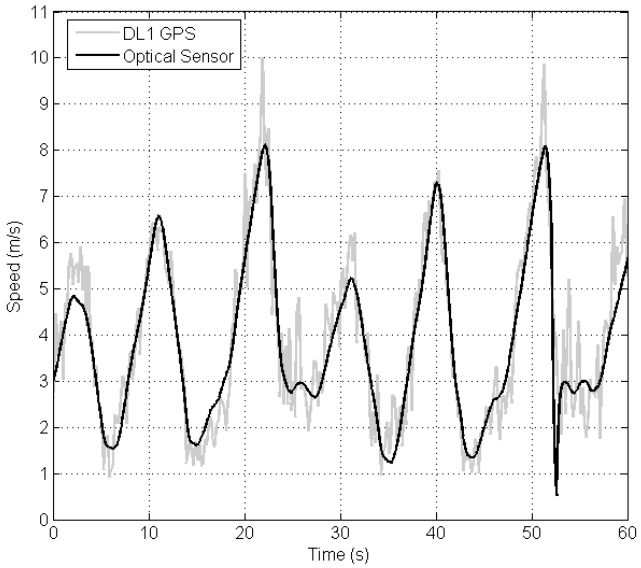

Figure 4.6: Optical speed sensor and DL1 GPS speed signals.

The sensor used to measure the cabin tilt angle was initially calibrated with a single linear gain for both left and right titling, as had been the case on the previous controller installation. However, it was noted that with this calibration the cabin appeared to tilt further in one direction than the other. Thanks to the kinematics of its installation, the tilt angle sensor extension has a non-linear relationship to the cabin tilt angle. Previous works [35] [51] had noted asymmetric tilting performance, perhaps caused by the same incorrect tilt sensor calibration.

Whilst calibration of the tilt angle sensor could have been performed by moving the cabin through its entire tilt range in small increments, and logging the sensor voltage output, the practical difficulties associated with gathering accurate tilt angle measurements meant an alternative approach was sought. Instead, the tilt sensor output was logged with the cabin at three tilt angles (-45°, 0º & 45º) and two separate linear sensor gains derived, Figure 4.7. Once calibrated, the cabin was moved through 5° increments using the manual mode in the controller program and a digital inclinometer used to check the true tilt angle. A close correlation was noted.

The output from the active steering LVDT was found to be non-linear. By measuring the actuator extension with digital callipers, and logging the LVDT output voltage, Figure 4.8 was produced. By fitting a polynomial to the data, Equation (4.10), and replicating it in the controller software, the sensor was calibrated to account for the non-linearity.

$$y = 0.00009x^5 - 0.0003x^4 - 0.007x^3 + 0.02x^2 + 1.0069x + 13.561 \quad (4.10)$$

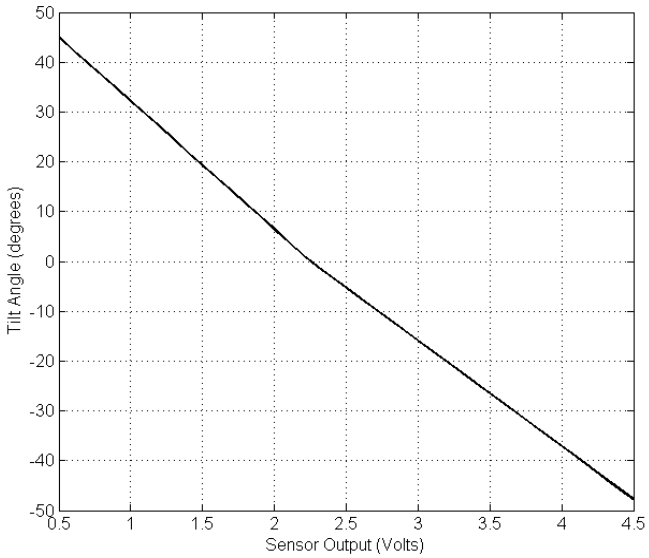

Figure 4.7: Two-stage tilt sensor calibration.

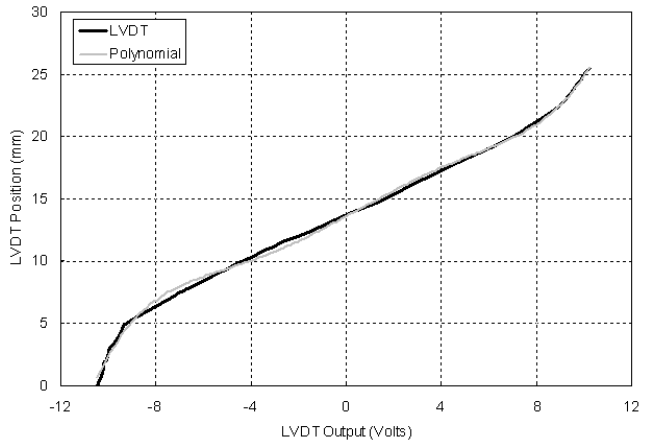

Figure 4.8: Active steering LVDT calibration polynomial.

4.3. Controller Software

4.3.1. Control Strategy

In [36] Berote *et al.* propose a SDTC strategy in which both DTC and STC systems work simultaneously to achieve a common tilt angle demand throughout the entire speed range of the CLEVER Vehicle. The proposed controller used the driver's steer demand and the vehicle's speed to estimate the lateral acceleration, and hence the tilt angle required to stabilise the vehicle. A variable active steering gain changed the magnitude of the steer angle alterations in response to the vehicle's forward speed, with smaller alterations being generated at higher speeds. It is this strategy that forms the basis for the SDTC system implemented in this thesis, Figure 4.9.

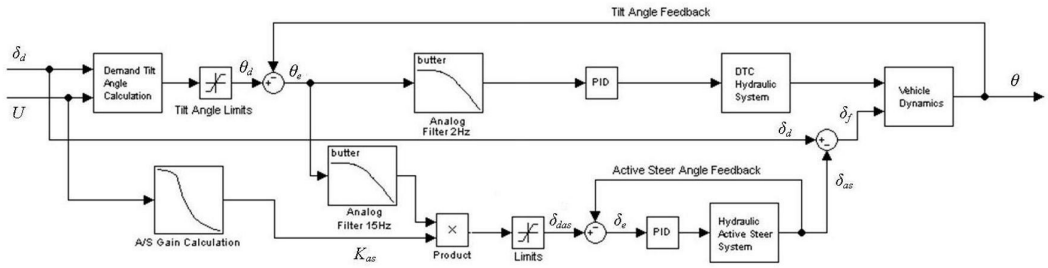

Figure 4.9: SDTC system block diagram.

The demand tilt angle (θ_d) is calculated as follows:

Using small angle approximations, assuming no tyre slip and ignoring both front wheel camber angle and rear wheel steering angle (δ_r), the cornering radius (R) is given by:

$$R = \frac{L}{\delta_d} \tag{4.11}$$

Where L is the vehicle wheelbase and δ_d is the driver's demand steer angle.

The lateral acceleration ($\ddot{y}$) is obtained from the cornering radius (R) and the vehicle's forward speed (U):

$$\ddot{y} = \frac{U^2}{R} \tag{4.12}$$

Using small angle approximations, the tilt angle (θ_d) required for balanced cornering is given by:

$$\theta_d = \frac{\ddot{y}}{g} \tag{4.13}$$

An additional empirically derived 'over-lean' factor of 1.2 is then applied to the equilibrium angle to compensate for the reduced effective tilt angle (arising from the rear module roll angle and the tilting kinematics) and the mass of the non-tilting rear module [51]. Note that the maximum magnitude of the over-lean factor is limited, too high and the driver may perceive a lateral acceleration away from the corner centre.

$$\theta_d = 1.2 \times \left(\frac{\ddot{y}}{g} \right) = 1.2 \times \left(\frac{U^2}{gL} \delta_d \right) \tag{4.14}$$

The current tilt angle (θ) is subtracted from the demand tilt angle to generate an error signal (θ_e):

$$\theta_e = (\theta_d - \theta) \tag{4.15}$$

The tilt angle error (θ_e) is then used in the closed loop negative feedback Direct Tilt Control (DTC) system.

Simultaneously, the active steering controller generates an active steer demand angle (δ_{das}) that is a function of the tilt angle error (θ_e) multiplied by a non-linear speed dependent active steering gain (K_{as}). The active steer demand angle is used in a second negative feedback position control loop with a Linear Variable Differential Transformer (LVDT) mounted on the active steering actuator used to provide position feedback. The resulting active steer angle (δ_{as}) is mechanically subtracted from the driver's steer demand (δ_d) to generate a new front wheel steer angle (δ_f).

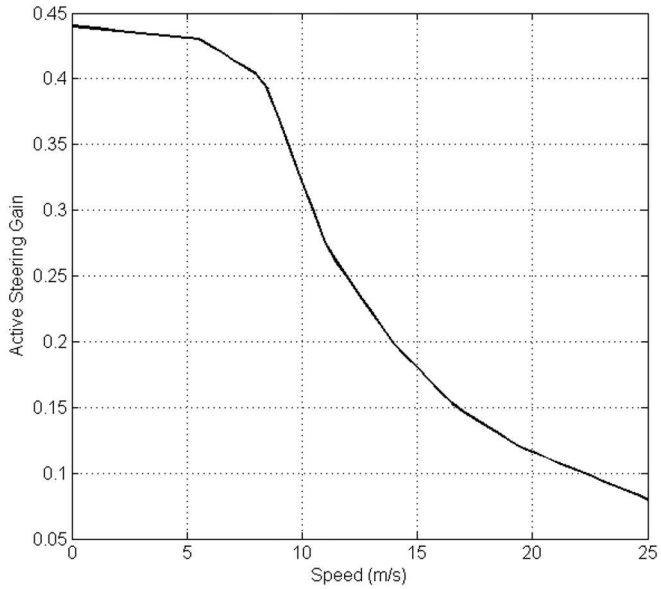

Figure 4.10: Active steering gain (K_{as}) curve, as used in the SDTC controller [35].

Values for the active steering gain (K_{as}) were obtained by Berote in [35], Figure 4.10. Berote used simulations of the CLEVER Vehicle's response to a ramp steer input to determine the gain value which resulted in the response/demand lateral acceleration amplitude ratio closest to 1 (or 0dB) over a range of frequencies and at a variety of speeds.

4.3.2. Controller Software Implementation

Having made the decision to use 'xPC Target Embedded Option' to generate the controller code from Simulink models, a Simulink model of the control system was required. Whilst the core of the tilt control model is quite simple, this accounts for only a fraction of the complete controller with additional features such as input signal calibration and filtering, data logging, emergency stop modes, tilt control mode selection, LED display drivers, and switch inputs with de-bounce filtering all adding considerable complexity. The high processing power of the controller hardware means that despite the complexity, the software can run at 1000Hz with ample capacity to spare.

The controller model consists of 4 main sub-systems:

1. Instrumentation – Responsible for converting analog sensor inputs from a voltage reading into SI units for distribution to other subsystems, principally the tilt controller. It also accepts digital inputs, applies de-bounce filters and uses them to trigger mode selection logic circuits.
2. Tilt Controller – Uses information from the instrumentation subsystem to calculate the demand tilt and active steer angles. It also uses the current tilt and active steer angle data to calculate error signals and applies PID control. The tilt controller has 4 different user selectable operating modes which are covered in more detail in Sub-section 4.3.3.
3. Dashboard Driver – Uses information from the Instrumentation subsystem to determine which of the 12 dashboard indicator LEDs should be illuminated. Applies pulse width modulation to reduce the effective output voltage to a level compatible with the LED lamps and to vary the intensity of illumination.
4. Outputs – Gathers analog and digital output signals from the Tilt Controller and Dashboard Driver subsystems, applies various safety limits and outputs to National Instruments I/O card.

4.3.3. Controller Modes

The tilt controller sub-system contains 4 further sub-systems each calculating output signals to the tilt and active steering valves for a different mode of operation. A 4 position switch is then used to pass the output of one of the modes depending on the user's choice. Whilst computing all 4 modes in parallel uses more processing power than necessary, the high performance of the controller CPU and the simplicity of the calculations render the effect insignificant.

The 4 modes are briefly described as:

1. Stationary – Both the tilt and active steer valve outputs are set to 0V.
2. Manual Mode – Uses manual tilt angle inputs from dashboard mounted switches and the current tilt angle to generate an error signal (θ_e). Applies PID control to determine the voltage output to the tilt valve. The active steering demand angle (δ_{asd}) is set to 0º and PID control used to control the steer valve accordingly.
3. Direct Tilt Control – As per Manual Mode except that steer and speed inputs are used to calculate the demand tilt angle (θ_d).
4. Steering Direct Tilt Control – As DTC except the active steering demand angle (δ_{asd}) is calculated from the tilt angle error and vehicle speed.

4.3.4. Data Logging

Data logging is performed by 5 'Filescope' blocks within the controller software. Each of these blocks records multiple signals to the controller's Compact Flash memory in '.dat' format; to reduce the volume of data recorded to manageable levels, each Filescope is set to record data only every tenth time step. The resulting 100Hz data is still of sufficiently high resolution for the purposes of analysing the CLEVER Vehicle's dynamics and for trouble shooting.

The 5 file scopes are named and organised as follows:

1. ain – Located within the instrumentation sub-system, this filescope records raw data from all the analog input channels.
2. din – Located within the instrumentation sub-system, records raw data from all digital input channels.
3. ins – Again located within the instrumentation sub-system, this filescope records processed analog and digital data as distributed to other areas of the controller.
4. cnt – Located within Tilt Control sub-system, records the calculated equilibrium angle, the resulting tilt demand angle and the tilt angle error. The active steering demand angle and active steering error are also logged.
5. val – Located within the Outputs sub-system, this block records the output signals to the tilt and active steer valves both before and after the application of safety limits.

4.3.5. Signal Filtering

The original TD40 controller installed on the CLEVER Vehicle in 2006 used a signal conditioner, with 15Hz low pass filters implemented in hardware, on the analog signal

inputs for anti-aliasing purposes. In addition, the tilt controller used a software implemented low pass filter on the tilt angle error signal, [10]; this filter served two purposes. Firstly, it removed un-wanted high frequency tilting motions which occurred in response to signal noise. Secondly, the filter acted to limit the speed of the tilting response to the benefit of both passenger comfort and vehicle stability (through reduced DTC actuator torque). In [10], Drew noted that the cut-off frequency of the tilt angle error filter represented a compromise between responsiveness and vehicle stability. He performed a sensitivity analysis, using cut-off frequencies from 1Hz to 6Hz, in order to determine a suitable compromise cut-off frequency. A value of 2Hz was chosen, higher cut-off frequencies allowed the DTC system to generate large moments which could de-stabilise the vehicle, whilst frequencies lower than 2Hz caused the vehicle to feel un-responsive.

The revised xPC controller dispenses with the pre-sampling 15Hz hardware filters in favour of a higher sampling rate of 1000Hz (up from 150Hz) and software filtering. Given that the roll dynamics of the CLEVER Vehicle have been shown to occur at less than 3Hz [10], the sampling rate of 1000Hz represents a far larger degree of oversampling than is necessary to prevent significant aliasing. As per Drew, a 2Hz software filter is implemented on the tilt angle error feed to the DTC actuators; the tilt angle error signal fed to the active steering system is subject to a filter with a higher cut-off frequency of 15Hz reflecting the faster response required. Frequencies above 15Hz were found to result in too much oscillation of the front wheel in response to noise and road inputs.

4.3.6. Safety Systems

The controller software incorporates a number of safety features aimed at preventing harm to the driver or other people in close proximity to the CLEVER Vehicle.

A prominent emergency stop button is located within easy reach of the driver. As well as physically grounding the signal to the tilt valve, it overrides the output in software to both the active steer and tilt valves setting them to 0V regardless of operating mode. Triggering the emergency stop button results in all 12 LEDs on the dash display illuminating with maximum intensity, if accidently triggered at speed the driver is warned and can take appropriate action to bring the vehicle to a safe stop.

To prevent fast tilting movements when the vehicle is stationary, and possibly in close proximity to people, a low speed safety system limits the maximum active steer and tilt valve openings at vehicles speeds below 2m/s. Furthermore, a second higher maximum

valve opening limit of 44% (including dead band compensation) is applied in all modes and at all speeds. The valve opening limit is carried over from the original CLEVER Vehicle software un-modified. Its value originates from a peak flow analysis conducted by Drew [10] which found that a flow of 101l/min was required to perform a -45° to +45° tilt at 0.33Hz. This is considered to represent the worst-case tilt requirement.

It is not possible to switch between the 4 operating modes at speeds greater than 2m/s to prevent the potentially dangerous situation where the vehicle returns upright whilst cornering at speed. Note that it is possible to select stationary or manual modes at speeds below 2m/s and then accelerate to higher speeds; this facilitates comparison of the vehicle's dynamics with and without tilting.

In order to prevent a sudden tilting motion to +45º occurring in response to a disconnected or severed tilt sensor cable, a minimum value of 0.2V is accepted from the tilt sensor (nominal operating range +0.5V to +4.5V). Should the signal from the tilt sensor fall below 0.2V the emergency stop mode is triggered.

De-bounce filters are used on the dash button digital inputs to prevent accidental rapid changes in tilt demand whilst in manual mode and accidental skipping of several modes when using the mode select button.

Drivers of the CLEVER Vehicle have noted a lack of roll stability feedback at the extremes; the result is that the vehicle can capsize unexpectedly denying the driver an opportunity to take corrective action. To provide some form of feedback, the tilt angle indicator LEDs flash in an increasingly urgent fashion as the rear suspension reaches full extension; however, it has been noted by drivers that in such situations their attention is focused elsewhere.

4.4. System Response Characteristics

4.4.1. DTC System Response

Given that the DTC control loop within the new xPC tilt controller is in effect identical to that implemented by Drew and Barker, using the same PID gains should result in the same step response characteristics. However, the scaling of signal inputs to integer values between 0 and 4095 required by the old TD40 controller, the subsequent amplification (by an un-known factor) of the valve control output signal in a separate signal conditioner, and the in-ability to interrogate the now broken TD40 make obtaining the gain values used difficult.

An alternative approach of empirically tuning the gains in the new tilt controller to achieve a satisfactory response was pursued. In [10] Drew states that the tilt control system has a step response time constant (the time taken for the response to reach 63.2% of the demand) of $\tau \approx 0.15$s, this figure was used as a target when tuning the gains in the new controller.

The step response of the DTC system was tested by creating a bespoke software program for the tilt controller which generated an un-filtered step in the tilt demand signal from -5º to +5º. The tests were performed with the vehicle stationary on a level laboratory floor, a 75kg driver and the wheels free to rotate (in order to facilitate the rear wheel steer function which is coupled to the tilt action). P, I & D gains of 1.7, 0 & 0.1 (when acting upon a tilt angle error in radians and producing a valve control signal of ±10V) were found to produce a time constant of $\tau \approx 0.165$ which was deemed acceptable, Figure 4.11.

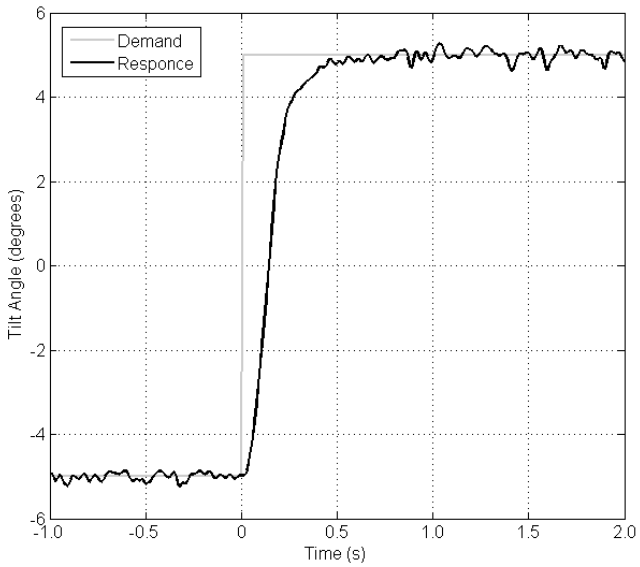

Figure 4.11: DTC -5º to +5º system step response.

Some time after the above mentioned gain values of the DTC system were determined, a series of further step response tests were performed at a range of step sizes from ±1º to ±7°. These later tests showed that τ in fact varied between 0.16 and 0.21 depending on step size. A variable τ is characteristic of a non-linear system (which the CLEVER Vehicle DTC system is known to be). Despite this finding, the system gains were maintained at 1.7, 0 & 0.1 during all subsequent experiments and simulations (except where stated in Chapter 7) on the basis that in reality the response is influenced to a greater extent by the speed of the driver's steer inputs and the filtering of the tilt angle error. In addition, no direct comparison was to be drawn between the CLEVER Vehicle's performance with new and old controllers, rather the new controller would enable comparison of DTC and SDTC modes by switching between them.

4.4.2. Active Steering System Response

To ensure that the active steering system hardware was able to achieve the required dynamic response, a sine sweep test was performed. The test was performed under closed loop control (with all software filtering removed and a simple proportional gain of 100) as attempts to perform the test in open loop quickly result in the actuator drifting into its end stops. It is not safe nor practical to conduct the sine sweep with the vehicle travelling forwards at a representative speed, therefore two tests were conducted; the first with the front wheel of the CLEVER Vehicle lifted clear of the ground (Figure 4.12) and the second with the wheel on the ground whilst stationary (Figure 4.13). The true system performance in use is expected to lie somewhere in between these two extremes. In both cases, the steering input arm (see Figure 4.3) was fixed in place to prevent movement.

In the worst case scenario, with the front wheel on the ground and the vehicle stationary, the amplitude reaches the -3dB point at approximately 28.9rad/s or 4.6Hz. This is considered sufficiently higher than the human driver's bandwidth so as not to hinder the system performance. Equally, the phase lag is small up to 3Hz (18.8rad/s), indicating good performance in the anticipated operating range.

Figure 4.14 shows the active steering system demand signal (δ_{das}) generated when a human driver applied a ramp steer input as quickly as possible whilst driving the CLEVER Vehicle at 10m/s. Also shown is the demand signal before application of the 15Hz filter and actuator stroke limits of ±5.6° (see Figure 4.9); finally the hydraulic active steering system's measured response is plotted. The 15Hz filter and the response characteristics of the hydraulic system contribute to a lag of approximately 0.025s. In the context of other lags associated with the vehicle's dynamics and tyre characteristics (such as the tyre relaxation length), this is not considered likely to have a significant detrimental impact on the SDTC system's performance.

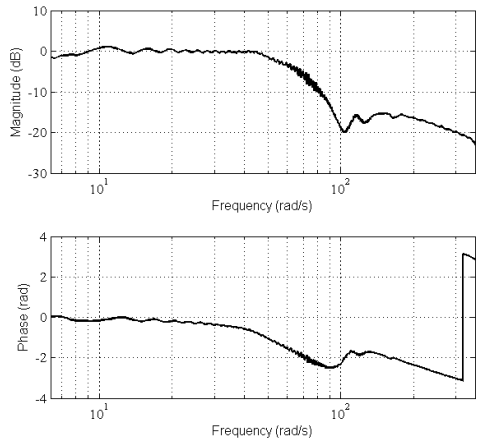

Figure 4.12: Active steering system Bode plot, front wheel off ground.

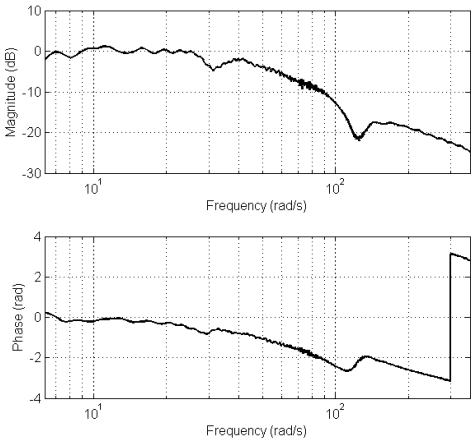

Figure 4.13: Active steering system Bode plot, front wheel on ground.

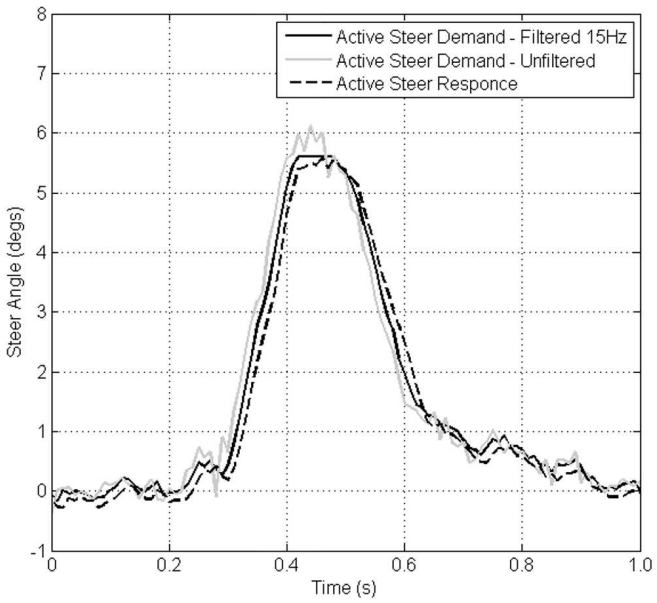

Figure 4.14: Active steering system demand (filtered & un-filtered) and measured response.

4.5. Concluding Remarks

This chapter has introduced the active steering hardware installed upon the CLEVER Vehicle prototype in order to facilitate the testing of a Steering Direct Tilt Control system. The active steering system uses a miniature hydraulic actuator and is installed 'in-series' to allow the control system to make small alterations to the driver's intended front wheel steer angle.

The active steering hardware is capable of modifying the front wheel steer angle by only ±5.8º (which is reduced further to ±5.6° in software). Whilst this angle represents only a fraction of the ±30º maximum front wheel steer angle of the CLEVER Vehicle, it is anticipated that it will be sufficient to facilitate testing of the SDTC system even if some saturation does occur under severe conditions.

Fitment of the new active steering hardware has necessitated the installation of a new controller with greater processing power and a larger number of analog inputs and outputs. The new control hardware is descried as well as installation and calibration of the necessary sensors. The SDTC system logic has been introduced along with a description of its implementation in software, the associated data logging and signal filtering strategy.

Finally, the DTC system step response has been matched to that of the previous CLEVER Vehicle controller and the active steering system shown to provide good performance in the required operating frequency range.

Chapter 5. Modelling of a Narrow Tilting Vehicle

The research presented within this thesis builds upon earlier work conducted at the University of Bath. As a result a simulation model of the CLEVER Vehicle was pre-existing. This chapter aims to introduce the simulation model, describe how it represents the vehicle dynamics and to introduce refinements made to the simulation model by the author. The simulation model output will also be extensively validated by comparing its output to data logged during testing of the prototype CLEVER Vehicle.

The simulation model will be used in later chapters to examine the roll stability of the CLEVER Vehicle. Validation of the simulation model is therefore concerned principally with frequencies below 3Hz at which the roll dynamics of the CLEVER Vehicle occur [35].

5.1. CLEVER Vehicle Simulation Model

A simulation model of the CLEVER Vehicle developed in MATLAB Simulink and SimMechanics was presented by Berote in [35]. Since the purpose of the simulation model is the study of the lateral dynamics behaviour of the CLEVER Vehicle, longitudinal dynamics resulting from aerodynamics drag, driving torque and braking are deliberately omitted.

The complete CLEVER Vehicle simulation model is a hybrid of multi-body and 1D techniques. The multi-body element is used to model the roll dynamics whilst lateral and yaw dynamics are modelled in a 1D sub-system. Additional sub-systems are used to model the hydraulic DTC system, tyre behaviour and control system logic.

5.1.1. Roll and Tilt Dynamics

The multi-body component (Figure 5.1) of the CLEVER Vehicle model is used to simulate the roll dynamics and the associated changes in load supported by each of the three wheels; it does not model the lateral and yaw dynamics (see section 5.1.2).

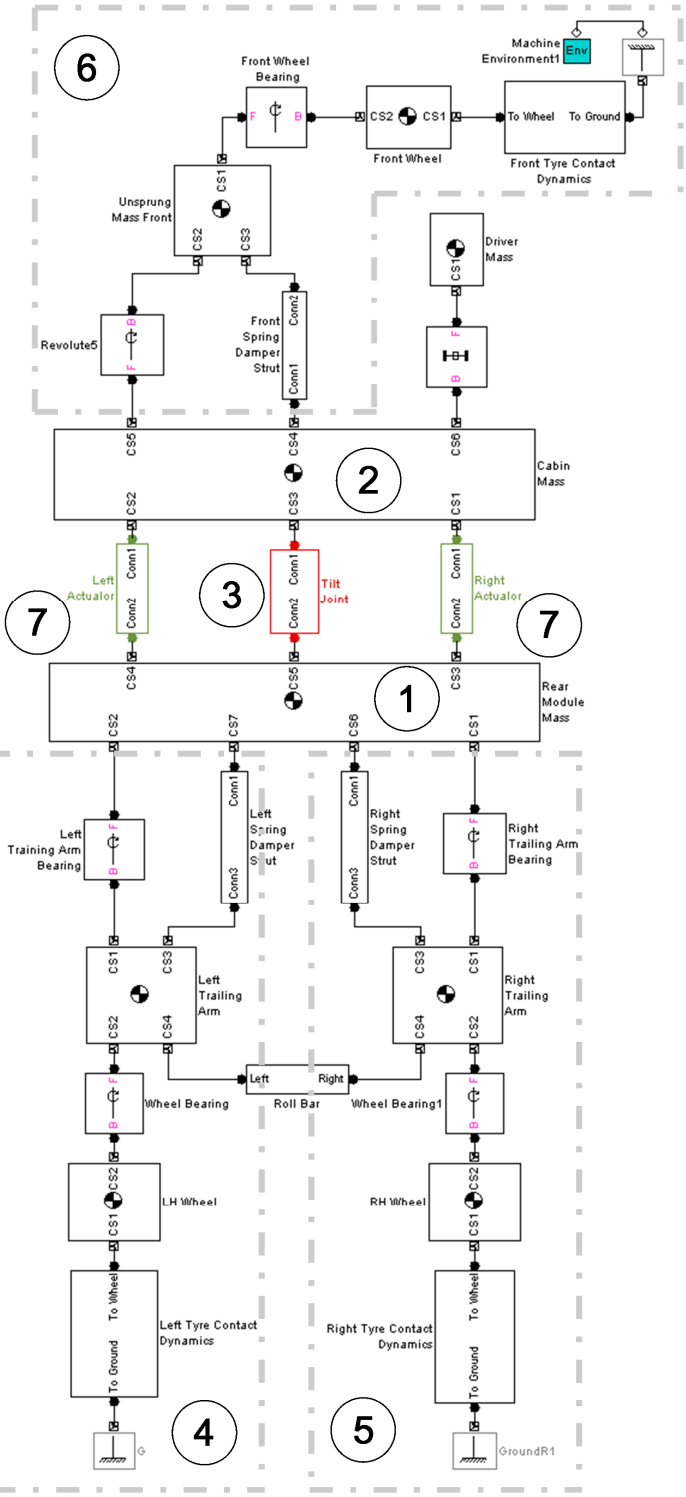

Figure 5.1: Multi-body simulation model of CLEVER Vehicle.

The multi-body representation of the rear module (1) is constrained in yaw as well as the X (longitudinal) direction, but has freedom in the Y (lateral) and Z (vertical) directions as well as the roll and pitch axes. The front cabin (2) is able to rotate about the tilt joint (3), this results in the lateral displacement of the front tyre contact patch and changes in the height of the tilt bearing (with associated pitch angle changes). The tilt joint sub-system incorporates a velocity dependent linear friction model. The rear trailing arms (4) & (5)

are attached to the rear module via revolute joints orientated in the Y axis and a pair of spring & damper struts; the spring & damper struts incorporate spring stiffness, pre-load, separate damping rates in compression and rebound, bump stops and stroke limits. An anti-roll bar links the two trailing arms.

The front suspension (6) pivots about a revolute joint linking it to the cabin, no steer axis is provided. The single acting hydraulic tilt actuators (7) generate a moment between the cabin and the rear module. Lateral tyre forces are applied to the multi-body model though the three tyre contact dynamics sub-system blocks (modelling of the tyre dynamics is discussed in Section 5.1.3). The tyre contact dynamics blocks also contain sensors to measure the vertical tyre loads which are needed in the lateral tyre force calculations.

5.1.2. Lateral and Yaw Dynamics

The lateral and yaw dynamics of the CLEVER Vehicle are modelled in a sub-system separate from the multi-body roll dynamics (Figure 5.2). The equations underpinning the lateral and yaw dynamics model are described in Equations (5.1) to (5.10).

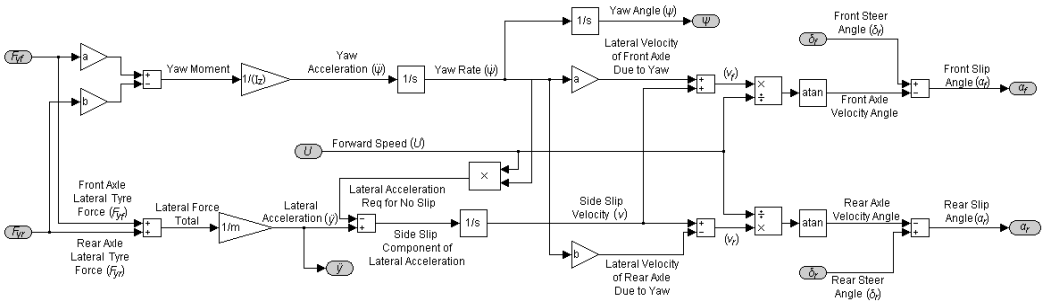

Figure 5.2: Lateral dynamics simulation model.

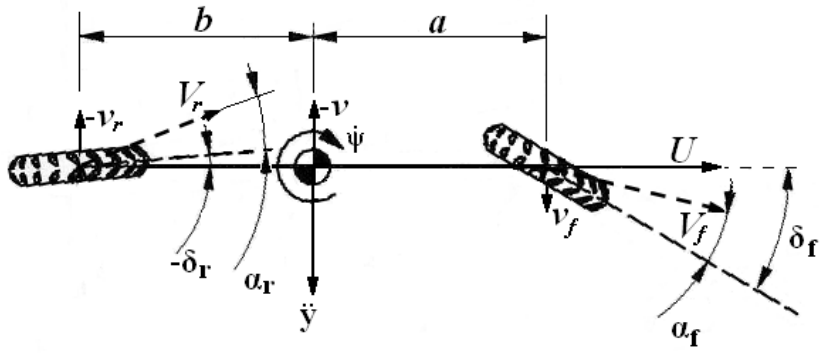

Figure 5.3: Bicycle model for lateral and yaw dynamics.

The forces which lead to the lateral acceleration of the vehicle are produced by the tyres on the front and rear axles. The lateral acceleration ($\ddot{y}$) of the vehicle's centre of gravity can be calculated as follows:

$$\ddot{y} = \frac{F_{yf} + F_{yr}}{m} \tag{5.1}$$

The yaw moment and yaw acceleration are given by:

$$M = aF_{yf} - bF_{yr} \tag{5.2}$$

$$\ddot{\psi} = \frac{aF_{yf} - bF_{yr}}{I_z} \tag{5.3}$$

The yaw acceleration can be integrated to find the yaw rate:

$$\dot{\psi} = \int \frac{aF_{yf} - bF_{yr}}{I_z} \tag{5.4}$$

Whilst at steady state the yaw acceleration will be zero, in the transient conditions of corner entry, a non-zero yaw acceleration will have existed and hence the integral of yaw acceleration will remain non-zero until the turn is completed.

In the absence of tyre slip, the lateral acceleration required to follow a curved path (or centripetal acceleration) ($\ddot{y}_c$) is given by:

$$\ddot{y}_c = \dot{\psi} U \tag{5.5}$$

However; since tyres generate much of their lateral force through slip (the rest being generated through camber thrust) there is almost always a slip element. The side slip velocity of the centre of gravity (v) will have a negative value and is calculated by:

$$v = \int \ddot{y} - \ddot{y}_c \tag{5.6}$$

When there is a non-zero yaw rate, the side slip velocities of the front and rear axles will differ from that of the centre of gravity and are given by:

$$v_f = \left[\int \ddot{y} - \ddot{y}_c\right] + a\dot{\psi} \tag{5.7}$$

$$v_r = \left[\int \ddot{y} - \ddot{y}_c\right] - b\dot{\psi} \tag{5.8}$$

The front and rear tyre slip angles are given by:

$$\alpha_f = -\tan^{-1}\left(\frac{v_f}{U}\right) + \delta_f \tag{5.9}$$

$$\alpha_r = -\tan^{-1}\left(\frac{v_r}{U}\right) + \delta_r \tag{5.10}$$

Where δ_f and δ_r are the front and rear wheel kinematic steer angles. Once computed, the front (α_f) and rear (α_r) slip angles are used in the Magic Formula tyre force calculations.

5.1.3. Tyre Modelling

The highly complex nature of tyres makes modelling their behaviour a challenging exercise. In the past many different approaches have been taken to the modelling of tyre behaviour. These models can generally be classified as being one of two types; theoretical or empirical. Theoretical models attempt to capture the mechanics of the tyre structure and its interaction with the road surface whilst empirical models attempt to derive mathematical formulas which fit measured data.

Perhaps the most widely used empirical tyre models are Pacejka's 'Magic Formulas' [29]. The Magic Formulas are a cluster of formulas used principally to calculate the longitudinal tyre force, lateral tyre force and the self-aligning torque in both pure slip conditions and combined slip conditions. Some of the elements of the Magic Formula equations are easily identified as relating to real world parameters (for example slip angle and camber angle) whilst others are more abstract; for this reason Pacejka's Magic Formulas are often referred to as a semi-empirical model.

As well as the standard Magic Formulas for car tyres, there are additional variations to account for the large camber angles encountered in motorcycle dynamics and simplified versions that are both easier to implement and computationally faster. Each Magic

Formula has an array of 'sub-formulas' which are used to calculate various parameters which are then fed into the main formulae. Given the number of variations, and the complexity of the formulas, it is considered beyond the scope of this thesis to cover them all in detail; instead this section will focus exclusively on the formulas used in the CLEVER Vehicle simulation model.

Since the CLEVER Vehicle simulation model is confined to the investigation of lateral dynamics only, the 'pure slip' versions of the Magic Formulas are used. These formulas exclude the influence of longitudinal slip, which may result from braking or driving torque, and do not compute the self-aligning torque, which whilst an important source of driver feedback, does not have a significant influence on the lateral dynamics.

Front Wheel Tyre Model

When the cabin of the CLEVER Vehicle is tilted, the front wheel can adopt large camber angles. It is therefore necessary to use a tyre model which holds under such conditions. Pacejka presents a Magic Formula for a motorcycle tyre in [29] which remains valid at large camber angles. It is this model that is used to represent the front wheel in the CLEVER Vehicle simulation model and is described in this section.

The lateral force produced by a motorcycle tyre is given by:

$$F_y = D\sin\left[C\arctan\left\{B\left(\alpha_{Feq} + S_H\right)\right\}\right] + S_V \tag{5.11}$$

Where C is an empirical parameter. In the absence of longitudinal forces $\alpha_{Feq}=\alpha$ and B and D are given by:

$$B = \frac{C_{F\alpha}}{(CD)} \tag{5.12}$$

$$D = \frac{d_4 F_z}{\left(1 + d_7 \gamma^2\right)} \tag{5.13}$$

Where d_4 and d_7 are empirical parameters, F_z the vertical load and γ the camber angle.

In order to accommodate large camber changes, a series of horizontal and vertical shifts are applied to the curve. These shifts are given by:

$$S_{Hf} = \frac{C_{F\gamma}\gamma}{C_{F\alpha}} \tag{5.14}$$

$$S_V = d_6 F_z \gamma \tag{5.15}$$

$$S_H = S_{Hf} - \frac{S_V}{C_{F\alpha}} \tag{5.16}$$

Where d_6 is an empirical parameter.

The front tyre used on the CLEVER Vehicle was created specifically for the project, thus parameter values are; instead the example parameter values from Pacejka [29] are used in Equations (5.11) to (5.16), along with cornering stiffnesses in slip ($C_{F\alpha}$) and camber ($C_{F\gamma}$) from Berote [35]. These parameter values are listed in Table 5.1.

Table 5.1: Front tyre parameters taken from [29] and [35].

Parameter	***Value***
C	1.6
$C_{F\alpha}$	$9.74F_z$
$C_{F\gamma}$	$0.86F_z$
d_4	1.2
d_6	0.1
d_7	0.15

Using the parameter values from Table 5.1 and a vertical load of F_z=1342N, the lateral force produced by the front tyre at slip angles between -10° and 10°, and at a range of camber angles, is illustrated in Figure 5.4.

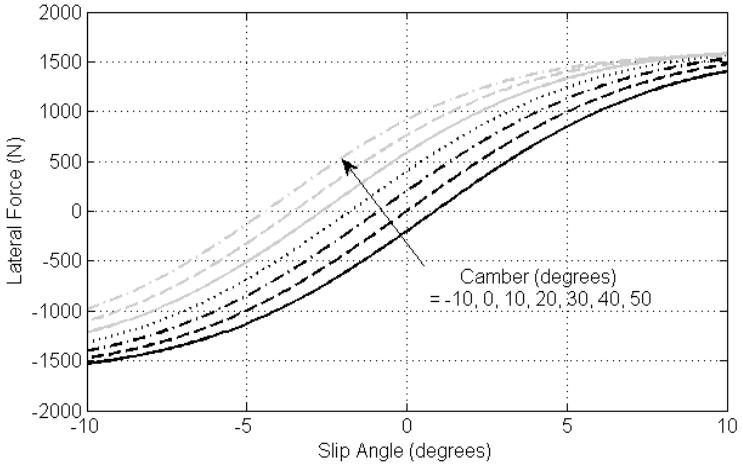

Figure 5.4: Front tyre Magic Formula output.

In order to incorporate the influence of the rear module roll, the camber angle of the front wheel is measured from the multi-body representation of the CLEVER Vehicle. In addition, both the camber and steer angles are subject to the kinematic calculations presented in Chapter 3 before being used in the Magic Formulas.

So as to remain valid in transient conditions, the tyre force output of the front tyre Magic Formula is subjected to the relaxation length calculation described in Chapter 3.

Rear Wheel Tyre Model

The rear wheels of the CLEVER Vehicle are not subjected to the large camber variations that occur at the front wheel, but are subject to large vertical load variations. Therefore, the standard (car) versions of the Magic Formulas are appropriate (as opposed to the motorcycle tyre version described previously). The following formulas are again taken from Pacejka [29] and use the 'similarity method' to adjust a tyre slip/force curve to account for variations in vertical load (F_z) and camber angle (γ).

Under pure slip conditions, the slip/force curve remains approximately the same shape regardless of load and camber angle; thus by multiplication and shifts of the horizontal and vertical axes, tyre performance under conditions other than the reference condition can be calculated. The reference condition is considered to be the tyre freely rolling with a nominal vertical load of F_{z0} and zero camber angle ($\gamma=0$).

The following Magic Formula can be used to calculate the lateral force generated at the reference condition:

$$F_{y0} = D_{y0} \sin\left[C_y \arctan\left\{B_{y0}\alpha - E_y\left(B_{y0}\alpha - \arctan\left(B_{y0}\alpha\right)\right)\right\}\right] \qquad (5.17)$$

Where E_y is the 'curvature factor' which influences the curvature of the lateral force graph in the region of the peak F_y value. The stiffness factor (B_{y0}) is calculated as:

$$B_{y0} = \frac{C_{F\alpha 0}}{C_y D_{y0}} \tag{5.18}$$

Where $C_{F\alpha 0}$ is the tyre cornering stiffness in slip at the reference condition, C_y is a measured tyre parameter, and D_{y0} is the 'peak factor' which influences the maximum lateral force produced. The peak factor and cornering stiffness ($C_{F\alpha}$), as a function of load (F_z), are given by:

$$C_{F\alpha} = c_1 c_2 F_{z0} \sin\left\{2\arctan\left(\frac{F_z}{c_2 F_{z0}}\right)\right\} \tag{5.19}$$

$$D_{y0} = \mu_{y0} F_{z0} \tag{5.20}$$

Where c_1 and c_2 are empirical parameters and μ_{y0} is the road surface friction coefficient at the reference condition (nominally of value 1 on dry tarmac).

Now that all the parameters needed to calculate the reference curve are established, variations in the load (F_z) and camber angle (γ) can be introduced.

Firstly, by multiplying the lateral force at the reference condition (F_{y0}) by the ratio of the actual and reference vertical loads (F_z and F_{z0} respectively), a new lateral force value is produced (F_y):

$$F_y = \frac{F_z}{F_{z0}} F_{y0} \tag{5.21}$$

Multiplying the lateral force by the ratio of the actual and reference vertical loads in Equation (5.21) has the unintended consequence of altering the slope of the slip/force relationship (and thus the cornering stiffness). To correct for this, the slip angle (α) is replaced by the equivalent slip angle (α_{eq}):

$$\alpha_{eq} = \frac{F_{z0}}{F_z}\alpha \tag{5.22}$$

Now that the un-intended alteration of the slip/force slope has been addressed, a modification can be introduced to represent the true variation of the tyre cornering stiffness with varying load (see Equation (5.19)). The expression for the equivalent slip angle can be expanded as follows:

$$\alpha_{eq} = \frac{C_{F\alpha}}{C_{F\alpha 0}}\frac{F_{z0}}{F_z}\alpha \tag{5.23}$$

Whilst large camber changes alter the peak magnitude of the slip/force curve, small changes (±6º) can be approximated as horizontal shifts in the slip/force relationship [29]. The horizontal shift (S_{Hy}) of the force curve in response to a camber angle (γ) is given by:

$$S_{Hy} = \frac{C_{F\gamma}}{C_{F\alpha}}\gamma \tag{5.24}$$

Where the cornering stiffness in camber ($C_{F\gamma}$) is calculated as:

$$C_{F\gamma} = c_5 F_z \tag{5.25}$$

With c_5 being an empirical parameter.

The horizontal shift of the graph in the presence of a non-zero camber angle leads to a new expression for the equivalent slip angle (α_{eq}):

$$\alpha_{eq} = \frac{C_{F\alpha}}{C_{F\alpha 0}}\frac{F_{z0}}{F_z}\left(\alpha + S_{Hy}\right) \tag{5.26}$$

Finally, the equivalent slip angle (α_{eq}) is used to re-calculate the reference lateral force:

$$F_{y0}(\alpha_{eq}) = D_{y0}\sin\left[C_y \arctan\left\{B_{y0}\alpha_{eq} - E_y\left(B_{y0}\alpha_{eq} - \arctan\left(B_{y0}\alpha_{eq}\right)\right)\right\}\right] \tag{5.27}$$

And Equation (5.21) is re-written to become:

$$F_y = \frac{F_z}{F_{z0}} F_{y0}(\alpha_{eq}) \tag{5.28}$$

As with the front tyre, the rear tyres used on the CLEVER Vehicle were created specifically for the project and no parameter values are available. Instead the example parameter values from Pacejka [29] are used in Equations (5.17) to (5.28); these values are listed in Table 5.2.

Table 5.2: Rear tyre parameter values.

Parameter	*Value*
C_γ	1.3
E_γ	-1
F_{z0}	3000N
c_1	8
c_2	1.33
c_5	1
μ_{y0}	1

Using the parameter values from Table 5.2, the rear wheel tyre forces at the reference load and the CLEVER Vehicle static rear wheel load of 1280N are found, Figure 5.5.

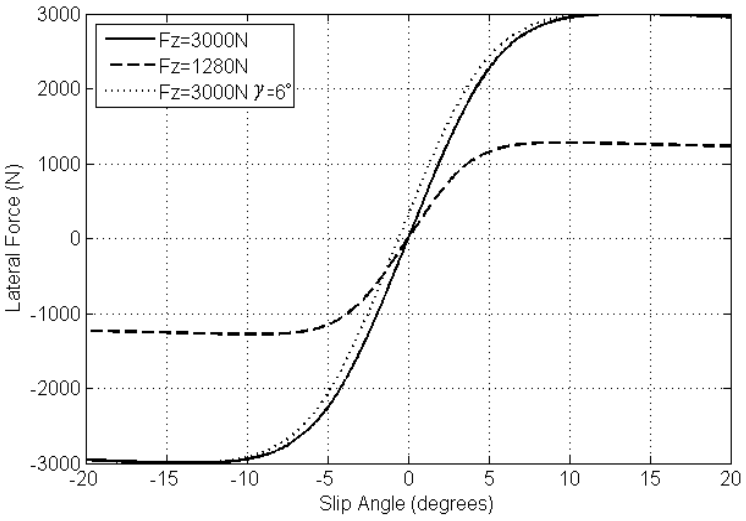

Figure 5.5: Rear tyre Magic Formula output.

As with the front tyre, the rear tyre force output was subjected to the relaxation length calculation described in Chapter 3.

5.1.4. Hydraulic Direct Tilt Control System

The hydraulic Direct Tilt Control (DTC) system consists principally of an engine driven gear pump, a proportional valve and a pair of single-acting hydraulic actuators mounted between the cabin and the non-tilting rear module, Figure 5.6.

As a result of the kinematics of the actuator installation geometry, the lever arm length of the actuators varies in a non-linear fashion throughout the tilting motion. This non-linearity is captured in the multi-body part of the CLEVER Vehicle model.

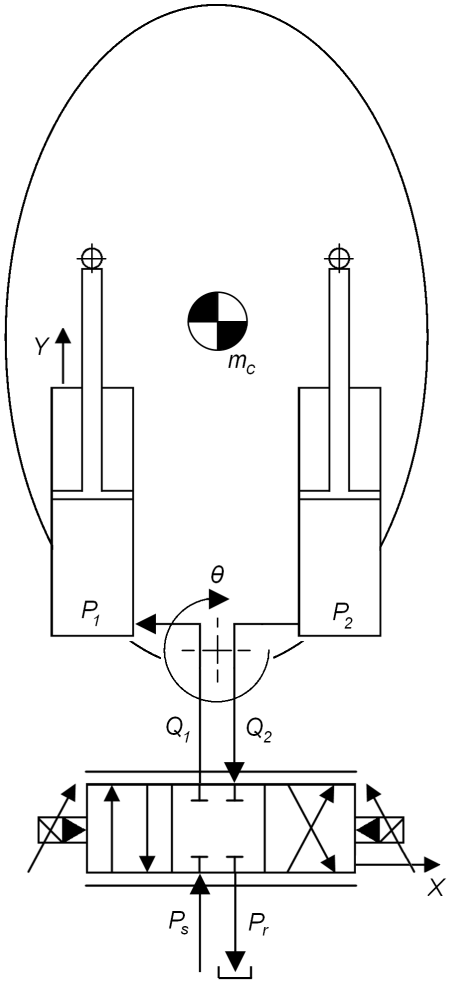

Figure 5.6: Hydraulic DTC system schematic.

Actuator Force Calculations

The 'actuator force' Simulink model is shown in Figure 5.7. Whilst the 1D hydraulic model neglects the actuator piston mass, the actuator piston masses are included in the multi-body model (Figure 5.1) and thus influence the inputs to the actuator force model.

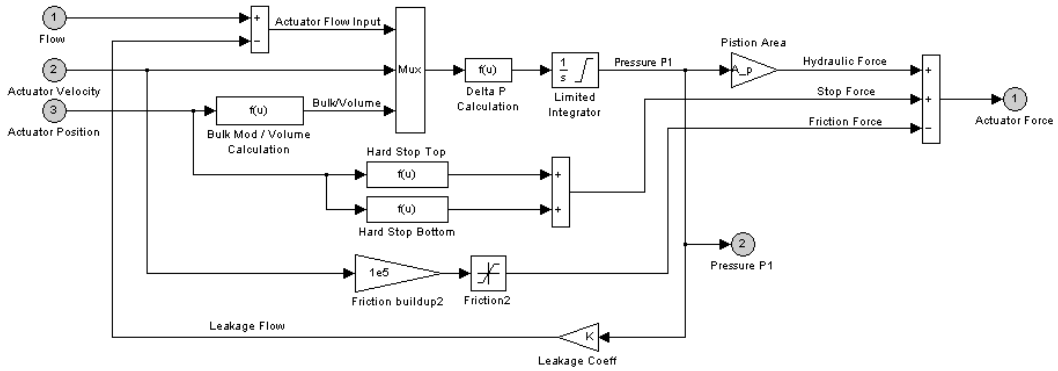

Figure 5.7: Hydraulic DTC actuator force model.

The force produced by a single-acting hydraulic actuator is a result of the pressure (P) within the actuator and the area (A_p) on which that pressure is acting. To find the actuator pressure in a dynamic system, the flow rate in to (or out from) the actuator and the rate of actuator volume change must be considered.

The effective bulk modulus (β) of a hydraulic fluid (a measure of its compressibility) is given by [55]:

$$\beta = -\frac{V\Delta P}{\Delta V} \tag{5.29}$$

Where ΔV is the volume strain. Re-arranging Equation (5.29) gives the pressure change:

$$\Delta P = -\beta \frac{\Delta V}{V} \tag{5.30}$$

The volume strain rate is the difference between the flow rate (Q) and the actuator volume change rate ($A_p U_p$):

$$\frac{\Delta V}{dt} = Q - A_p U_p \tag{5.31}$$

U_p being the actuator velocity. The pressure change rate is:

$$\frac{\Delta P}{dt} = \beta \frac{Q - A_p U_p}{V} \tag{5.32}$$

Note that the volume (V) changes throughout the actuator stroke

$$V = V_0 + A_p Y \tag{5.33}$$

Where V_0 is the volume at the initial actuator position and Y is the actuator displacement.

The pressure is found by integration:

$$P = \beta \int \frac{Q - A_p U_p}{V_0 + A_p Y} dt \tag{5.34}$$

and the actuator force is given by pressure and the piston area:

$$F = A_p \times P \tag{5.35}$$

$$F = \beta A_p \int \frac{Q - A_p U_p}{V_0 + A_p Y} dt \tag{5.36}$$

Valve Flow Rate

The Direct Tilt Control valve is a 4 way proportional valve and is modelled as four orifices, two of which are opened when tilting right and the opposing two are opened when tilting left. The flow through each orifice is found using the orifice equation [55].

$$Q = K_v X \sqrt{\Delta P} \tag{5.37}$$

Where K_v is the 'valve constant', X is the spool displacement and ΔP is the pressure difference across the orifice. The pressure difference across the supply (ΔP_s) and return (ΔP_r) orifices is given by:

$$\Delta P_s = P_s - P_1 \tag{5.38}$$

$$\Delta P_r = P_2 - P_r \tag{5.39}$$

Where P_s is the nominal supply pressure, P_r the return pressure and P_1 and P_2 are the pressures in the extending and retracting actuators respectively, as calculated in Equation (5.34).

The proportional valve is over-lapped giving a dead-band of approximately ±13.5% in the centre of the spool stroke. The dead-band is incorporated into the valve model and the valve controller compensates by adding ±13.5% to the valve demand signal such that the spool moves rapidly through the dead-band. The spool dynamics are not modelled as the manufacturer's data sheet [56] shows the -3dB cut-off frequency to be approximately 40Hz for a 25% spool opening. This response is considered sufficiently fast so as not to influence the tilting performance.

5.2. Simulation Model Refinements

A number of refinements to the simulation model supplied by Berote, have been made by the author; whilst many of the refinements are peripheral, and do not impact upon the simulation output, the more significant changes are detailed in the following sub-sections.

5.2.1. Controller Gains

Chapter 4 details how the proportional and derivative gains in the CLEVER Vehicle prototype were tuned such that the step response of the revised control system matched the responses published by Drew [10]. Subsequently, simulation tilt controller gain values were adjusted to match the real controller; the proportional gain increased from 1.0 to 1.7 and the derivative gain from 0.0 to 0.1. No integral gain is used.

5.2.2. Active Steering System

In order to implement a Steering Direct Tilt Control (SDTC) strategy, it was necessary to install an active steering system on the CLEVER Vehicle prototype. The installation and performance of the active steering system is detailed in Chapter 4. The simulation model was modified to reflect both the physical installation of the active steering system and the associated control logic.

Whilst the active steering model contains the actuator stroke limits, it was not deemed necessary create a detailed model of the active steering hydraulic system's dynamics. In practise the performance is so fast, and the force output high enough, that the output tracks the demand very closely.

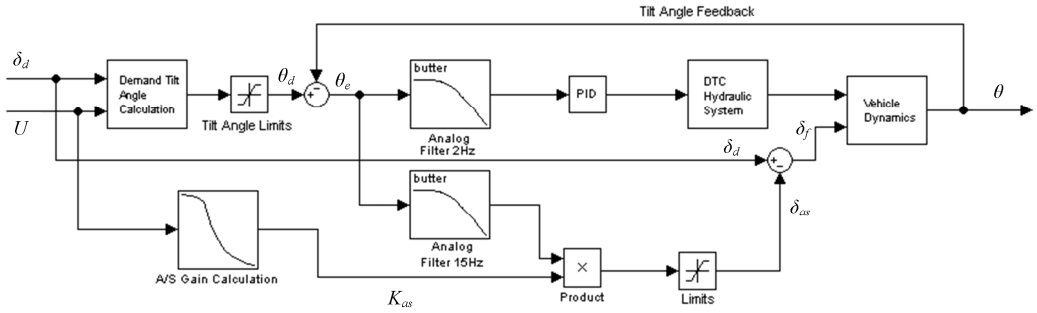

Figure 5.8: Active steering simulation block diagram.

5.2.3. Filtering

Low Pass Filters (LPFs) were added to the simulation model in order to replicate those used in the prototype CLEVER Vehicle controller. A 2Hz Butterworth LPF is used on the tilt angle error to remove un-wanted noise and subsequent 'fidget' of the tilting cabin. A 15Hz Butterworth LPF is used on the active tilt angle error signal used by the active steering system. The higher frequency reflects the faster response required from the active steering system. The origin of the filtration strategy is discussed in Chapter 4.

5.2.4. Masses

Installation of the active steering system, and the associated controller hardware, led to changes in the vehicle's total mass and the mass distribution. The simulation model was altered to match the prototype vehicle in its revised configuration and now gives near identical static wheel loads.

5.2.5. Path calculation

The simulation model was modified by the addition of a new sub-system to calculate the displacement in the longitudinal (X) lateral (Y) directions (Figure 5.9). This enabled the plotting of the vehicle trajectory in response to a series of steer inputs and examination of the influence of the active steering system on the vehicle's path following capability, see Chapter 7.

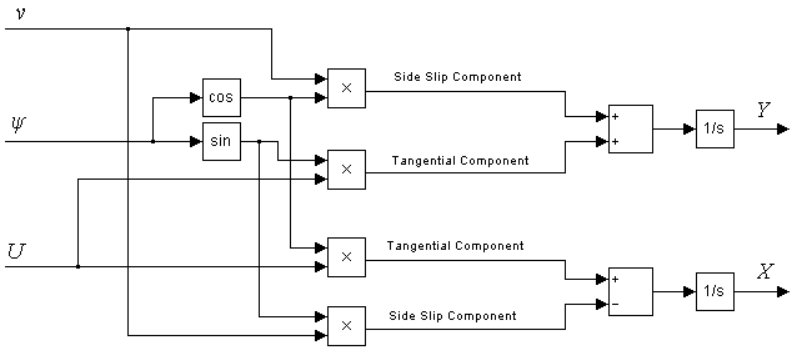

Figure 5.9: Lateral and longitudinal position calculation.

The X and Y displacements are found from the side slip velocity (v), yaw angle (ψ) and the speed (U):

$$X = \int \left[\left(U \times \cos\psi \right) - \left(v \times \sin\psi \right) \right] \tag{5.40}$$

$$Y = \int \left[\left(U \times \sin\psi \right) + \left(v \times \cos\psi \right) \right] \tag{5.41}$$

5.3. Simulation Model Validation

Extensive validation of the CLEVER Vehicle simulation model was performed by Berote in [35]. Using a three-poster rig to excite the vehicle across a range of frequencies, Berote was able to demonstrate that the multi-body element of the simulation model captured the major modes in bounce and roll, but that due to friction and frame flexibility (particularly at the tilt joint), unexpected nonlinearities were present in the measured data which were not captured by the simulation model. None-the-less, Berote concluded that the simulation model captured the major modes and that modelling the frame flexibility would not serve the purposes of the research as it would be better to stiffen the vehicle if it were ever to reach production. In addition, Berote provided verification of the lateral dynamics sub-system model (at low accelerations), in steady state and quasi-steady state conditions, by presenting data showing a good correlation between the simulated and measured lateral acceleration and rear module roll angle signals.

In this section, further validation of the simulation model is presented in order to demonstrate that the revised simulation model provides a good representation of the CLEVER Vehicle's performance, and to examine the simulation performance at higher lateral accelerations.

5.3.1. Validation of the Lateral Dynamics, DTC System, and Roll Dynamics Models

In this sub-section, the results of simulations conducted using steer and speed inputs (Figure 5.10) logged during testing of the prototype CLEVER Vehicle are presented; the simulation output is then compared to data logged during the testing. Test procedures and data logging are discussed further in Chapters 6 & 7.

The steer and speed inputs used in the simulations were recorded whilst driving around a car park on the university campus. Each lap took approximately 20s to complete and consisted of two straights, one featuring a lane change manoeuvre part way along its length, and two 180° right turns. The CLEVER Vehicle was operated in DTC mode, and the speed and steer inputs where severe enough to generate peak lateral accelerations of approximately 7m/s^2, (Figure 5.11). Pervious validation had been restricted to maximum lateral accelerations of 3m/s^2.

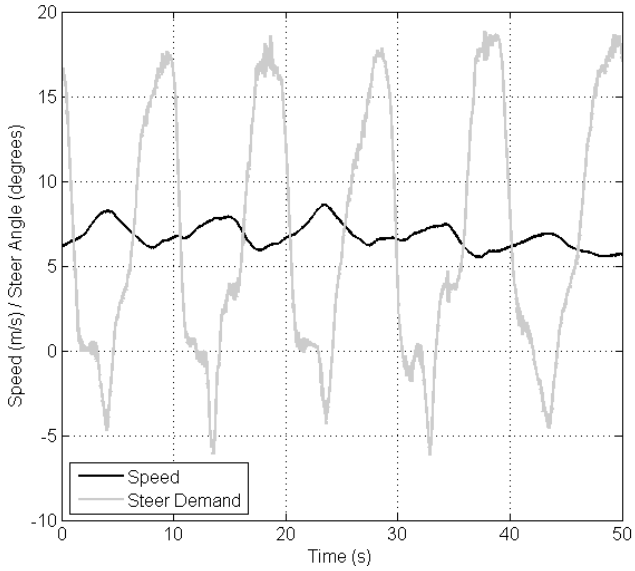

Figure 5.10: Logged speed and steer inputs used to validate the model.

The lateral acceleration data presented in Figure 5.11 shows that whilst the simulation model captures the major acceleration modes, some higher frequency behaviour is evident in the measured data that does not appear in the simulation data. Although not presented here, simulations have been performed which demonstrate that the discrepancy between simulated and measured lateral acceleration is, at least in part, due to the data logger (with integrated accelerometer) position on the prototype CLEVER Vehicle. Ideally, the accelerometer would be mounted at the vehicle's roll centre which, given the rear module's trailing arm suspension, occurs at ground level. Unfortunately this is not

practical and the data logger is mounted high on the rear module where it is subject to additional lateral accelerations resulting from both the roll angle and roll acceleration of the rear module. Additional sources of error include the unknown tyre parameters (generic tyre properties are used in the Magic Formula tyre models) and of course noise on the measured data due to road inputs. The simulation model is considered to offer acceptable reproduction of the lateral acceleration.

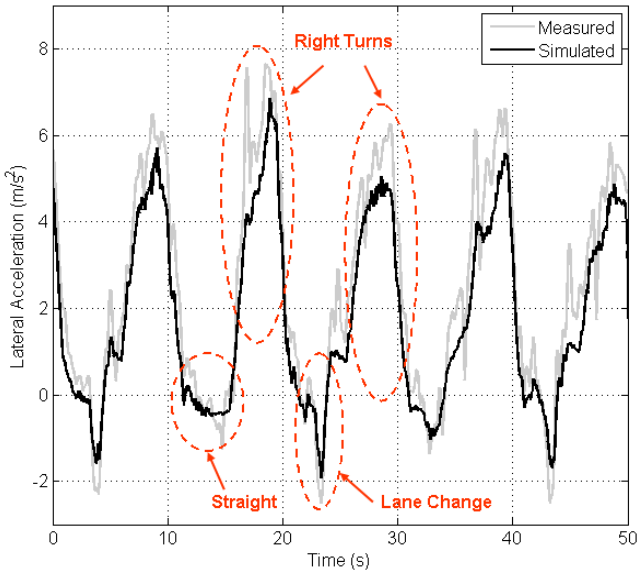

Figure 5.11: Measured (filtered at 3Hz) and simulated lateral acceleration.

The performance of the hydraulic DTC system model is confirmed by comparing the measured and simulated tilt angle responses, (Figure 5.12). Since the demand tilt angle is calculated from the steer and speed inputs (which are identical in both the simulation and the measured data), the demand tilt angle in simulation is identical to that produced by the vehicle mounted controller. Other than a small amount of noise visible in the measured data, the measured and simulated tilt angle responses are almost indistinguishable.

Finally, examining the simulation model's reproduction of the rear suspension displacement serves two purposes; firstly, the roll angle of the rear module influences the camber angle of all three wheels and thus the lateral dynamics. Secondly, the rear suspension displacement provides a measure of how successfully the simulation model replicates the roll dynamics of the CLEVER Vehicle; examination of the vehicle's roll stability is the primary use of the simulation model within this thesis.

Displacements of the left and right hand wheels are presented in Figure 5.13 & Figure 5.14. The measured data is subject to some noise as a result of surface irregularities; a shallow drainage gully running along the centre of the test area is thought responsible for

the sudden compression of both wheels simultaneously at t≈9, t≈29 and t≈49s. More significant discrepancies between the simulated and measured left hand suspension displacement occur at t≈25 and t≈35, these discrepancies are not thought to be caused by road inputs as they occur when the vehicle is at different positions within the test area. However, given that corresponding discrepancies are not present in the right hand suspension position data, the simulation model is thought to be replicating the vehicle's roll dynamics acceptably. An alternative explanation may be high friction in the left hand trailing arm bearing. Un-modelled longitudinal dynamics and small changes in the vehicle's weight distribution may also contribute to smaller discrepancies elsewhere in the suspension position data. None-the-less, the simulation model replicates the measured suspension displacement well.

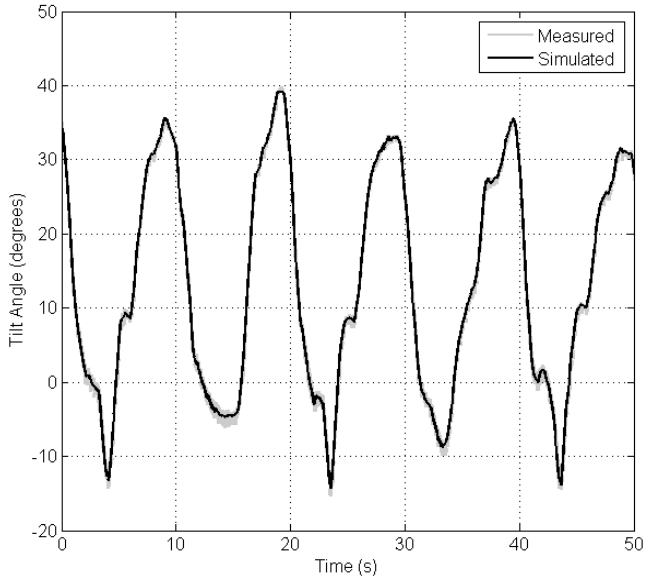

Figure 5.12: Measured and simulated tilt response during vigorous driving.

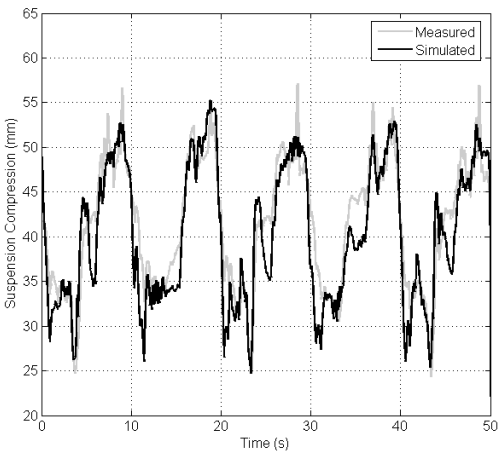

Figure 5.13: Measured and simulated left suspension displacement.

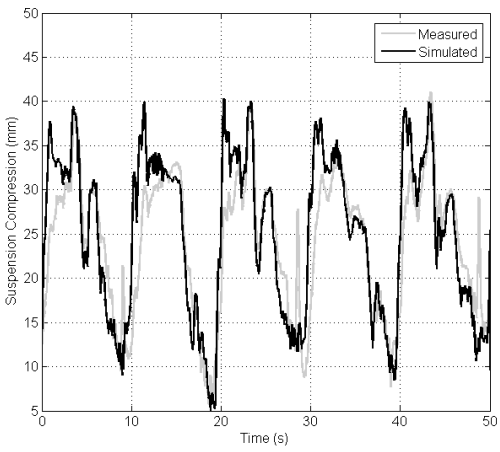

Figure 5.14: Measured and simulated right suspension displacement.

5.3.2. Validation of Active Steering Model

Verification of the active steering system required the use of a new set of steer and speed inputs, this time logged by the CLEVER Vehicle prototype whilst being driven in Steering Direct Tilt Control (SDTC) mode (Figure 5.15). The track layout is identical to the earlier DTC case and thus the steer and speed inputs are similar.

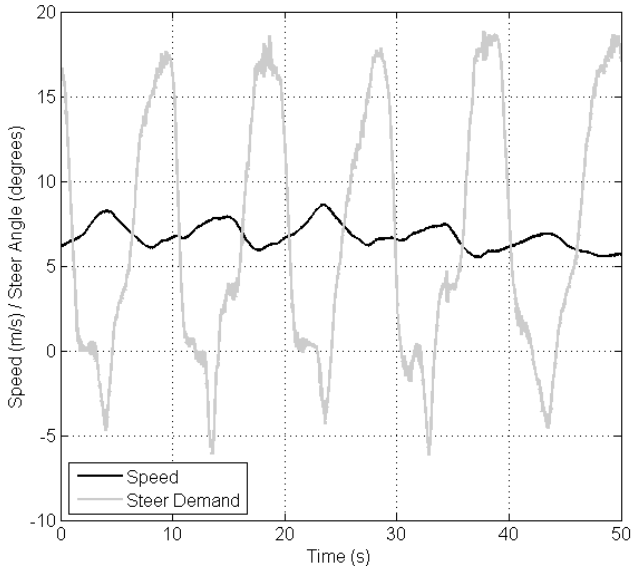

Figure 5.15: Logged speed and steer inputs used to validate the active steering model.

Figure 5.16 and Figure 5.17 show the active steer angle measured when driving the prototype vehicle and the active steer angle generated by the simulation model. It is noted that the active steering angle in the measured data is slightly larger in magnitude than the active steering angle produced by the simulation model during highly transient phases. This discrepancy is due to differences in the measured and simulated tilt angle error (Figure 5.18 and Figure 5.19). Note that reproduction of the tilting response in simulation remains extremely good; but, since the magnitude of the tilt angle error (θ_e) is small in comparison to the tilt angle (θ), seemingly trivial discrepancies in the tilting response have a more conspicuous influence on the active steering angle.

Despite the small differences in the tilt angle error signals, the active steering system behaviour in simulation is a good representation of the measured behaviour of the real system.

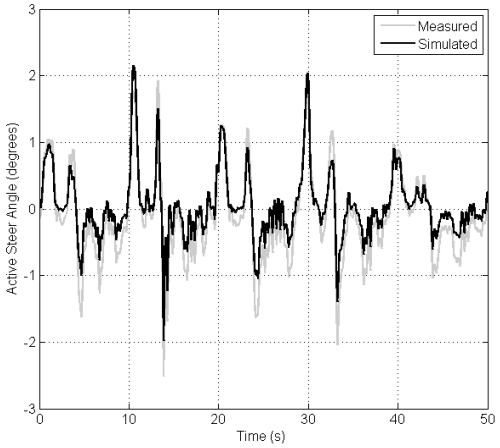

Figure 5.16: Measured and simulated active steer angles (both filtered at 3Hz).

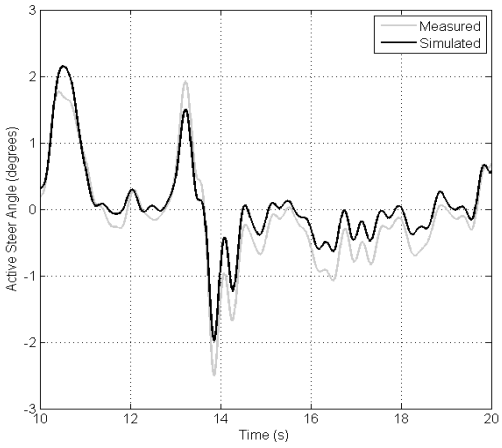

Figure 5.17: Extract from measured and simulated active steer angles.

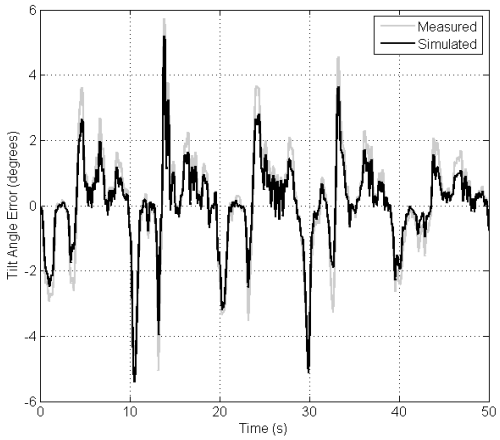

Figure 5.18: Tilt angle error (both filtered at 3Hz).

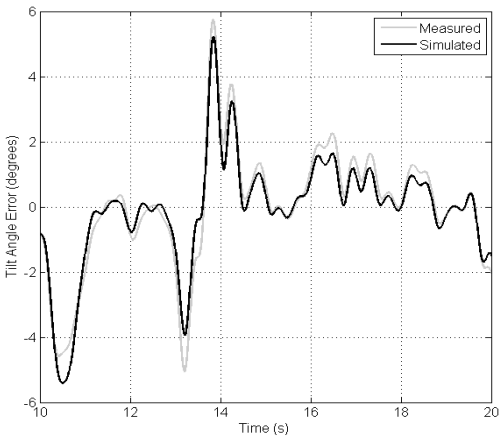

Figure 5.19: Extract from tilt angle error.

5.4. Concluding Remarks

In this chapter, the simulation model originally supplied by Berote has been introduced and modelling of the roll dynamics, lateral dynamics, tyres and hydraulic system explained. Changes made to the simulation model by the author (notably the filtering strategy, controller gains and the inclusion of the active steering system) were also discussed.

The performance of the simulation model was verified by using steer and speed inputs measured during testing of the prototype vehicle, and comparing the simulation output to the measured data. Using inputs recorded in Direct Tilt Control (DTC) mode, the lateral acceleration response of the vehicle was replicated satisfactorily by the simulation model, particularly at lower frequencies. Some discrepancies remain at higher frequencies but these are thought to be largely down to the positioning of the accelerometer on the

prototype vehicle. The tilting response of the vehicle was replicated extremely well by the simulation model, as was the rear suspension displacement once the influence of surface irregularities was negated.

Using a second set of steer and speed inputs, this time logged using the prototype CLEVER Vehicle in Steering Direct Tilt Control (SDTC) mode, the simulation model's ability to replicate the active steering system response was examined. Whilst small differences in the measured and simulated tilt angle errors did cause some difference in the magnitude of the active steering angle, the overall behaviour is replicated well by the simulation model.

The very good correlation between the simulated and measured dynamic behaviour of the CLEVER Vehicle means that the simulation model can confidently be used for assessing the vehicle's dynamics and developing further control strategies.

Chapter 6. Roll Stability of a Steering Direct Tilt Control System

This chapter examines the roll stability performance of the Steering Direct Tilt Control strategy proposed by Berote [35]. A number of experiments were performed using the prototype CLEVER Vehicle operating in both Steering Direct Tilt Control (SDTC) and Direct Tilt Control (DTC) modes. The results recorded in the two modes are compared to ascertain the stability improvement provided by the more advanced SDTC system.

This chapter expands on results published by Robertson *et al*. [57] which provided experimental verification of SDTC system performance during highly transient manoeuvres.

6.1. The Test Environment

The results presented in this chapter were obtained during test sessions performed in a car park at the University of Bath, Figure 6.1. The car park in question was predominantly flat with a slight camber to aid drainage into the shallow gully that runs along the centre line. The longest straight measures approximately 90m in length and 16m in width. The road surface was in excellent condition having been re-surfaced within the year preceding testing and having a minimal number of irregularities such as drain covers.

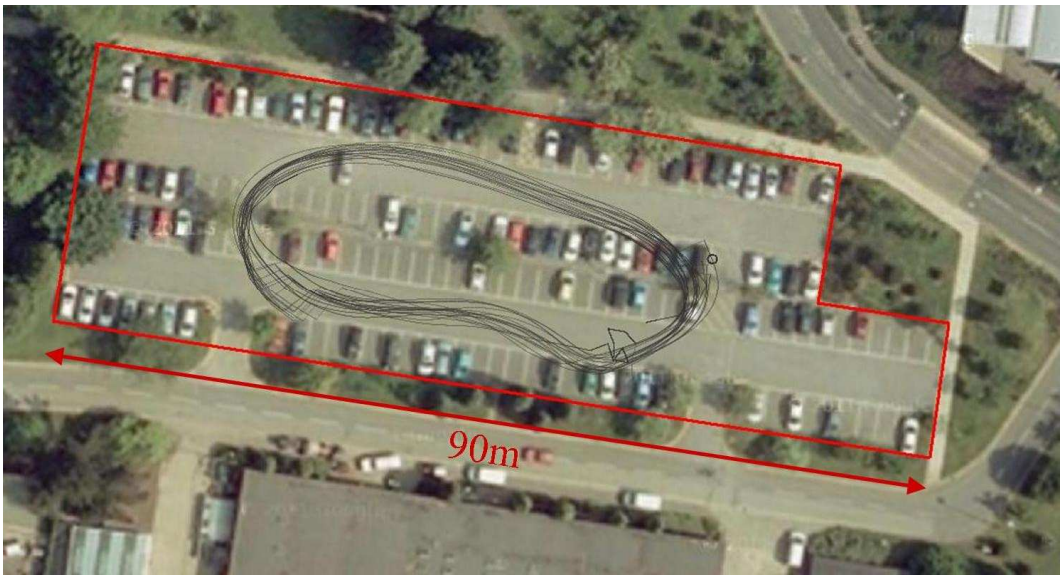

Figure 6.1: Satellite image of the test environment and a typical GPS trace of the vehicle's path. ***Imagery ©2013 GeoEye, Getmapping plc, Infoterra Ltd & Bluesky DigitalGlobe, Map Data ©2013 Google.***

The limited length of the test environment meant it was not practical to obtain test results at speeds significantly greater than 10m/s and the restricted width influenced the range of steer inputs that were possible. Despite these constraints, it was possible to investigate a wide range of steady state and transient manoeuvres at high lateral accelerations.

Clarification of Front Wheel Steer Angle Values

Reference is made in this chapter to multiple variants of the front wheel steer angle (δ). In the interests of clarity the different front wheel steer angle parameters, and their meanings, are listed in Table 6.1.

Table 6.1: Front wheel steer angles.

Symbol	Description
δ_d	Steer demand angle – The demand front wheel steer angle generated by the driver's steer inputs.
δ_{as}	Active steering angle – The alteration to the front wheel steer angle produced by the active steering system.
δ_f	Front wheel steer angle – The front wheel steer angle that results from the combination of both the driver's steer demand angle and the active steering angle.

6.2. Wheel Load Calculations

With direct measurement of the vertical load supported by each of the wheels not possible, where this information is presented, it has been estimated using the suspension rate curves shown in Figure 6.2. The curves were generated by placing the CLEVER prototype on a set of calibrated vehicle scales, applying a roll moment to the chassis, and recording both the suspension positions and the vertical wheel loads. Generating the suspension rate curves in this fashion encompasses the rear anti-roll bar's influence on the wheel loads, but excludes damping forces. Whilst attempts were made to calculate them, damping forces are omitted from the wheel load estimation as differentiation of the suspension position data (to determine the velocity) introduced unacceptable levels of error. The trailing arm rear suspension does not introduce any linkage forces which could influence the suspension positions in the presence of lateral forces.

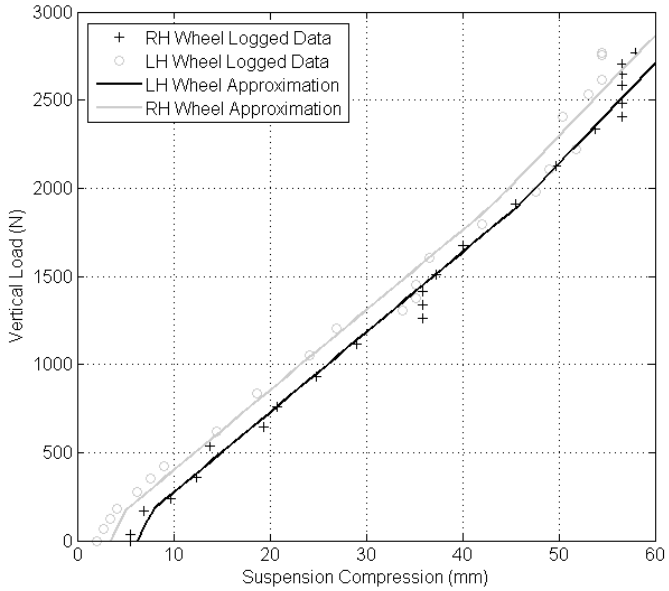

Figure 6.2: The 3 stage linear approximation of the rear wheel rates used to obtain estimations of the vertical loads (F_{zl} & F_{zr}).

6.3. Quasi-Steady-State Performance

A number of quasi-steady-state tests were performed by driving the CLEVER Vehicle prototype in a circle in both DTC and SDTC modes, with the principal goal of verifying the lateral acceleration estimate used within the tilt control system. Given the restricted width of the test facility, the turn radius was kept constant and the forward speed varied to achieve a range of lateral accelerations. Inevitably, the human driver was not able to generate perfect steer and speed inputs so some oscillation of the lateral acceleration is evident. The tests were performed in both DTC and SDTC modes and in both left and right hand turns. Since in quasi-steady-state conditions, the active steering system has little influence, and the vehicle is symmetrical, only results for left hand turns in DTC mode (Figure 6.3) are presented here.

In order that the correct demand tilt angle (θ_d) is generated by the controller, it is important that the lateral acceleration ($\ddot{y}$) is accurately estimated. In conditions with a low level of transience, a comparison between the controller estimate (based on the speed and steer angle) and the measured lateral acceleration shows a good correlation, Figure 6.4.

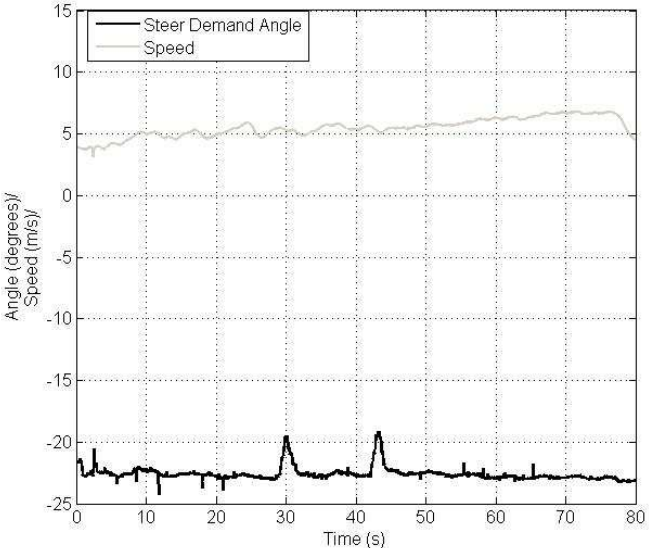

Figure 6.3: Steer demand angle and vehicle speed during quasi-steady-state test.

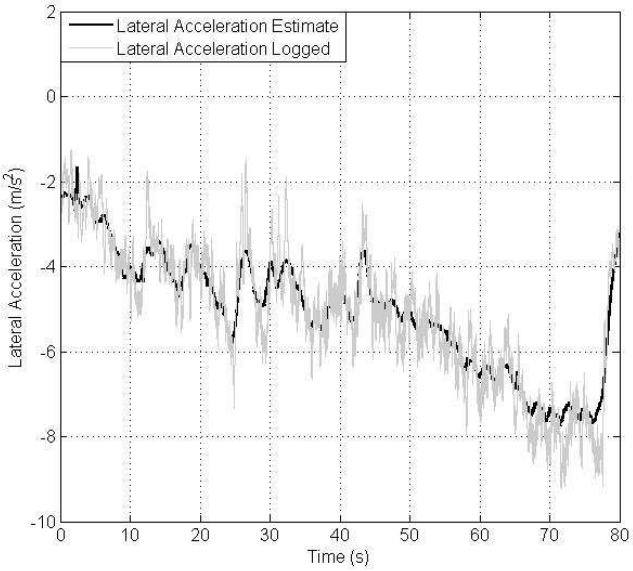

Figure 6.4: Controller estimated and measured lateral accelerations during quasi-steady-state test.

Due to space restrictions, the data logger (with integrated accelerometers) used to measure the lateral acceleration is mounted high on the rear module of the CLEVER Vehicle, well above the roll axis. In highly transient conditions, it is subject to additional lateral accelerations resulting from the roll acceleration of the rear module; this causes the measured lateral acceleration data to deviate from the controller estimate. For this reason, the controller estimate is used throughout this thesis as the preferred lateral acceleration signal.

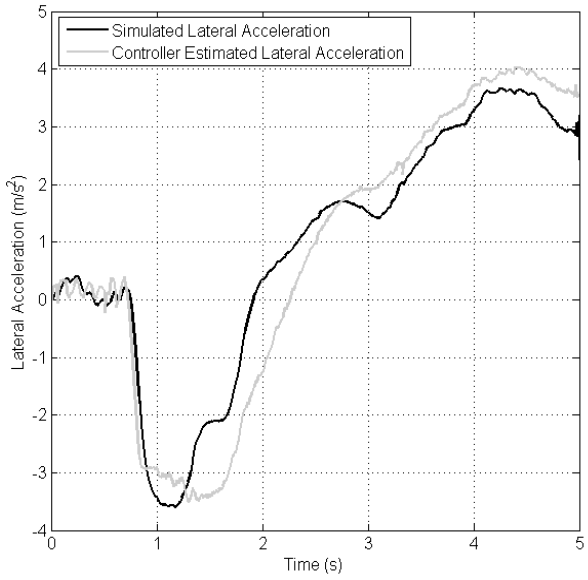

Figure 6.5: Simulated lateral acceleration and controller estimate of lateral acceleration.

Although selected as the preferred signal, it is known that the controller estimate of lateral acceleration has limitations, particularly in highly transient situations. To quantify the influence of these limitations the controller's estimate of lateral acceleration in response to a harsh ramp steer input (performed in DTC mode) is compared to the simulated lateral acceleration response (calculated by dividing the non-linear tyre forces by the vehicle mass), Figure 6.5. Whilst the peak magnitude of the lateral acceleration is similar in both cases, there are some differences in transient behaviour, particularly around t≈1.5s.

Given that it is based only upon the vehicle speed and the demand front wheel steer angle (δ_d), the controller estimate of lateral acceleration excludes several factors which will affect the transient response. These include the lateral force applied to the non-tilting base as the cabin mass is moved towards the turn centre by the DTC actuators, the tyre slip characteristics and the camber thrust generated by the front wheel as the cabin tilts. The faster initial response of the controller estimate (t≈0.9s) may be attributed to the inclusion of the tyre relaxation length in the simulation model which delays the generation of lateral forces in response to steer inputs.

Figure 6.6 shows the tilt angle demand and response signals during the quasi-steady-state tests. As one would expect in conditions with a low degree of transience, the tilt angle tracks the demand very well. The maximum tilt angle of -45° is reached at t≈58s; this corresponds to a lateral acceleration of ≈6.25m/s^2 (Figure 6.4). The vertical load estimates for each of the rear wheels obtained using the wheel rate graphs (Figure 6.2) are shown in Figure 6.7. At lateral accelerations of up to 5m/s^2, the increase in load on the outside wheel matches the reduction in load on the inside wheel and the total load remains roughly constant. However, at higher lateral accelerations and larger suspension displacements, a discrepancy appears and the total rear axle load reduces. One possible explanation for the discrepancy is that at higher lateral accelerations, the outside wheel generates a larger proportion of the total lateral force; this higher lateral force may lead to increased friction in the trailing arm bearings and suppressed displacement. Alternatively, the wheel rate curves may not be accurate at the extreme ends of the suspension travel. Despite the discrepancies, the displacement / load relationship curves are considered sufficiently accurate to provide a good indication of the vehicle's roll stability.

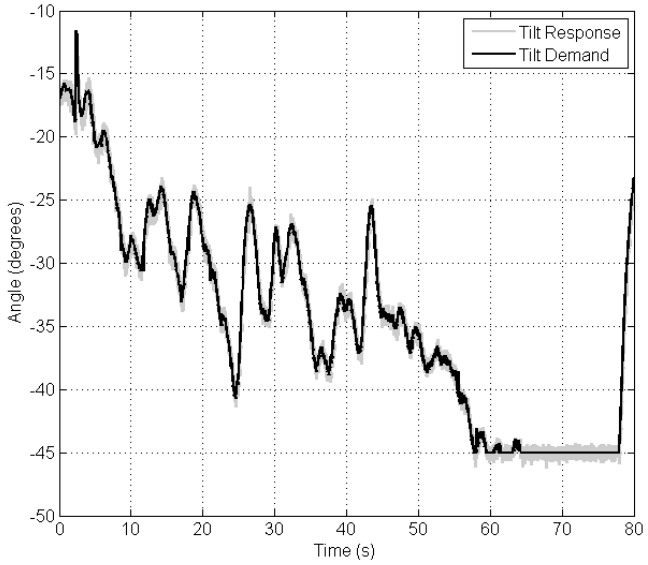

Figure 6.6: Tilt angle demand and response during quasi-steady-state test.

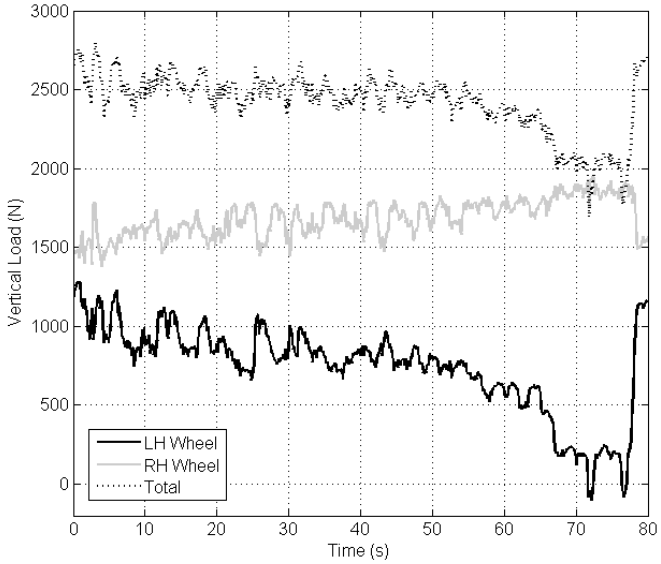

Figure 6.7: Left, right and total wheel loads during quasi-steady-state test.

6.4. U-turn Manoeuvre

A series of 180° right handed U-turn manoeuvres of approximately 10m radius were undertaken at a speed of approximately 7m/s in both DTC and SDTC modes with the intention of assessing the impact of the SDTC strategy on the roll stability. In total the manoeuvre was performed 54 times, 24 times in DTC mode and a further 30 times in SDTC mode.

Despite the manoeuvre generating lateral acceleration demands approaching 6m/s^2, as the rate at which these lateral accelerations were generated was comparatively low (Figure 6.8), the influence of the active steering system was very small. The estimated lateral acceleration response (calculated from the front wheel steer angle (δ_f), as opposed to the driver's steer demand (δ_d) – the two may differ as a result of the active steering) is little different to the demand. During the transient turn-in and turn-out phases modest active steer angles are apparent (Figure 6.9) but, for the most part, the active steer angle remains close to zero and the SDTC system performed much like a DTC system. As a result of the small active steer angles, any difference in response between DTC and SDTC modes was so small that it was indistinguishable amongst the inevitable variation in the steer and speed inputs. Only limited SDTC results are presented for this manoeuvre.

It should be remembered that a lack of roll stability afflicts the CLEVER Vehicle during highly transient conditions, and not at steady-state; thus the fact that SDTC and DTC performance is similar during the U-turn manoeuvre does not highlight a short-coming of the SDTC strategy.

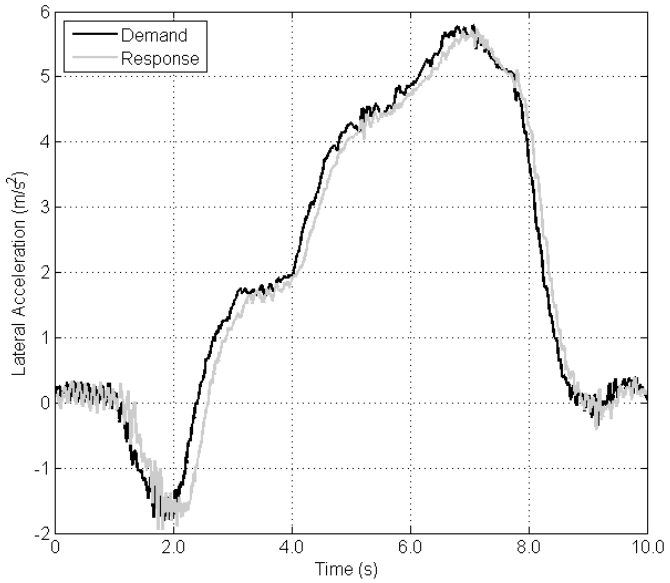

Figure 6.8: Estimated lateral acceleration demand and response during U-turn manoeuvre in SDTC mode.

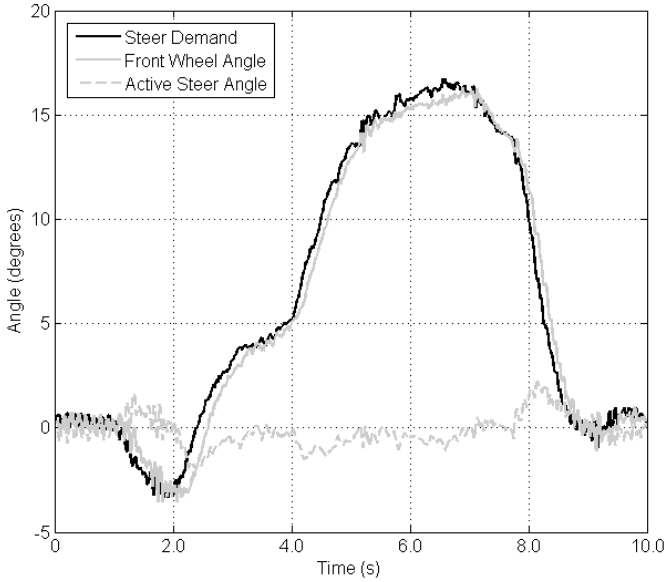

Figure 6.9: Steer angles during U-turn manoeuvre in SDTC mode.

6.5. Harsh Ramp Steer Experiment Results

Experimental results were obtained for a series of rapid ramp steer inputs made by a human driver at three speeds between 6m/s and 10m/s in both DTC and SDTC modes.

The ramp steer inputs were made as quickly as possible by the driver in DTC mode, typically taking less than 0.3s to reach the demand value. The magnitude of the steer inputs was chosen to take the CLEVER Vehicle close to its roll stability limit; they were therefore smaller at higher speeds. Because of the restricted width of the test facility each ramp steer input had to be followed, after a short dwell, by a reversal of the steer demand. The steer inputs used in the DTC case were then replicated as closely as practically possible in the SDTC case.

Inevitably, it was not possible to obtain perfectly consistent results from one test run to the next. To counter the variations in the speed and steer inputs each manoeuvre was completed multiple times. For each of the three forward speeds, one manoeuvre completed in DTC mode and one completed in SDTC mode were selected for comparison. The manoeuvres selected provide the best match of the lateral acceleration demand curves at each speed.

6.5.1. Results at 6m/s

Figure 6.10 to Figure 6.17 show the test results recorded at a speed of 6m/s. A total of 51 steer input manoeuvres (31 DTC and 20 SDTC) were conducted at a nominal speed of 6m/s (Figure 6.10) with the resulting peak lateral acceleration demands ranging from 2.5 to 4m/s^2. The selected DTC and SDTC cases each show a lateral acceleration demand of approximately 3m/s^2 (Figure 6.11). Despite the modest size of the lateral acceleration, the CLEVER Vehicle was observed to be close to its roll moment limit during these tests with frequent lifting of the inside wheel when in DTC mode.

Figure 6.12 shows that although no countersteering action is produced, the SDTC case has a lower front wheel steer angle rate. In turn, the rate at which the lateral acceleration response builds is attenuated (Figure 6.11). In Figure 6.13 the active steering angle (δ_{as}) is shown to track the demand (δ_{das}) very well, and no saturation of the active steer angle occurs. Tilt angle tracking performance is not improved in the SDTC case (Figure 6.14 & Figure 6.15) implying that the tilt actuators are not force saturated in the DTC case, and that it is the filtering of the tilt angle error (θ_e) in the controller that limits the speed of the tilting response (see Chapter 4). Small reductions in the suspension position and vertical load variations (Figure 6.16 & Figure 6.17) are observed when in SDTC mode; this suggests a modest reduction in the DTC tilt actuator torque and a small improvement in vehicle stability. The effectiveness of the SDTC strategy is limited at this slow speed.

The limitations of using suspension displacement as a measure of vertical wheel load are evident in Figure 6.16 and Figure 6.17. During testing the inside wheel was observed to lift clear of the ground in DTC mode, however the data shows some wheel load remaining. Whilst the anti-roll bar's influence on the wheel load has been accounted for, it is possible that damping and friction forces restrict the suspension displacement slightly.

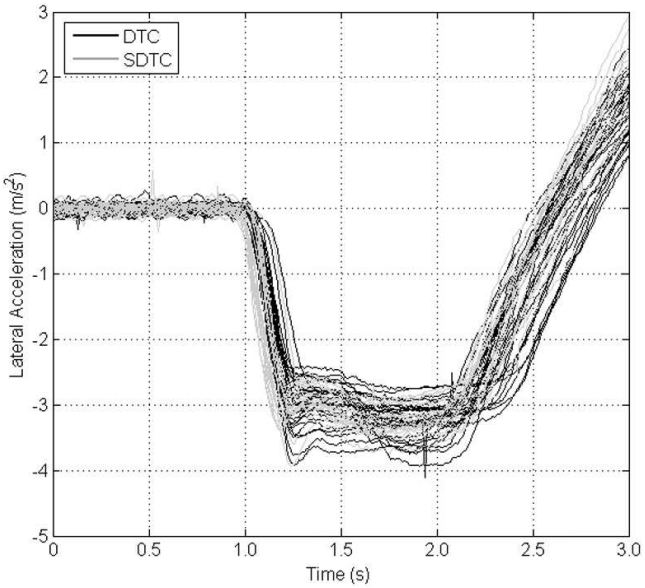

Figure 6.10: 6m/s - Lateral acceleration demand curves for 31 steer inputs in DTC mode and 20 steer inputs in SDTC mode.

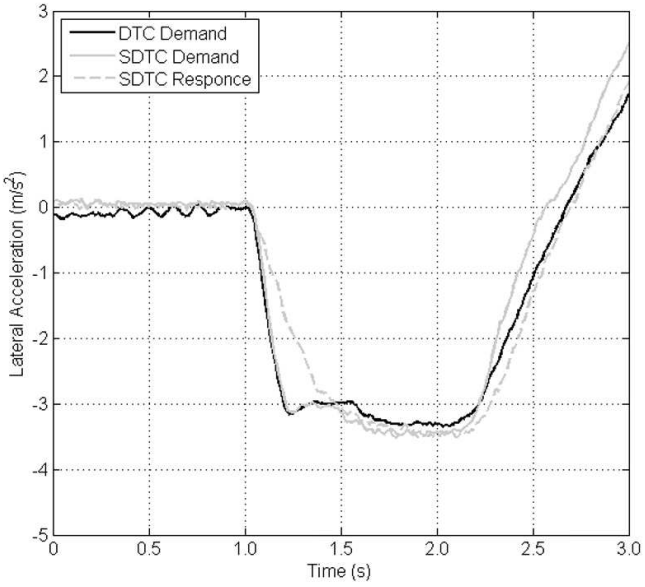

Figure 6.11: 6m/s - Lateral acceleration demand in the selected DTC and SDTC cases, and the resulting lateral acceleration response in the SDTC case.

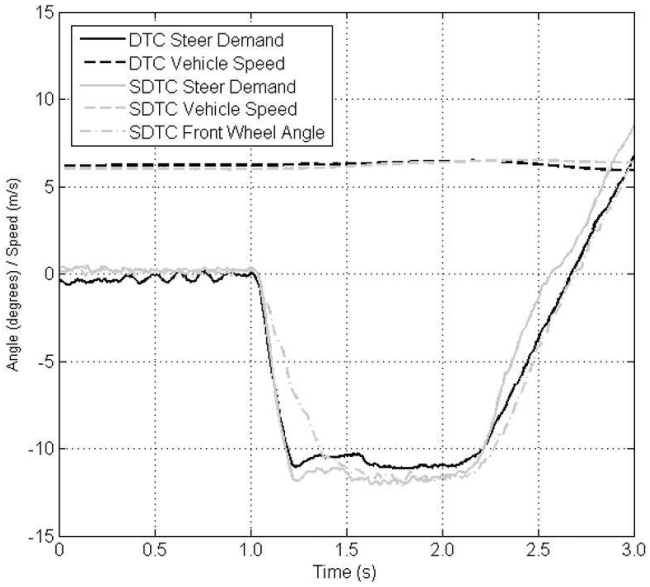

Figure 6.12: 6m/s - Steer demand (δ_d) and speed (U) inputs for both DTC and SDTC cases, and the resulting front wheel steer angle (δ_f) in the SDTC case.

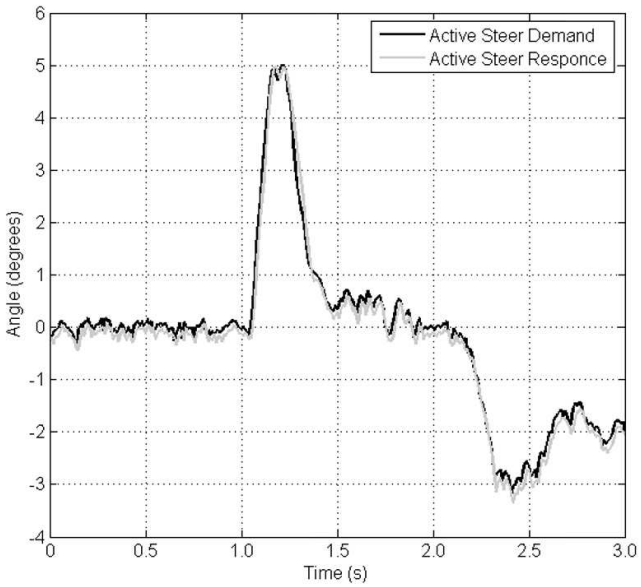

Figure 6.13: 6m/s - Active steer demand (δ_{das}) and response (δ_{as}) in SDTC mode.

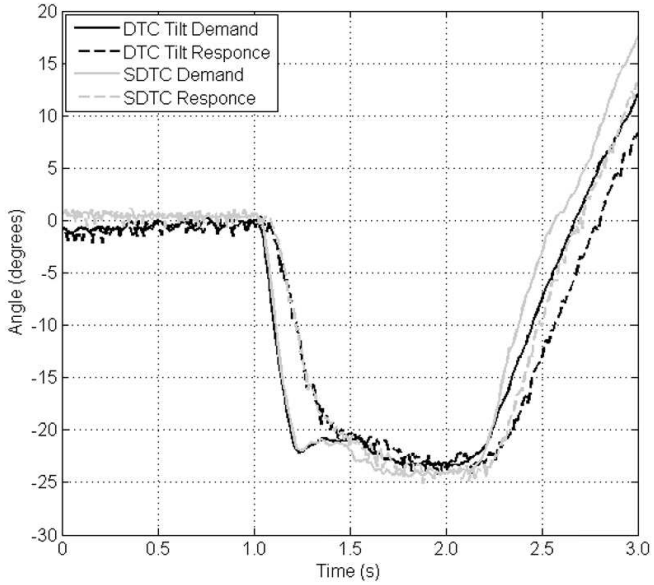

Figure 6.14: 6m/s - Tilt angle demand (θ_d) and response (θ) in DTC and SDTC cases.

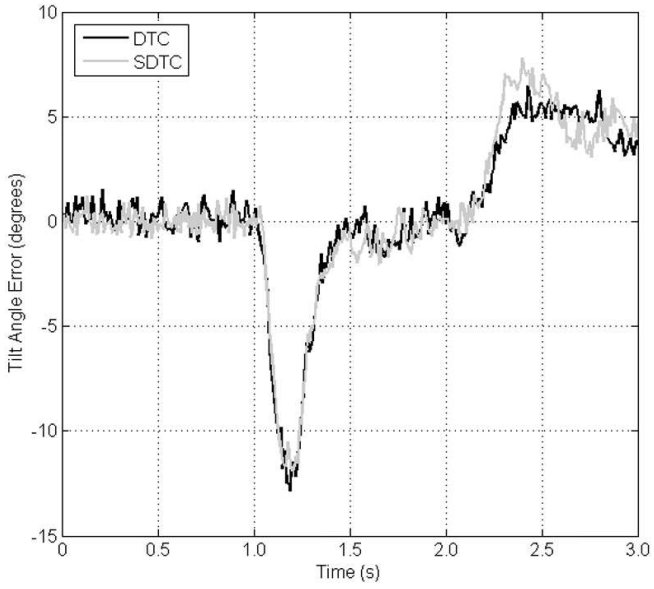

Figure 6.15: 6m/s - Tilt angle error (θ_e) in DTC and SDTC.

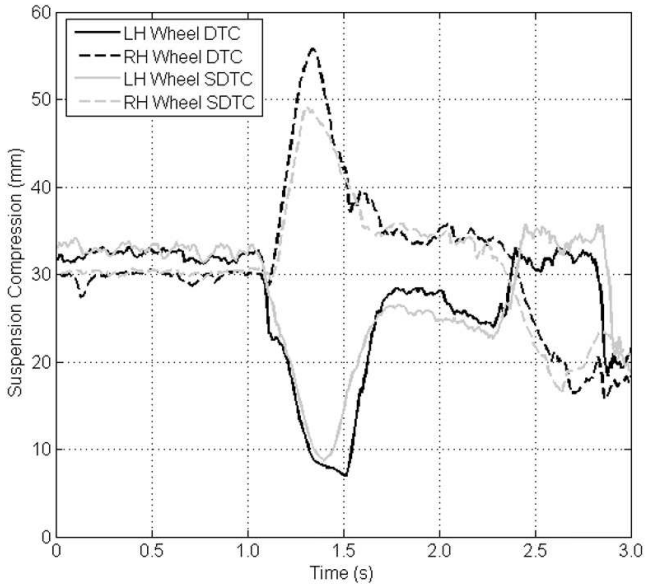

Figure 6.16: 6m/s - Rear suspension positions during the steer input manoeuvre.

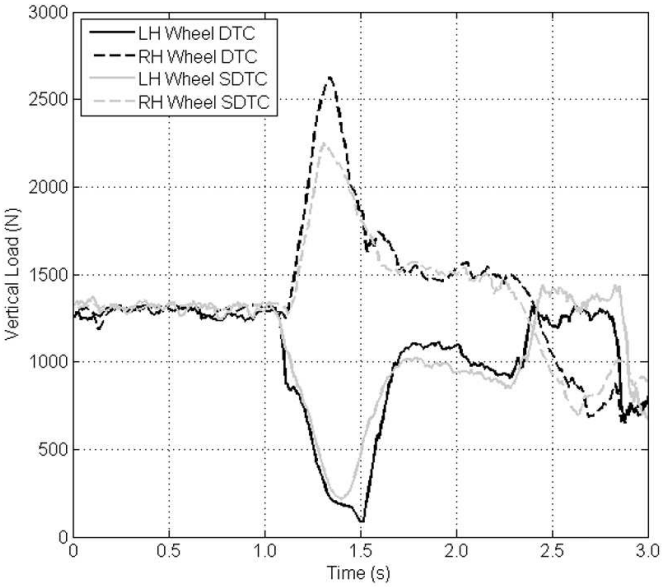

Figure 6.17: 6m/s - Vertical wheel loads estimated from the suspension position data.

6.5.2. Results at 8m/s

Figure 6.18 to Figure 6.25 show the test results recorded at a speed of 8m/s. 42 steer input manoeuvres were conducted in DTC mode and 24 in SDTC mode (Figure 6.18) resulting in peak lateral acceleration demands of between approximately $3m/s^2$ and $5m/s^2$. It is noted that the driver exhibits a tendency to generate larger lateral acceleration demands in SDTC mode than DTC mode despite attempting to remain consistent; it is thought that the reduced steering torque requirement in SDTC mode is responsible. It is also noted that front wheel shimmy is evident in Figure 6.20. Despite efforts to reduce it, some backlash remains in the steering linkages of the prototype CLEVER Vehicle which causes the wheel shimmy phenomena.

As was the case at 6m/s, no countersteering action is generated by the SDTC system in response to the selected steer input at 8m/s (Figure 6.20). However, in this instance, the magnitude of the steer demand (δ_d) is reduced and a larger proportion of it is attenuated momentarily by the active steering (which nears saturation, Figure 6.21). The increased effectiveness of the active steering at 8m/s is also evident in the lateral acceleration curves (Figure 6.19), where the lateral acceleration response in SDTC mode is delayed to a greater extent than was the case at 6m/s. By delaying the onset of the lateral acceleration, the DTC actuators may apply a smaller moment between the tilting cabin and non-tilting rear module whilst achieving a similar tilting response (Figure 6.22).

At a forward speed of 8m/s, when operating in SDTC mode the CLEVER Vehicle shows considerably smaller variations in suspension displacement than occur in DTC mode (Figure 6.24). When comparing the minimum inside wheel vertical loads of 97N and 458N (Figure 6.25) to the nominal 1280N static value, a reduction in wheel load variation from 1183N to 822N is observed. This represents a 29% reduction in the load transfer in the SDTC case. Since the tilt response remains similar in both the DTC and SDTC cases (Figure 6.22 & Figure 6.23), the reduced load transfer must result from the lower tilt moment generated by the DTC actuators, rather than from any greater balancing action of the tilted cabin mass.

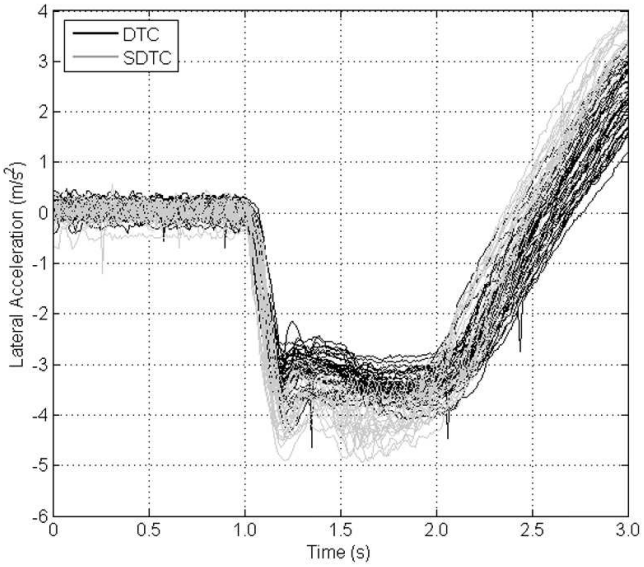

Figure 6.18: 8m/s - Lateral acceleration demand curves for 42 steer inputs in DTC mode and 24 steer inputs in SDTC mode.

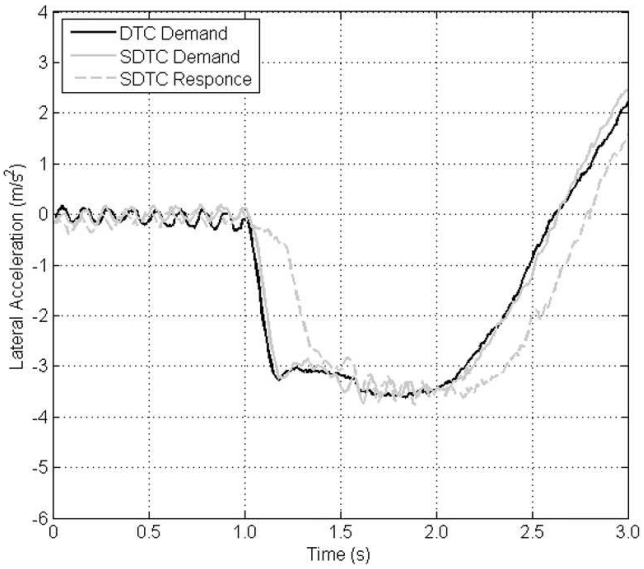

Figure 6.19: 8m/s - Lateral acceleration demand in the selected DTC and SDTC cases, and the resulting lateral acceleration response in the SDTC case.

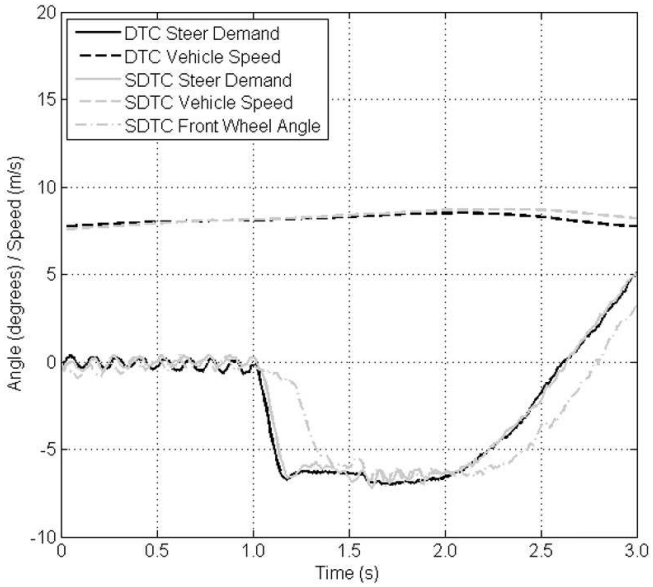

Figure 6.20: 8m/s - Steer demand (δ_d) and speed (U) inputs for both DTC and SDTC cases, and the resulting front wheel steer angle (δ_f) in the SDTC case.

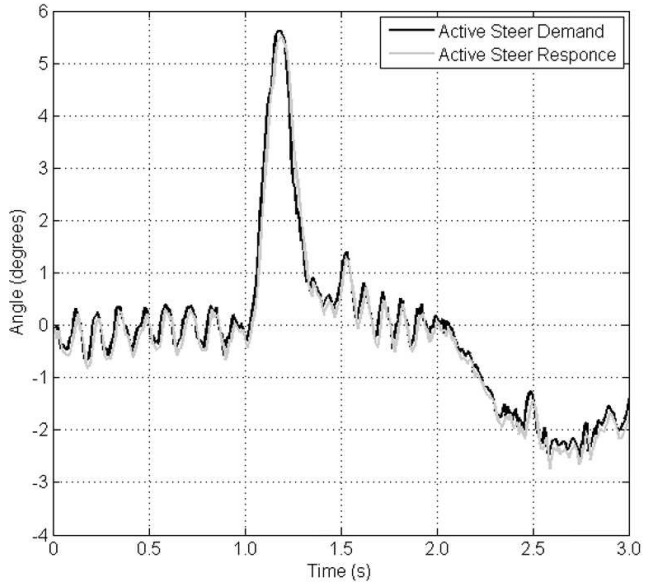

Figure 6.21: 8m/s - Active steer demand (δ_{das}) and response (δ_{as}) in SDTC mode.

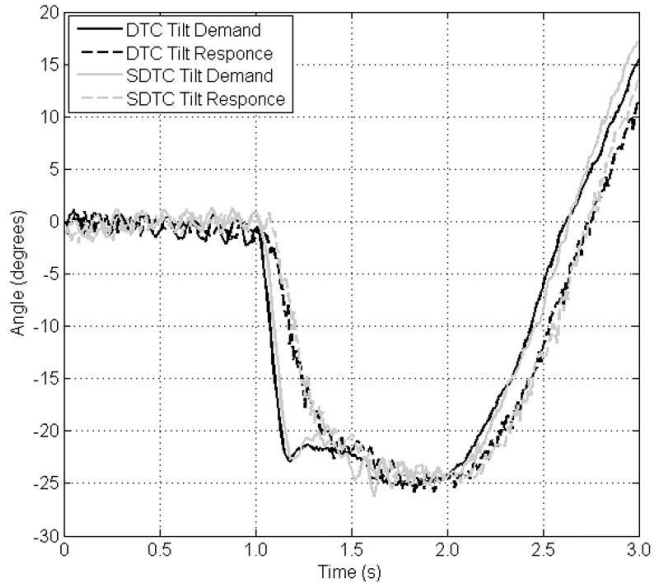

Figure 6.22: 8m/s - Tilt angle demand (θ_d) and response (θ) in DTC and SDTC cases.

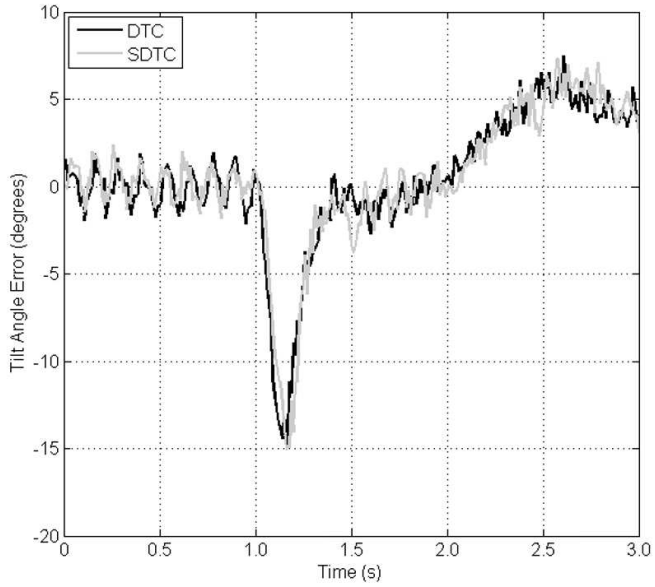

Figure 6.23: 8m/s - Tilt angle error (θ_e) in DTC and SDTC.

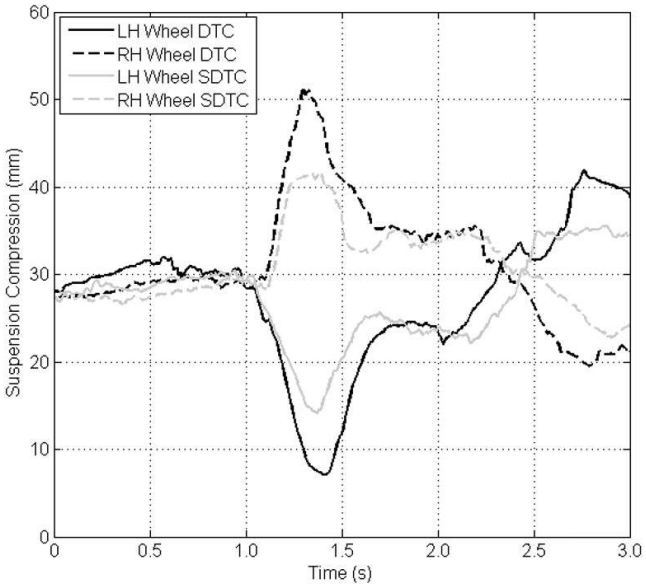

Figure 6.24: 8m/s - Rear suspension positions during the steer input manoeuvre.

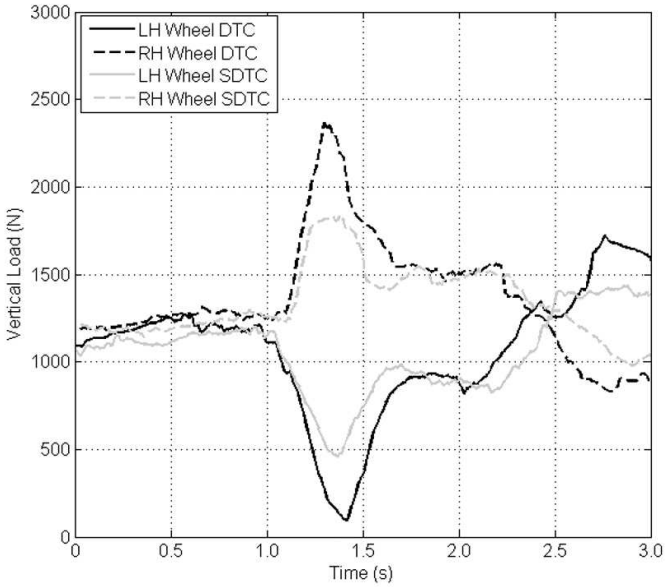

Figure 6.25: 8m/s - Vertical wheel loads estimated from the suspension position data.

6.5.3. Results at 10m/s

Figure 6.26 to Figure 6.33 show the test results recorded at a speed of 10m/s. 37 steer input manoeuvres were conducted in DTC mode and 32 in SDTC mode. As was noted at 8m/s, the lateral acceleration demand generated by the driver at 10m/s in SDTC mode is generally larger than that generated in DTC mode (Figure 6.26). In SDTC mode, lateral acceleration demands of up to 6m/s^2 were generated without rollover; in the DTC mode the lateral acceleration demand was normally limited to approximately 4m/s^2. On two occasions the driver generated a lateral acceleration demand significantly exceeding 4m/s^2 in DTC mode which lead to his having to take corrective action as the vehicle approached roll-over. On these occasions the lateral acceleration curves can be seen to rise rapidly at t≈1.6s and t≈1.9s.

In the two cases selected for comparison, the lateral acceleration demand (Figure 6.27) reached a peak value of approximately 4m/s^2. The lateral acceleration response in SDTC mode was delayed by approximately 0.25s as a result of the active steering action (Figure 6.28). Despite the reduced active steering gain at 10m/s (see Chapter 4), the active steering angle (δ_{as}) is seen to saturate (Figure 6.29). The higher vehicle speed results in a larger tilt angle demand (θ_d) and rate, and consequently an increased tilt angle error (θ_e) (Figure 6.31). Once again, the tilting response was similar in both DTC and SDTC modes (Figure 6.30).

Figure 6.32 and Figure 6.33 show a significant reduction in the suspension position and wheel load variations that occur during the ramp steer manoeuvre when in SDTC mode. In this mode the inside wheel experiences a minimum load of 560N, during the same manoeuvre conducted in DTC mode the minimum load is 79N. If the wheel load variations from the nominal static load of 1280N are considered, the 720N variation in SDTC mode represents a 40% reduction from the 1201N variation that occurs in DTC mode.

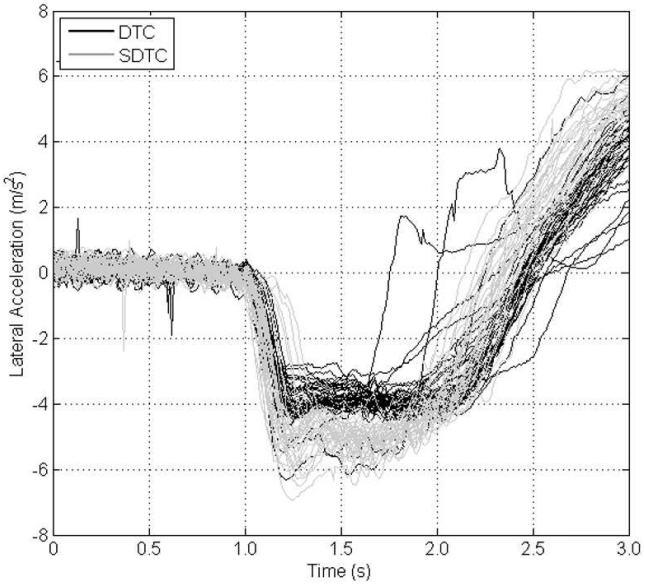

Figure 6.26: 10m/s - Lateral acceleration demand curves for 37 steer inputs in DTC mode and 32 inputs in SDTC mode.

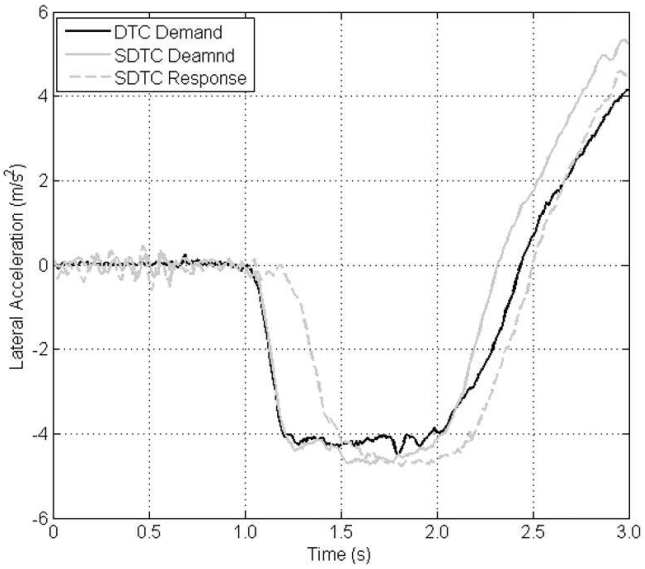

Figure 6.27: 10m/s - Lateral acceleration demand in the selected DTC and SDTC cases, and the resulting lateral acceleration response in the SDTC case.

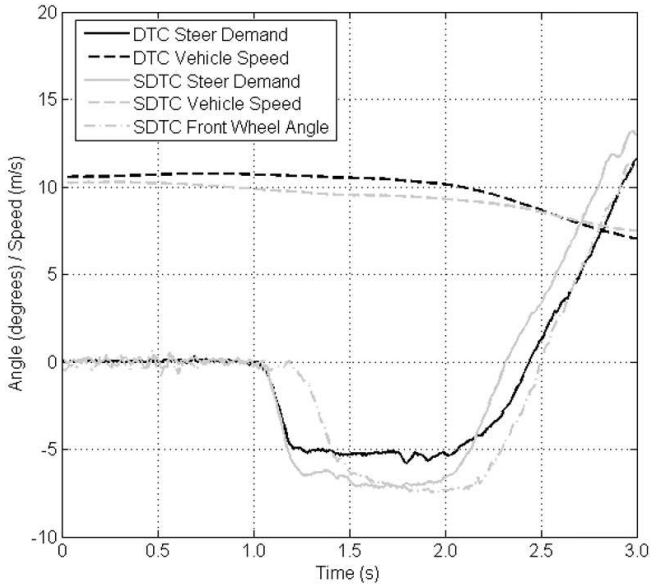

Figure 6.28: 10m/s - Steer demand (δ_d) and speed (U) inputs for both DTC and SDTC cases, and the resulting front wheel steer angle (δ_f) in the SDTC case.

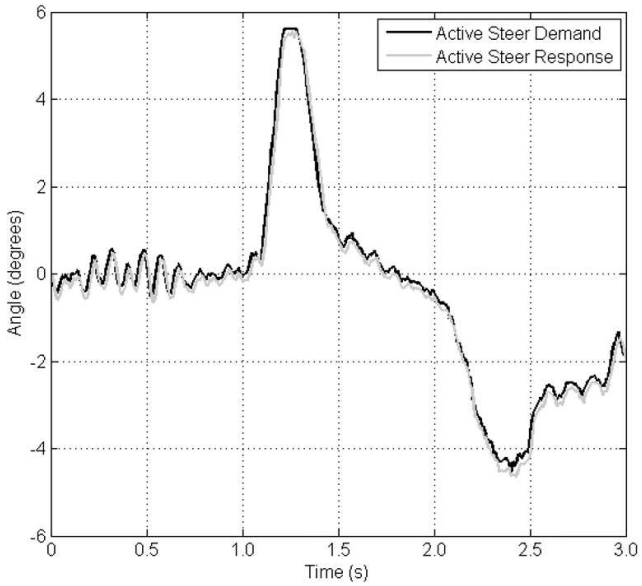

Figure 6.29: 10m/s - Active steer demand (δ_{das}) and response (δ_{as}) in SDTC mode.

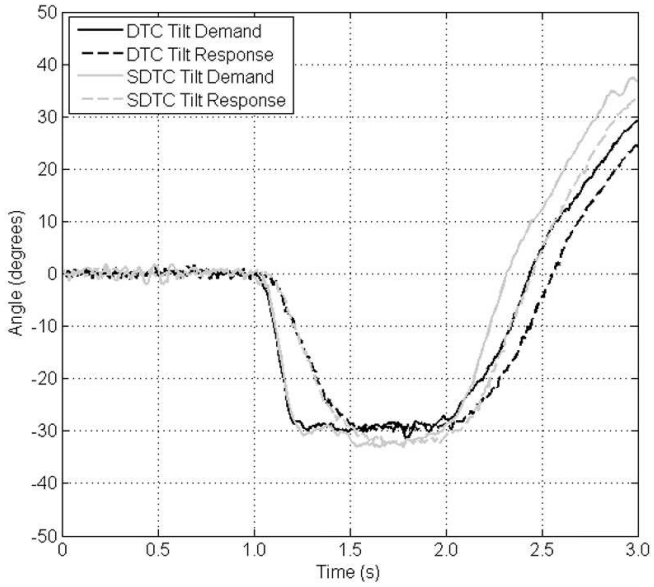

Figure 6.30: 10m/s - Tilt angle demand (θ_d) and response (θ) in DTC and SDTC cases.

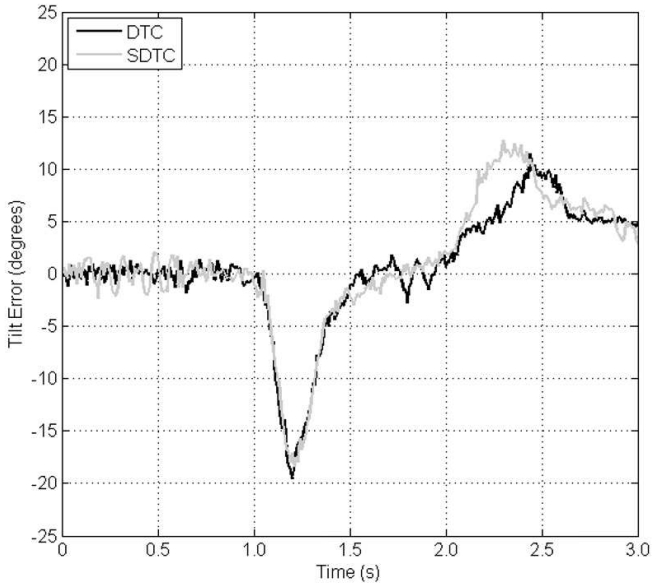

Figure 6.31: 10m/s - Tilt angle error (θ_e) in DTC and SDTC.

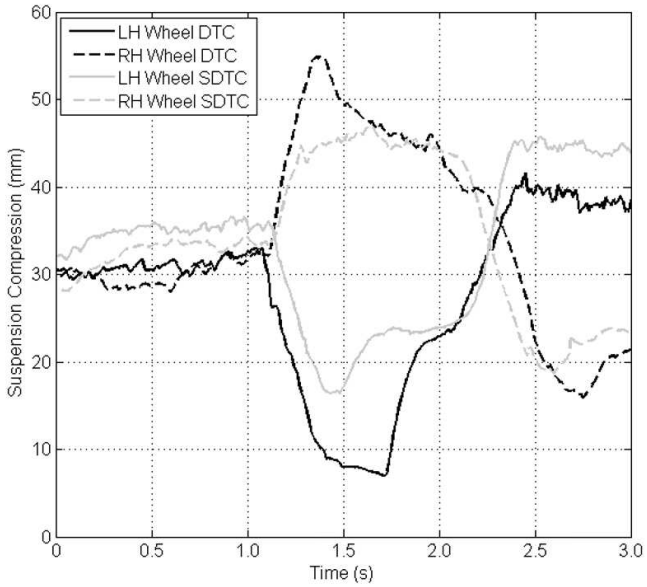

Figure 6.32: 10m/s - Rear suspension positions during step manoeuvre.

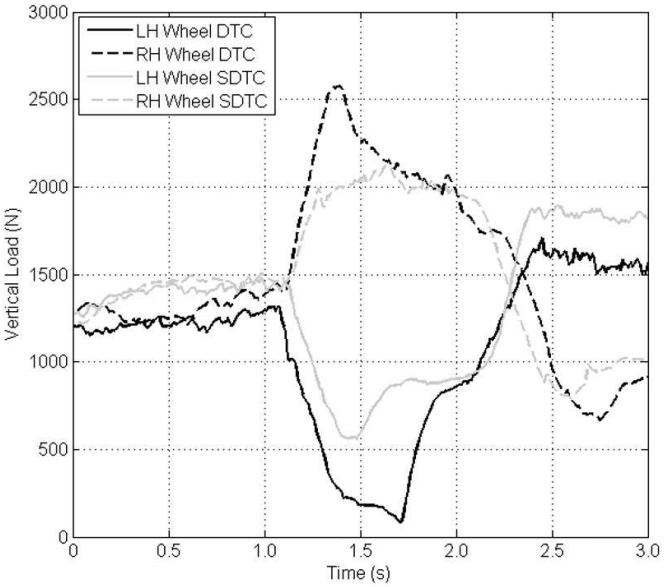

Figure 6.33: 10m/s - Vertical wheel loads estimated from the suspension position data.

6.6. Slalom Manoeuvre Results

A series of slalom manoeuvres were performed at a speed of approximately 8m/s in both DTC and SDTC modes. The slalom course was laid out with cones placed in a straight line and spaced approximately 8m apart. The driver then guided the CLEVER Vehicle to the alternate side of each cone. In a slalom situation, with its repeated switching between right and left hand lateral accelerations, the cabin roll inertia is expected to significantly influence the rear wheel loads, and thus the vehicle stability.

The test was performed 7 times in DTC mode and 11 times in SDTC mode and, as was the case with the step input experiments in Section 6.5, the two tests with the closest lateral acceleration demand curves were chosen for comparison. Figure 6.34 shows the lateral acceleration demand in the selected DTC and SDTC cases; also shown is the lateral acceleration response in SDTC mode. It is noted that the lateral acceleration demand in the SDTC case is higher, and of steeper gradient, than in the DTC case. Given that the same course was completed at approximately the same speed in both cases, the difference in the lateral acceleration demand curves may be attributed to either the driver having to use larger steer inputs in SDTC mode to compensate for the influence of the active steering on the vehicle trajectory (see Chapter 7), or increased driver confidence in the vehicle's stability in SDTC mode inadvertently leading to the use of a more aggressive driving style.

The driver's steer and speed inputs are shown in Figure 6.35, along with the resulting front wheel steer angle in the SDTC case. Thanks to the active steering, the front wheel steer angle lags the steer demand providing additional time for the cabin to tilt before the lateral acceleration is generated. The active steering angle is shown to track the demand well in Figure 6.36; saturation of the ±5.6º limits is evident at t≈1.3s. The large active steer angle is associated with the large tilt angle error that occurs in the SDTC case, Figure 6.37 and Figure 6.38. Whilst the tilt angle error in the SDTC case is larger, this does not indicate a slower tilting response. Rather, it is as a consequence of the larger steer demand angle rate (i.e. the gradient of the steer demand curve, Figure 6.35) generated by the driver in SDTC mode and the resulting lateral acceleration demand rate.

The wheel load plot, Figure 6.39, demonstrates that, despite the disparity in steer inputs, the vehicle is more stable in SDTC mode than DTC mode. Had the steer inputs in the two modes have been equivalent, a larger difference in wheel loading would be expected.

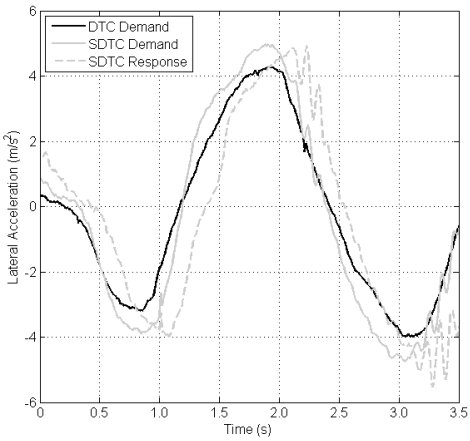

Figure 6.34: Lateral acceleration demand in DTC and SDTC, and the resulting lateral acceleration in SDTC.

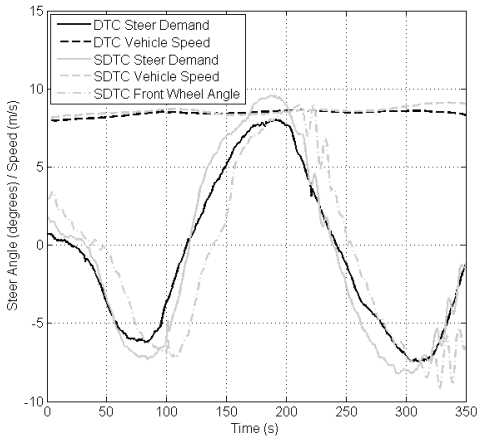

Figure 6.35: Steer demand (δ_d) and speed (U) inputs for both DTC and SDTC cases, and the resulting front wheel steer angle (δ_f) in the SDTC case.

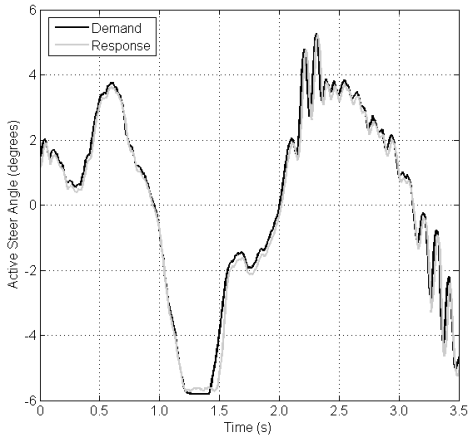

Figure 6.36: Active steer demand (δ_{das}) and response (δ_{as}) in SDTC mode.

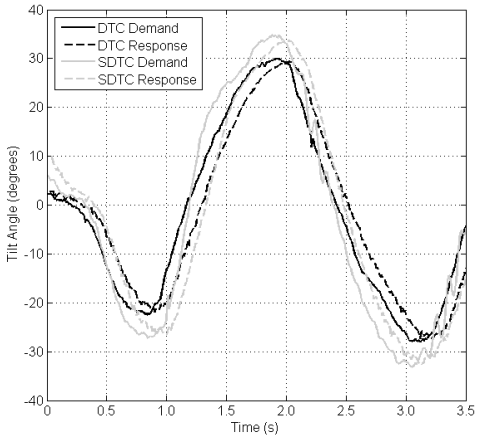

Figure 6.37: Tilt angle demand (θ_d) and response (θ) in DTC and SDTC cases.

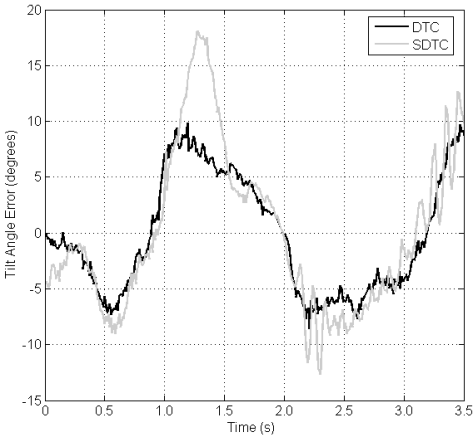

Figure 6.38: Tilt angle error (θ_e) in DTC and SDTC.

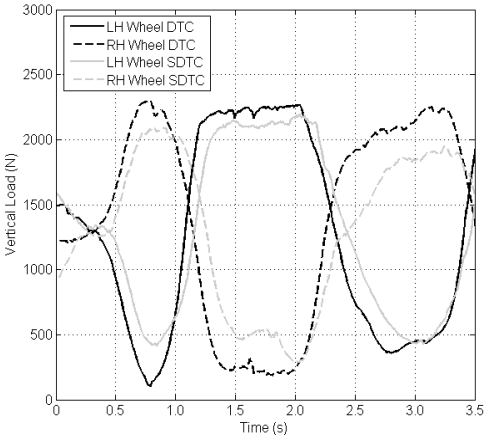

Figure 6.39: Vertical wheel loads estimated from the suspension position data.

6.7. Subjective Observations

During testing of the CLEVER Vehicle, a number of subjective observations were made by the driver.

Firstly, in SDTC mode the steering torque requirement (or steering weight) is reduced considerably. This is thought to be the result of the active steering acting to 'take up' the driver's steer input. This trait was considered a positive one by the driver as it reduced the physical effort required to pilot the CLEVER Vehicle. It was also noted that the driver did not feel significant levels of 'kickback' through the steering wheel from the 'in-series' active steering system, perhaps helped by the use of a worm type reduction steering box.

Despite the data showing no appreciable difference in tilt response, in SDTC mode the driver's perception was that the vehicle responded more quickly than it did in DTC mode. This may be due to a reduction in the rear module roll rate, and the associated increase in the true tilt angle rate that results. It may also result from the reduced steering torque requirement (described above) allowing larger, faster steer inputs to be made.

Delays in generating lateral acceleration, introduced by the active steering system in SDTC mode, felt like mild transient understeer. This is considered an acceptable characteristic as most drivers are familiar with a vehicle which understeers and the short duration of the sensation did not notably inhibit the driver's ability to control the vehicle's heading.

6.8. Concluding Remarks

This chapter provides experimental results showing the effectiveness of a combined Steering Direct Tilt Control system during both quasi-steady-state and highly transient manoeuvres. Suspension position data is used to estimate the vertical loads supported by each of the two rear wheels and therefore quantify the vehicle's roll stability.

In the quasi-steady-state and low transience U-turn manoeuvres, the tilt angle errors were small and the SDTC system behaved in the same way as a DTC system; no quantifiable stability improvement could be shown. The SDTC strategy is of course not intended to enhance the vehicle stability under these conditions.

Highly transient ramp steer input tests were performed at three different speeds and the effectiveness of the SDTC system was shown to vary as a function of speed. At lower speeds the stability improvement offered by the SDTC system over the DTC system was

small. However, small increases in the vehicle's forward speed yielded significant reductions in the wheel load variation experienced in SDTC mode. At 10m/s the wheel load variation in SDTC mode was 40% lower than that recorded in DTC mode, significantly enhancing the vehicle's roll stability.

In the slalom test, the SDTC strategy was shown to provide a modest improvement in roll stability despite the driver generating larger, faster, steer inputs. Because of the discrepancy in the steer inputs, the stability improvement could not be accurately quantified.

The improvements in transient roll stability occurred despite no countersteering action being achieved in any of the tests; rather, the active steering system reduced or delayed the steer inputs. Results published by Furuichi *et al.* [40] have shown that, whilst introducing a simple lag in the front wheel steer angle response improves NTV stability significantly, achieving a counter steering action leads to a faster tilting response and enhances stability yet further. There may be scope to increase the countersteering gains used on the CLEVER Vehicle to realise improved roll stability; this possibility is investigated in Chapter 7. Even without generating countersteer, the delay in the front wheel steer angle response provides the DTC actuators with an opportunity to begin tilting the cabin before large lateral accelerations are generated. This in turn reduces the moment applied to the rear module thus improving roll stability.

Finally, this chapter presents the subjective assessment that the driving characteristics of a Narrow Tilting Vehicle are not unacceptably compromised, and are in some ways enhanced, by the use of a Steering Direct Tilt Control strategy.

Chapter 7. Path Following Performance of a Steering Direct Tilt Control System

A feature common to both Steering Tilt Control (STC) and Steering Direct Tilt Control (SDTC) systems is the generation of a countersteering action in the early stages of a manoeuvre, [4] [33]. Countersteer, and other stabilising variations to the front wheel steer angle, may impact upon the trajectory followed by a STC or SDTC equipped vehicle in response to a series of steer inputs.

This chapter builds upon results published by Robertson *et al.* [58] and uses both simulation and experimental techniques to examine the extent of the SDTC system's impact on the vehicle's path, and whether a human driver is then able to adapt his or her steer inputs to compensate. The influence of the active steering gain on the vehicle's trajectory will also be examined.

7.1. Lane Change Manoeuvre Simulations

This section will use the CLEVER Vehicle simulation model introduced in Chapter 5 to compare the path followed, in response to a series of steer inputs, in Direct Tilt Control (DTC) mode and in SDTC mode. Furthermore, the affect on vehicle roll stability, when revised steer inputs are used to maintain acceptable path following, is investigated. Finally, the influence of higher DTC system gains on the performance of a SDTC system is considered.

Simulations were performed of the CLEVER Vehicle negotiating a path through a 'Lane Change Manoeuvre' or 'Elk Test' to BS ISO 3888-2:2002 [59]. This test was chosen as it is used widely in the automotive industry and encompasses transient behaviour; particularly rapid changes of direction that result in high lateral load transfers, known to be a weakness of the CLEVER Vehicle DTC system design.

BS ISO 3888-2:2002 describes a course to be laid out with cones on a suitable expanse of tarmac; the width of the course is a function of the vehicle width and differs in each section. In order to ensure that the CLEVER Vehicle remains within the track boundary, an additional boundary has been introduced half a vehicle width inside the cones to constrain the position of the rear module centre of gravity (CG_r), Figure 7.1.

7.1.1. Influence of Active Steering on Vehicle Trajectory

With the active steering system disabled (DTC mode), a series of steering inputs was empirically derived that would ensure that the CLEVER Vehicle successfully negotiated a path through the BS ISO 3888-2:2002 test at a speed of 10m/s (36km/h), Figure 7.1. Steering inputs were defined as a series of straight line ramp inputs which were then passed through a first order lag transfer function to smooth the transitions.

The simulation was then repeated in SDTC mode with the same steer inputs as the DTC example; this is termed the 'SDTC-Uncorrected' case. The resulting path followed by CLEVER was found to breach the track boundary by a significant margin. The difference in the two paths followed, with and without active steer, in response to the same steering inputs is significant. It highlights the fact that the presence of active steer means a driver must modify his/her steering inputs to some extent in order to maintain trajectory tracking performance.

A third simulation, the 'SDTC-Corrected' case, was conducted with the steer inputs adjusted such that CLEVER remained within the track boundaries with active steering engaged and followed a path similar to the DTC case.

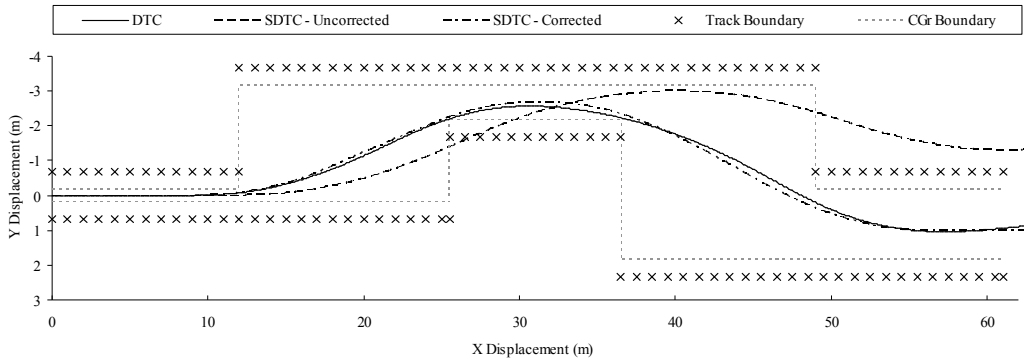

Figure 7.1: BS ISO 3888-2:2002 test track with CLEVER CG_r path.

Figure 7.2 is a plot of the front wheel steer angle (δ_f) and, where applicable, the corresponding demand steer angle (δ_d). The front wheel steer angle that allowed CLEVER to successfully negotiate the lane change test in the DTC case forms the demand signal in the SDTC-Uncorrected case; the SDTC-Uncorrected output can be seen to lag the demand as a result of the countersteering action.

The SDTC-Corrected demand leads both the uncorrected demand and the corrected output, thus counteracting the lag generated by the countersteering action of the active steering system. This is akin to the driver of the vehicle looking ahead and anticipating the required steer inputs some time in advance. Peak steer angle values, demand and

output, are higher in the SDTC-Corrected case. These higher values are required to offset the influence the stabilising countersteer has on the vehicle's yaw angle and resulting lateral displacement. In the SDTC-Corrected case some saturation of the active steering system's stroke limits is evident in the front wheel steer angle curve, notably between 1.7s and 2.2s. In these circumstances, a steering system subject to higher saturation limits would result in larger countersteering actions, and consequently, a different vehicle trajectory.

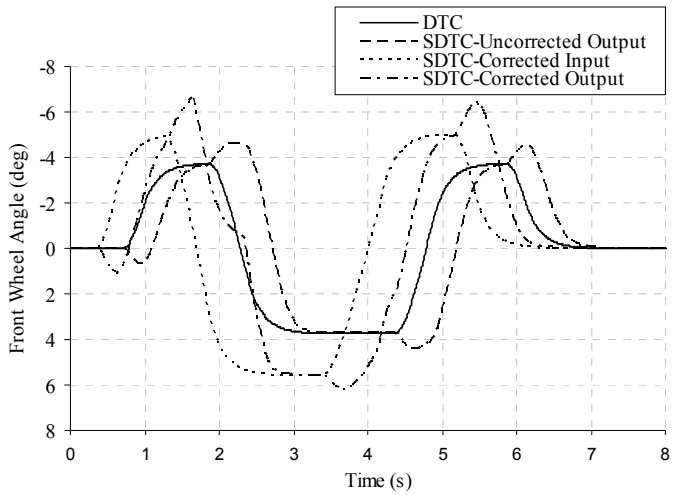

Figure 7.2: Steer demand and response curves for DTC, SDTC-Uncorrected and SDTC-Corrected cases.

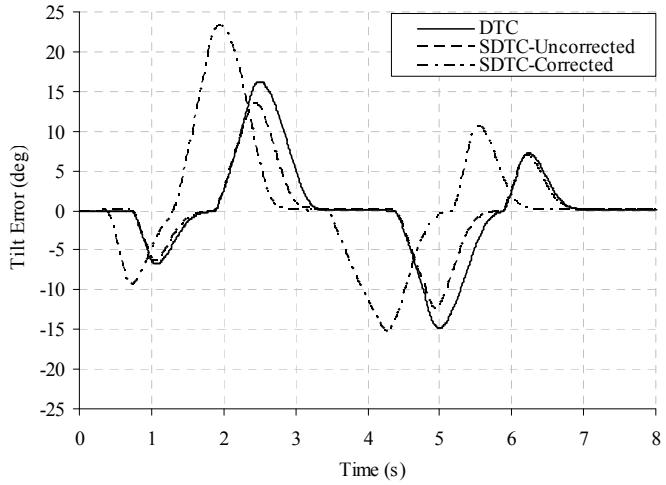

Figure 7.3: Tilt angle error in DTC, SDTC-Uncorrected and SDTC Corrected cases.

Figure 7.3 is a plot of the tilt angle error (θ_e) variation with respect to time. The tilt angle error in the SDTC-Uncorrected case peaks at a lower value than in the DTC case. Since the demand tilt angle is the same in both the DTC and SDTC-Uncorrected cases, the reduced tilt angle errors may be attributed to the additional contribution of the countersteering action to the total tilting moment. In contrast, the SDTC-Corrected case

results in significantly higher peak tilt angle errors, a consequence of the larger steer demands required to maintain trajectory control in the presence of countersteer. Since the active steering system's influence on the front wheel angle is a function of tilt angle error, it is these large tilt angle errors that generate the large countersteering actions visible in Figure 7.2.

The enhanced stability of the SDTC system can be demonstrated with a plot of the vertical load carried by each of the rear wheels, Figure 7.4 & Figure 7.5. In a perfectly balanced situation, such as straight line running, each of CLEVER's rear wheels carry a vertical load of approximately 1280N; a load of zero would indicate that the tyre has lifted clear of the ground.

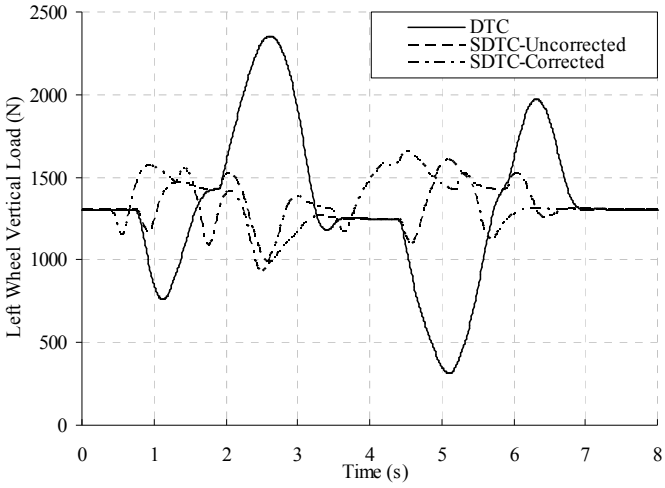

Figure 7.4: Left wheel vertical load in each of the three cases.

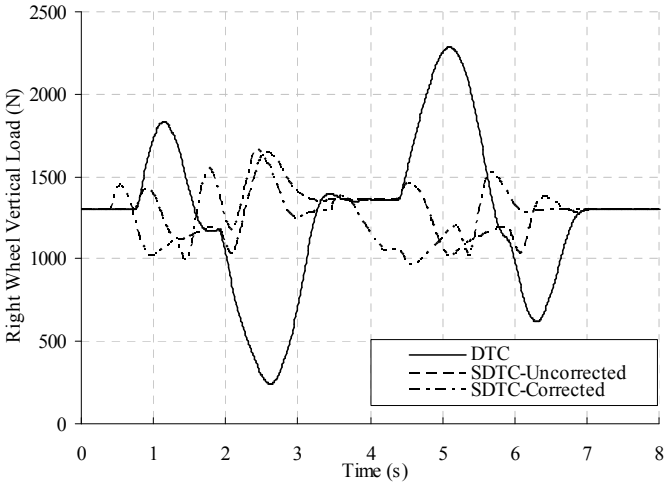

Figure 7.5: Right wheel vertical load in each of the three cases.

There are significant differences in the vertical wheel load variations that occur in the DTC case and the two SDTC cases. Without active steering, the vertical load on the left hand wheel reaches a minimum of approximately 300N during the lane change manoeuvre. With active steering, even with the more severe steer demands of the SDTC-Corrected case, the minimum load does not drop below 900N.

Fundamental to the operation of a DTC system is the torque applied between the tilting and non-tilting parts. In the case of CLEVER, this torque must be reacted by the roll stiffness and inertia of the rear module. In addition, there is an overturning roll moment induced by the lateral acceleration, the module's mass, and its centre of gravity height that also contributes to the reduction of the inside wheel vertical load. The active steering system's principal contribution to stability is to lower the moment produced by the DTC actuators during cabin tilting movements.

The larger steering inputs of the SDTC-Corrected case do not lead to significantly lower vertical wheel loads when compared to the SDTC-Uncorrected case; this can be explained by examining the timing of the peaks in Figure 7.2 and Figure 7.3. Thanks to the active steering system's ability to delay steer outputs, and the anticipatory nature of the steer inputs, the tilt angle error peaks occur before large amounts of front wheel steer angle and large lateral forces are generated.

Given the large reductions in rear wheel vertical load variation in both the SDTC-Uncorrected and SDTC-Corrected cases, active steering can be said to be a significant aid to stability in transient situations, even when path following is maintained.

7.1.2. Influence of Tilt Controller Gain on Trajectory

All simulations conducted previously in this chapter have utilised a PID controller in the DTC component of the tilt system with P, I, and D gains of 1, 0, and 0 respectively. Increasing the DTC system gains is likely to reduce the tilt angle error and active steering angle, and may lead to reduced vehicle stability.

Given that the SDTC system is expected to produce differing countersteering actions for each tilt gain examined, altered steer inputs would be required to keep the CLEVER Vehicle within the track boundary for each case. In the interests of providing a consistent basis for comparison, SDTC-Corrected steer inputs are not used in this section. Instead, the following results were obtained using the DTC steering inputs from Figure 7.2.

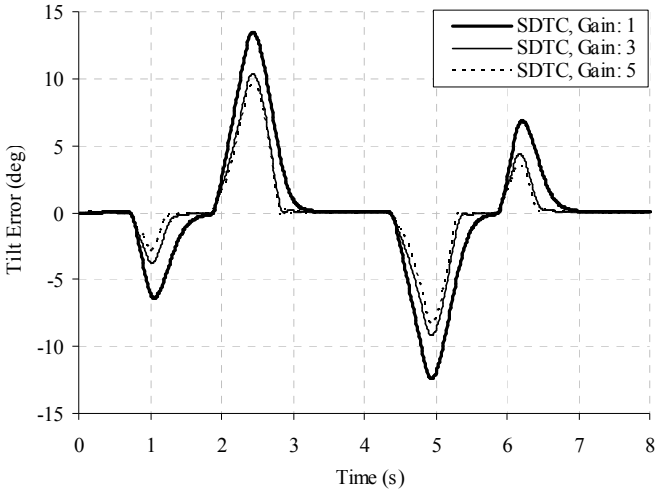

Figure 7.6: Tilt angle error with differing tilt controller gains.

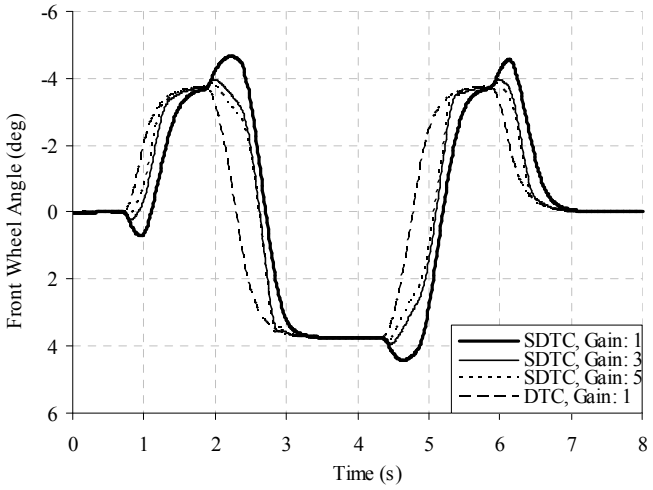

Figure 7.7: Front wheel steer angle response with differing tilt controller gains.

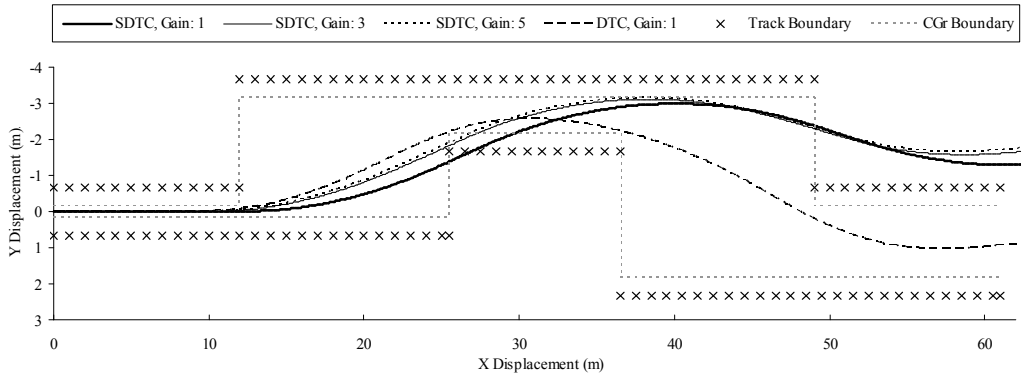

Figure 7.8: Path followed in response to DTC steer inputs with differing tilt controller gains.

Figure 7.6 illustrates that tilt angle error is considerably reduced by increasing the proportional tilt gain (in the DTC PID controller) from 1.0 to 3.0; a further increase in the gain from 3.0 to 5.0 yields a considerably smaller reduction in error. Simulations of further increases in tilt gain were performed; these yielded only very limited reductions in error and are omitted from the figure.

Since the active steering system's influence on the front wheel angle is a function of tilt angle error, it therefore follows that increased tilt gain results in reduced countersteering effect and a more immediate steering response. Figure 7.7 illustrates that both the amplitude and duration of countersteering actions do indeed reduce significantly as the tilt gain rises.

The impact of the reduced countersteering action upon the path followed by CLEVER is illustrated in Figure 7.8. Whilst increasing the tilt gain results in little improvement in the vehicle's position in the X≈50-60m region, it is worthy of note that Y displacement here is the cumulative result of a series of steering inputs. If the Y position is considered after a single steer input, X≈26m, significant improvement is shown. In the case of a vehicle being driven by a human driver, constant corrections are made in the form of steering inputs thus preventing the accumulation of multiple errors. The improved response to a single steer input may have a more significant positive effect upon the driver's ability to successfully navigate a path than is immediately apparent from Figure 7.8.

It is reasonable to assume that increased tilt gains, and reduced countersteering actions, will result in larger tilting moments being generated by the DTC component of the SDTC system; the associated variations in rear wheel loading could potentially have a negative impact upon the vehicle's stability. Figure 7.9 and Figure 7.10 are plots of the vertical load carried by the left and right hand rear wheels during the lane change manoeuvre for each of the tilt gains.

When operating in SDTC mode, vehicle stability is significantly better than in the DTC case, even when higher tilt controller gains are used. Whilst raising the tilt controller gains in SDTC mode does lead to a small decrease in stability, the deviation from the driver's intended path is reduced. The reduced deviation from the intended path may in turn lead to smaller steer inputs being generated by a human driver.

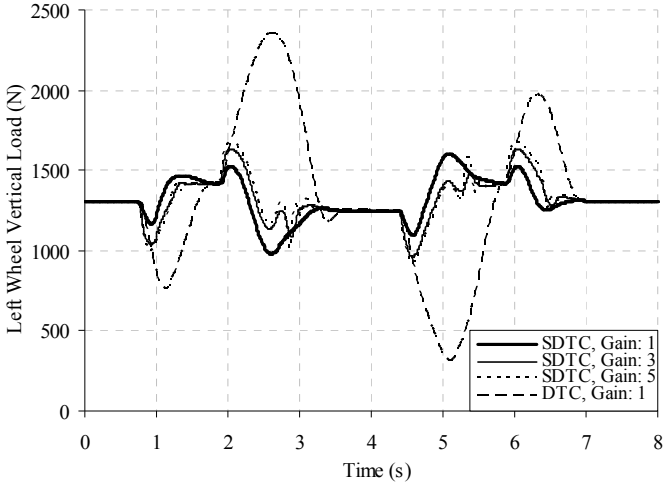

Figure 7.9: Left wheel vertical load with differing tilt controller gains.

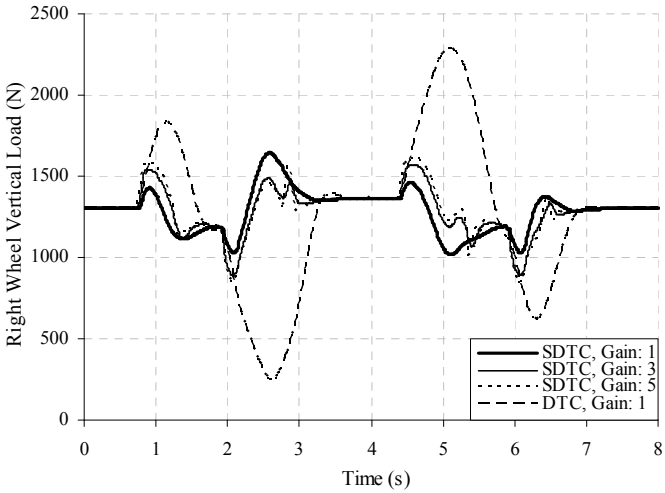

Figure 7.10: Right wheel vertical load with differing tilt controller gains.

7.2. Experimental Verification of Path Following Performance

Although the previous section has shown in simulation that the steer inputs required to successfully follow a path in SDTC mode differ from those used in DTC mode, the question of whether a human driver would be able to generate the necessary steer inputs has not been addressed. In this section a series of lane change experiments are performed using the prototype CLEVER Vehicle to examine the interaction between a human driver and the Steering Direct Tilt Control system.

7.2.1. Methodology

Given the difficulty of recording the path followed by the CLEVER Vehicle with sufficient precision, and that a steering robot was not available to provide consistent steer inputs, rather than log the path followed in response to a defined steer input, a path was defined and the steer inputs required to navigate it were logged.

The chosen path was a lane change manoeuvre (Figure 7.11) similar to that used in the simulations presented earlier in this chapter, but with the following alterations. In the interests of simplicity, and because of space constraints, only the first half of the manoeuvre was performed (i.e. the vehicle changed lane, but did not then return to the original lane). In addition, the lane widths were kept constant at 1.2m throughout to more precisely define the path and ensure consistency.

A series of three 'gates' were used to define the path, with small cones forming the boundaries between gates (Figure 7.12). Whilst the position of the gates was pre-determined by BS ISO 3888-2:2002, the intermediate cones were placed 0.6m either side of what the driver considered to be the 'natural line' between gates.

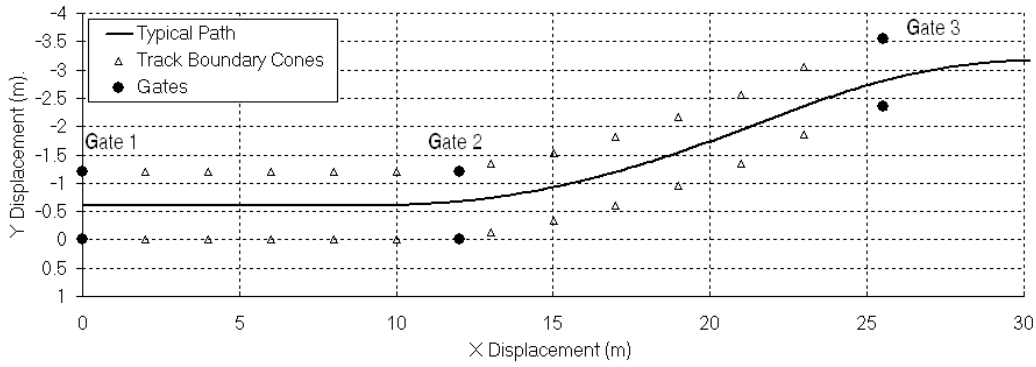

Figure 7.11: Test track layout.

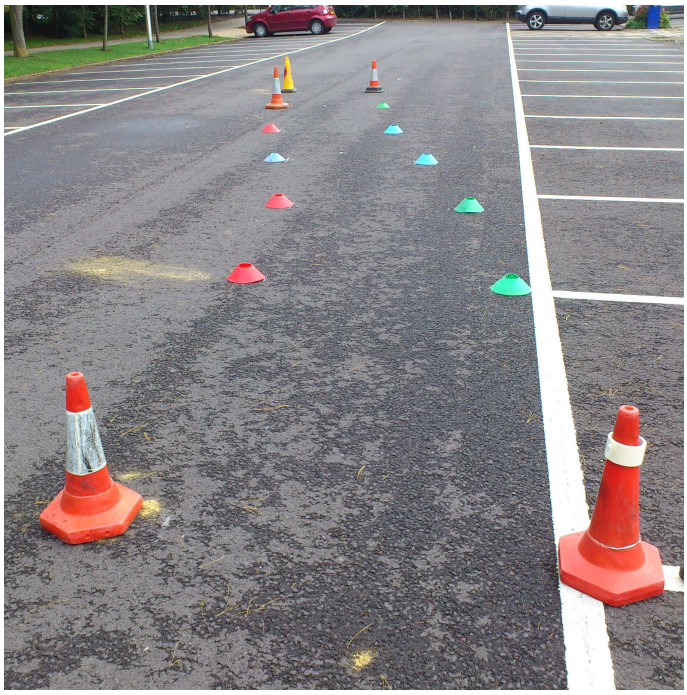

Figure 7.12: Test track with gates 2 (tall cones in foreground) and 3 (tall cones in distance) visible.

With the track defined, 24 attempts at the manoeuvre were performed in DTC mode and a further 29 in SDTC mode. In each mode, ten of the attempts were considered successful with no cones being hit. Data from the ten successful manoeuvres completed in each controller mode was averaged to reduce the influence of the inevitable variations in the human driver's steer and speed inputs on the results. The averaging process also had the benefit of smoothing the curves in a similar manner to filtering.

7.2.2. Results

The driver's steer inputs in the ten successful DTC and ten successful SDTC cases are shown in Figure 7.13. The steer demand in the SDTC case is consistently larger in peak magnitude than the steer inputs used in DTC mode. These larger steer inputs lead to larger lateral acceleration demands, Figure 7.14.

The averaged steer inputs, Figure 7.15, clearly show that in the SDTC case, the driver generates a larger and more rapid steer input. This more vigorous steer input is responsible for the 25% larger peak lateral acceleration demand shown in Figure 7.16. Because of the influence of the active steering, the front wheel steer angle response and the lateral acceleration response in the SDTC case lag the driver's demand. The SDTC steering response is a close match to the DTC steer angle up to t≈1.5s; the SDTC response then exceeds the DTC steer angle, reaching a peak of -6º (as opposed to -4.5º in the DTC case). The steer response in the SDTC case lags the demand, peaking around

0.2s later. This is a consequence of the active steering angle (Figure 7.17) which, when the steer demand rate is reversed in the second phase of the manoeuvre, adopts a negative value.

The steer inputs generated by the human driver in the SDTC case are consistent with the steer inputs derived in the SDTC-Corrected simulations (Figure 7.2), being both larger in magnitude and occurring earlier. Once again, the requirement for the driver to modify his steer inputs to maintain trajectory tracking performance when using a SDTC strategy is demonstrated.

Whilst the tilt angle error in the SDTC case is larger than the DTC case (Figure 7.9), because the demand occurs at an earlier time, the cabin tilting motion is always further advanced (Figure 7.8). The larger tilt angle error in SDTC stems from the more rapid, larger magnitude, steer inputs. Although the faster tilting response should result in improved vehicle stability in the SDTC case, since the tilting motion can begin before large lateral accelerations are generated, Figure 7.20 shows only a very small improvement.

The need for the driver to generate larger and more rapid steer inputs in order to follow his desired trajectory in SDTC mode could be responsible for the modest extent of the stability improvement; however, this effect was small in the SDTC-Corrected simulation case. Rather, the explanation lies within the gentle nature of lane change manoeuvre experiments, the relatively mild steer inputs generated lateral accelerations of only approximately $2m/s^2$. The active steering system's influence over the vehicle's stability is greater at higher speeds and lateral accelerations where it can in effect cap the lateral acceleration response at a safe level. Had a higher speed or more severe steer input been used, a larger difference in stability would be expected between the DTC and SDTC cases.

Finally, whilst the driver of the CLEVER Vehicle did notice the need to generate different steering inputs in the two control modes, after a short period of time the SDTC mode felt natural. This suggests that the ability to control the vehicle's heading does not present a barrier to the adoption of a SDTC strategy on a production vehicle.

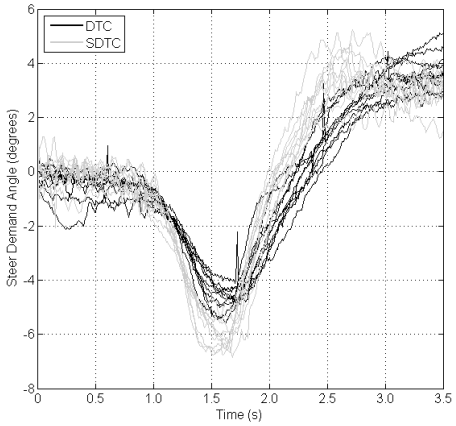

Figure 7.13: Steer demand curves for 10 manoeuvres in DTC mode and 10 in SDTC mode.

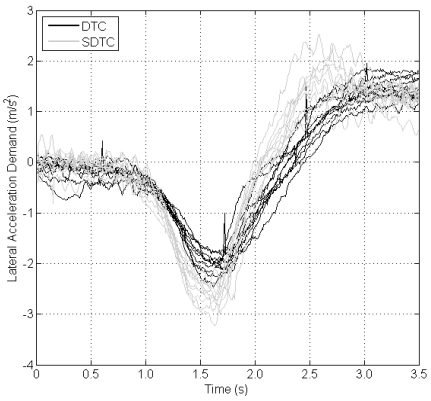

Figure 7.14: Lateral acceleration demand curves for 10 manoeuvres in DTC mode and 10 in SDTC mode.

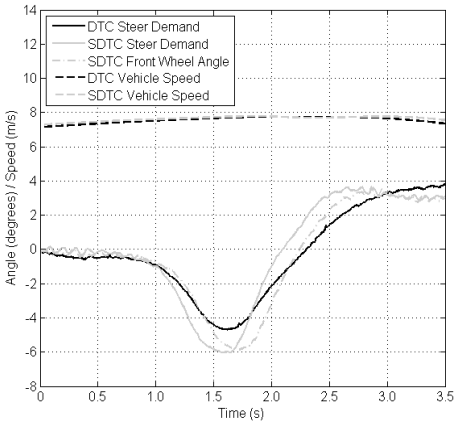

Figure 7.15: Averaged steer and speed inputs in DTC and SDTC modes.

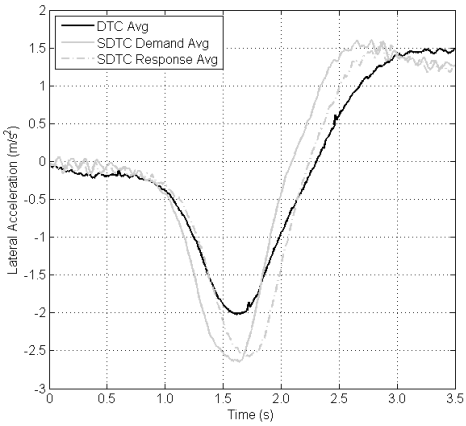

Figure 7.16: Averaged estimated lateral acceleration demand in DTC and SDTC mode and the lateral acceleration response in SDTC mode estimated from the front wheel steer angle response.

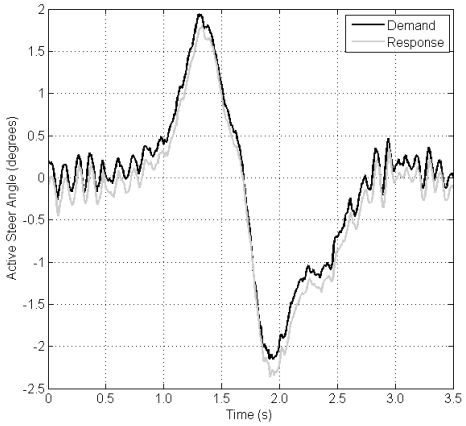

Figure 7.17: Averaged active steer demand and response in SDTC mode.

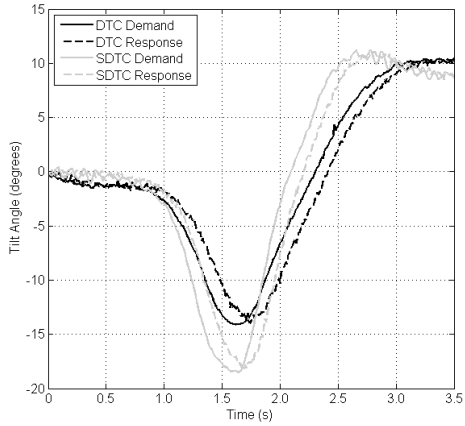

Figure 7.18: Averaged tilt demand and response in both DTC and SDTC modes.

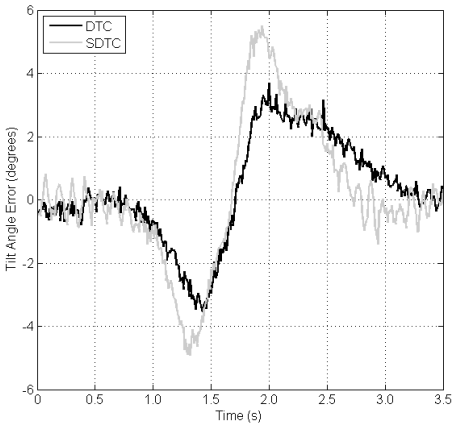

Figure 7.19: Averaged tilt angle errors.

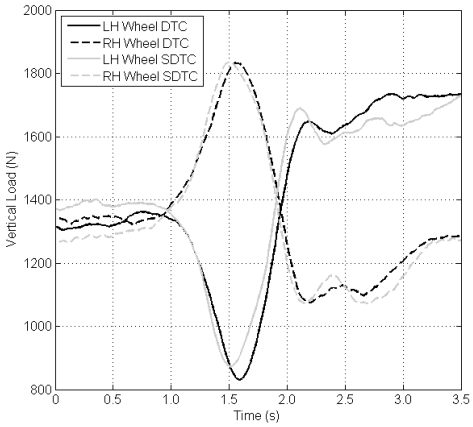

Figure 7.20: Vertical wheel loads estimated from averaged suspension position data.

7.3. Influence of Active Steering Gain on Trajectory

The active steering gain (K_{as}) used in the controller determines the magnitude of the active steering system's response to tilt angle errors and as such, it influences the trajectory followed by the CLEVER Vehicle. In this section, the simulation model of the CLEVER Vehicle was used to investigate the influence of the active steering gain on both path following and the roll stability performance.

Berote [35] derived active steering gain values (Figure 7.21) such that they eliminated overshoot (relative to the steady state value) of the lateral acceleration in response to a specific ramp steer input. It is these gain values which have been used in the simulations conducted so far in this thesis, and which are implemented in the CLEVER Vehicle controller. Berote noted that the 'optimum' gain value reduced at higher speeds where small changes to the front wheel steer angle had a large influence on the lateral acceleration.

The methods employed by Berote to find the optimum gain value were somewhat arbitrary (the over-shoot does not cause a stability issue and its brief duration means it is un-likely to be noticed by the driver), and have been found to be highly dependent on the tilt angle response of the CLEVER Vehicle. Small changes in simulation parameters, such as the DTC system's PID controller gains, result in relatively large changes to the lateral acceleration overshoot (Figure 7.22) and the associated gain values which emerge from Berote's selection process. If the same selection criteria are applied with the increased DTC PID gains of 1.7, 0 & 0.1 (Chapter 4), rather than the 1.0, 0 & 0.1 used by Berote, un-feasibly high active steering gains result.

This section will be used to show trends that occur in response to changes in the active steering gain value, rather than attempt to derive a new set of gain values.

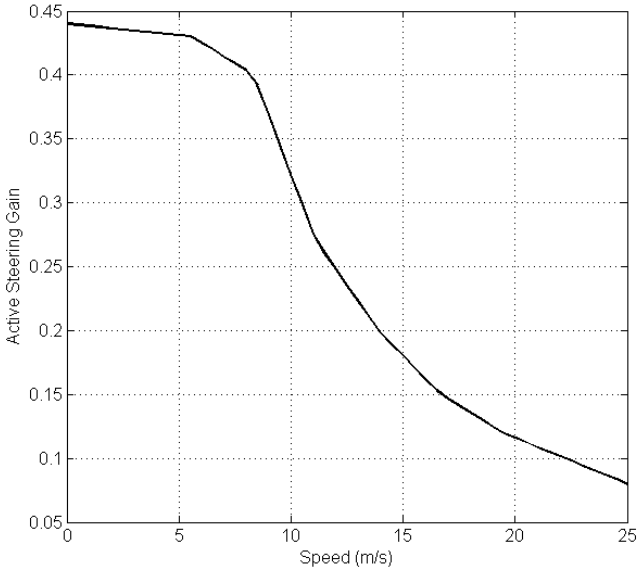

Figure 7.21: Berote's active steering gain curve [35].

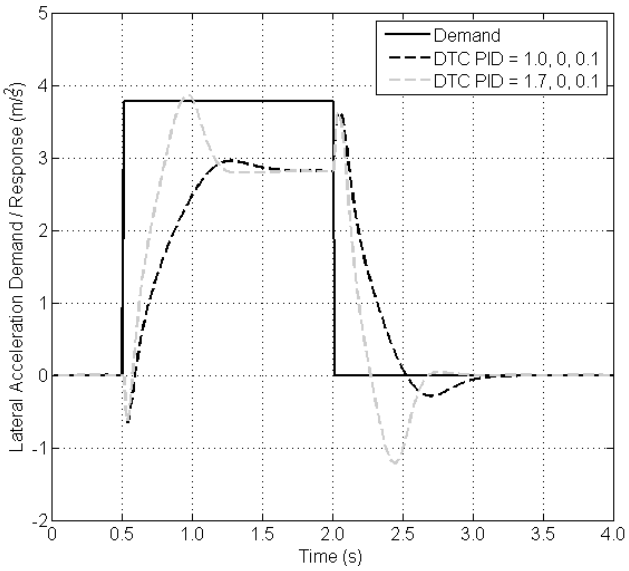

Figure 7.22: Influence of Direct Tilt Control Gains on the lateral acceleration response using Berote's active steering gain curve.

7.3.1. Active Steering Gain Simulations

The following simulations were conducted at a forward speed of 8.33m/s (30km/h) using a ramp steer input of magnitude 7º, occurring over a period of 1s, and filtered at 2Hz to smooth the transitions. The front wheel steer angle response is shown in Figure 7.23. At active steering gain values up to 0.4, no countersteering action is produced but the front wheel steer response is delayed slightly. At larger gain values a momentary countersteering action is evident and a larger delay in the response occurs.

Delaying the front wheel steer angle response has an impact upon the lateral acceleration, Figure 7.24, which is again delayed to a greater extent at higher active steer gain values. The lateral acceleration tends to over-shoot the steady state value briefly towards the end of the 'turn-in' and 'turn-out' phases. This over-shoot is reduced at higher active steer gain values; however, even at values as high as 1.0, some over-shoot remains. By delaying the lateral acceleration response, and generating short duration inverted lateral accelerations, the path followed by the CLEVER Vehicle is affected, Figure 7.25; the active steering system produces an understeer like handling characteristic. The difference in position at the end of the manoeuvre, relative to the non-active steer case, is approximately 2.26m with an active steering gain value of 1.0. Despite the countersteering action, the maximum inverse lateral displacement on turn-in is only 3.6mm. In a more severe manoeuvre, with larger lateral acceleration demand rates and larger tilt errors, a larger inverse lateral displacement would be expected.

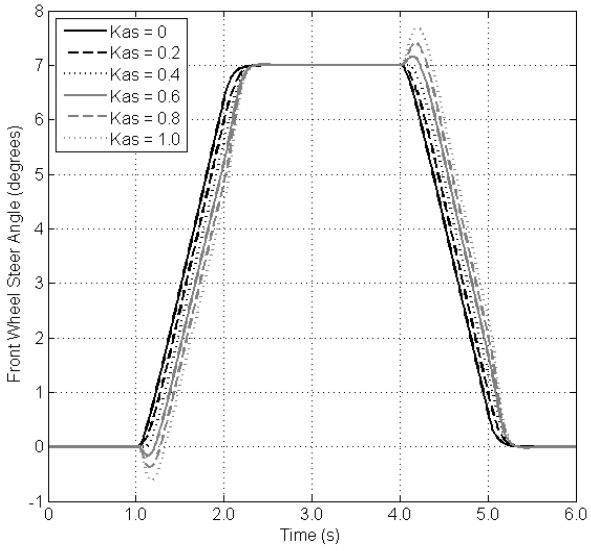

Figure 7.23: Front wheel steer angle during corner entry and exit manoeuvre with varying active steering gain values.

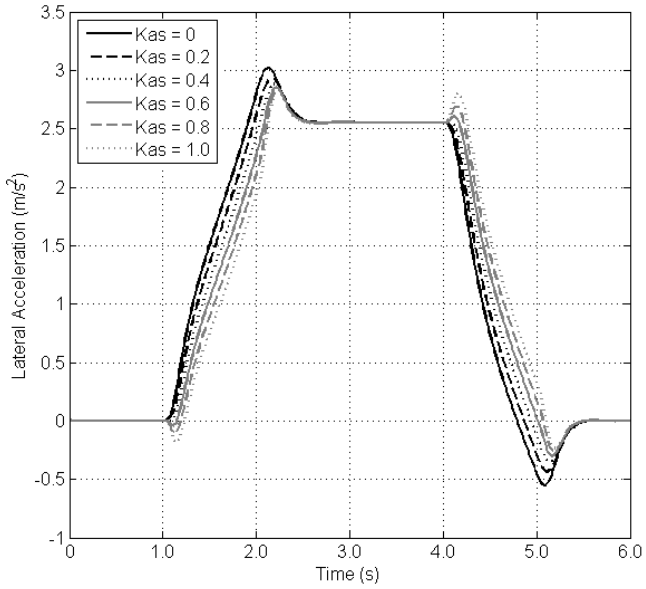

Figure 7.24: Lateral acceleration response with varying active steering gain values.

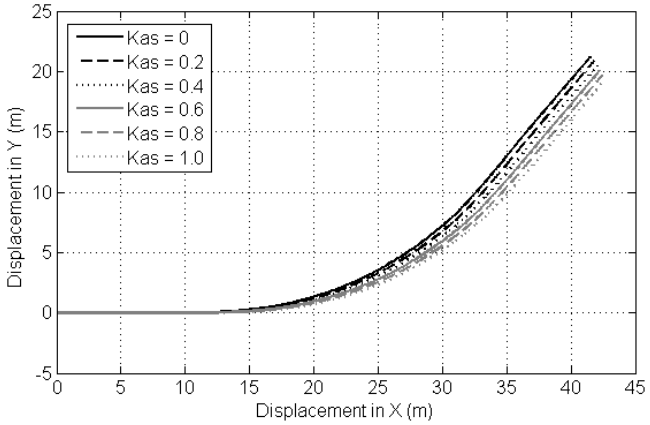

Figure 7.25: Paths followed with varying active steering gain values.

The influence of the active steering gain on vehicle stability can be illustrated by examining the left and right rear wheel loads, Figure 7.26 and Figure 7.27. Whilst the relatively gentle nature of the manoeuvre means that even with no active steering, the load transfer remains comfortably below a safe level, a substantial stability improvement is achieved by increasing the active steering gain.

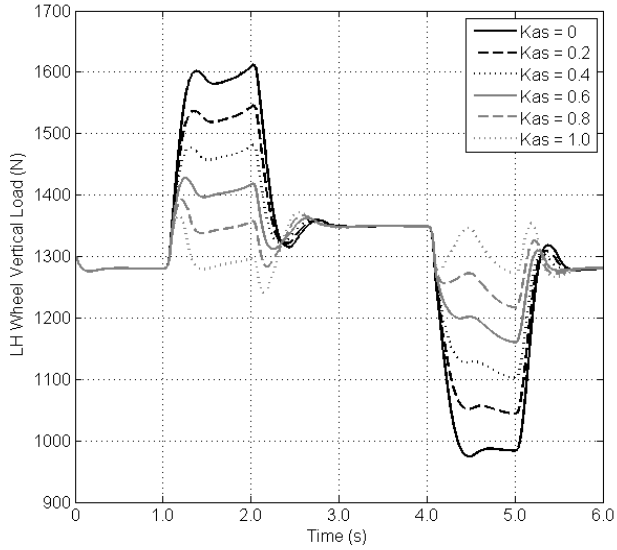

Figure 7.26: Left wheel vertical load at varying active steering gain values.

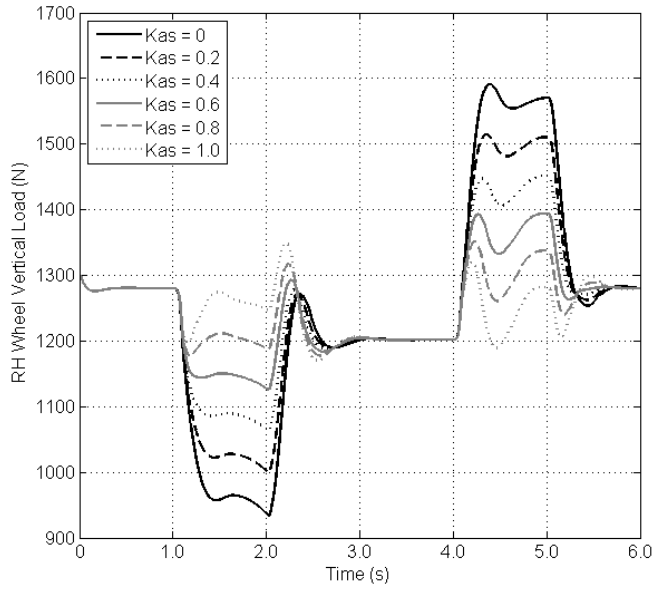

Figure 7.27: Right wheel vertical load at varying active steering gain values.

The peak inside (right) wheel load variation and displacement error (relative to the non-active steer case) at the end of the ramp steer manoeuvre, are shown relative to the gain value in Figure 7.28. The relationship between each of the parameters and the gain value is approximately linear within the selected range. Whilst in the previous section the driver was shown to be able to adapt his steer inputs to maintain path following in SDTC mode, the responsiveness of the vehicle is compromised. Therefore, the active steering gain selection represents a compromise between responsiveness and stability. Equally, it can be said that the active steering gain determines the relative influence of the DTC and STC components of the control system on the vehicle's behaviour.

It is concluded that defining an optimal active steering gain value is somewhat arbitrary and the upper gain limit is determined principally by the human driver's subjective assessment of acceptable responsiveness. It is therefore felt that a sensible approach to the selection of active steering gains for the CLEVER Vehicle, or any other NTV using a SDTC strategy, would be to determine a conservative baseline configuration in simulation, and then tune the gains using feedback from the human driver of a prototype vehicle.

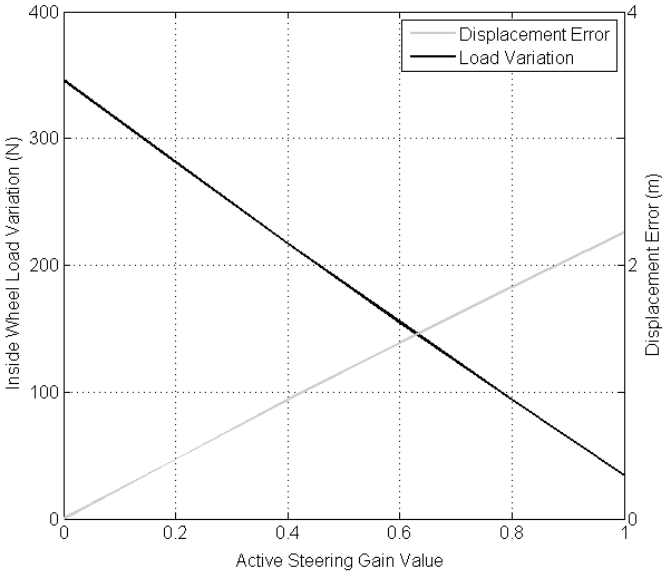

Figure 7.28: Influence of active steering gain on peak load transfer and vehicle position at t=6s.

For the sake of this thesis, an opportunity to tune the active steering gains using a human driver did not present itself. As a result Berote's gain curve (Figure 7.21) is retained for use in the next chapter.

7.4. Concluding Remarks

The CLEVER Vehicle simulation model has been used to show that the countersteering actions of a SDTC system have a significant influence on the trajectory followed by an NTV in response to a series of steer inputs whilst undertaking a lane change manoeuvre. A revised series of steer inputs were presented that successfully guided the SDTC equipped vehicle through the manoeuvre. Despite the revised inputs occurring at an earlier time and being larger in magnitude, they did not lead to a significant reduction in vehicle roll stability. Increasing the DTC gains was shown to lead to reduced active steering actions, better path following performance and a modest reduction in vehicle roll stability.

A series of experiments were performed using the prototype CLEVER Vehicle which confirmed the earlier simulation finding that in order for a driver to maintain path following when using a SDTC strategy, they must modify their steer inputs. Again, the revised steer inputs were found to occur earlier and be larger in magnitude. The human driver reported that generating the revised steer inputs felt natural after a short period of acclimatisation. Whilst only a modest roll stability improvement was recorded in SDTC mode, a more severe manoeuvre with higher lateral accelerations may have lead to greater differentiation between DTC and SDTC modes.

Finally, the influence of the active steering gain (K_{as}) on the vehicle's trajectory and its roll stability was examined. Higher gains were shown to promote improved stability whilst lower gains provide better path following, and therefore a more responsive handling characteristic. Gain values should be selected to provide an acceptable compromise between the two characteristics.

Chapter 8. Controller Sensitivity Study and Improvement.

In previous chapters, the performance of the Steering Direct Tilt Control (SDTC) system was studied assuming a 75kg payload and a vehicle operating on a clean, dry road surface. In this chapter, the performance of the vehicle in a variety of operating conditions will be examined with a view to implementing an adaptive controller if necessary. In addition, the use of a feed-forward control strategy will be explored with the aim of further improving the vehicle's transient roll stability

8.1. Payload - A Sensitivity Study

The majority of the testing and simulation of the CLEVER Vehicle has assumed that the vehicle is loaded with only a single occupant and no luggage. The design of the CLEVER Vehicle concept is such that a passenger can be accommodated behind the driver, and a small luggage compartment is provided behind the rear passenger's head.

The default mass value for the driver of the CLEVER Vehicle was 75kg. This is approximately the mass of the driver used in the experimental tests presented in Chapters 6 & 7, and has been used in all subsequent simulations. For the 75kg driver an inertia value of I_{xx}=8.2kgm^2 is assumed [35].

The addition of a passenger and luggage will increase both the mass and inertia of the cabin module; the impact of this increase will be studied in this section with a view to assessing the need for an adaptive controller.

8.1.1. Payload Mass and Inertia Simulations - DTC

Simulations were conducted in which the payload mass increased in 25kg steps to a maximum of 150kg. Corresponding increases in the inertia are also made. A constant speed input of 10m/s and a ramp steer input of -7° over 0.3s (Figure 8.1) were used.

Table 8.1: Payload, mass and inertia values.

Case	Payload Mass (kg)	Payload Inertia, I_{xx} (kgm^2)
1	75	8.20
2	100	10.93
3	125	13.67
4	150	16.40

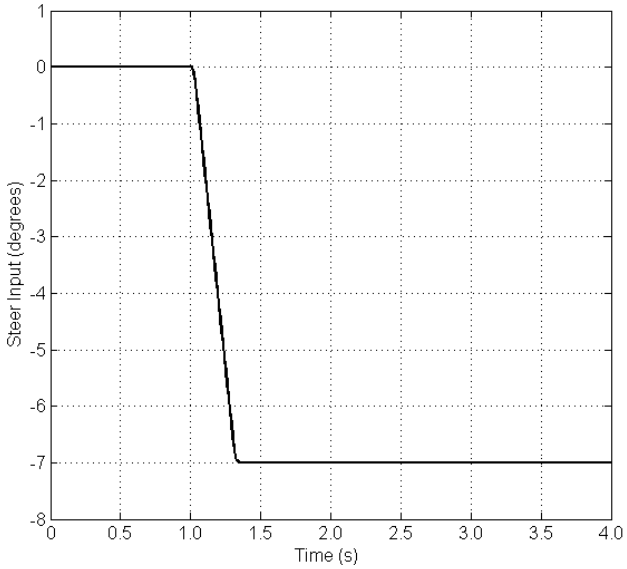

Figure 8.1: 7° ramp steer input filtered at 2Hz.

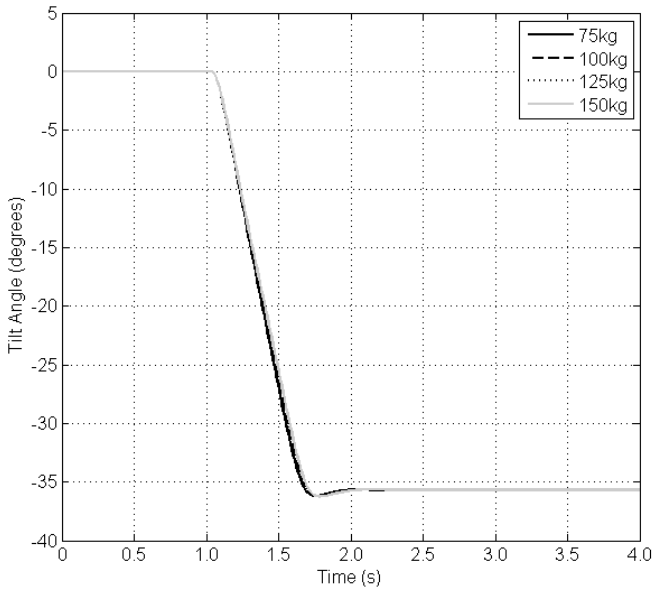

Figure 8.2: Tilt angle response at varying payloads in DTC mode.

The variations in payload have only a marginal affect on the tilt angle response, Figure 8.2. In order to maintain the tilting response at higher payloads it is necessary for the DTC system to generate a larger tilting moment. The effect on the roll stability is examined in Figure 8.3 which is a plot of the left (inside) wheel load during the ramp steer manoeuvre.

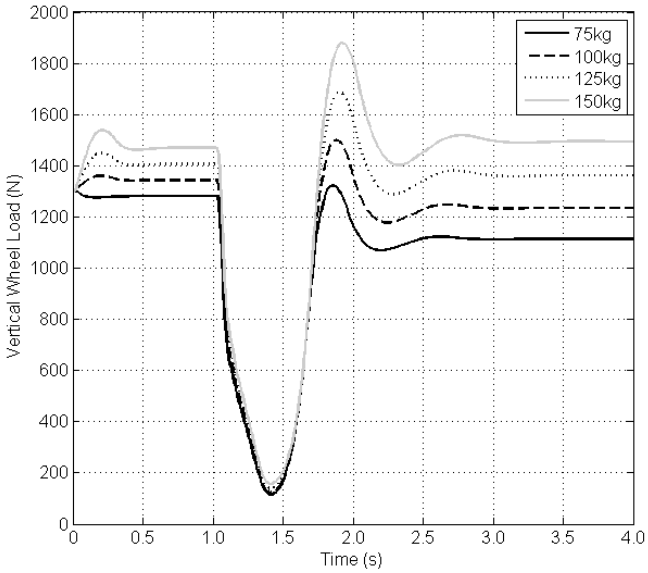

Figure 8.3: Left (inside) wheel load during ramp steer manoeuvre with varying payloads in DTC mode.

Increasing the payload mass inevitably increases the static rear wheel vertical load, in this way adding mass increases the available moment reserve. Figure 8.3 shows that, once the simulation has settled at a steady state but before the vehicle undertakes the ramp steer manoeuvre, the rear wheel vertical load is approximately 1280N with a 75kg payload and rises to 1470N with a 150kg payload. The moment reserve is therefore increased by 14.8% as a result of the higher payload. However, the minimum wheel load experienced during the manoeuvre is similar in all four cases; the increased tilting moment cancelling out the increased moment reserve. Using the minimum wheel load as a measure of vehicle stability, it would appear that the payload mass has a negligible impact in transient situations.

It is noted that once the vehicle has settled at a steady state with the steer angle applied, the inside wheel load does not match the nominal static value. At lower payloads, the inside wheel load during steady state cornering is reduced below the static value; at the highest payload, it is increased. Whilst the maximum 'over-lean factor' is limited to approximately 1.2 so that the driver does not perceive an inverse lateral acceleration (Chapter 4), there is some limited scope for creating a controller that reduces the over-lean factor (and therefore the demand tilt angle) at high payloads. Such a control strategy may, by reducing the tilting moment at very high payloads, realise a small improvement in transient stability.

8.1.2. Payload Mass and Inertia Simulations - SDTC

Having established that increased payload has a negligible influence on the vehicle stability when using a DTC strategy, the influence of increased payload in conjunction with a SDTC strategy was explored. The driver mass and inertia values shown in Table 8.1were again utilised.

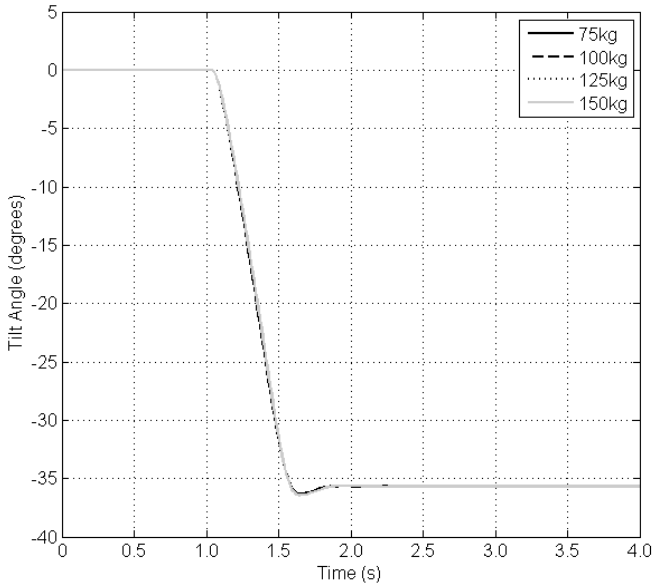

Figure 8.4: Tilt response at varying payloads in SDTC mode.

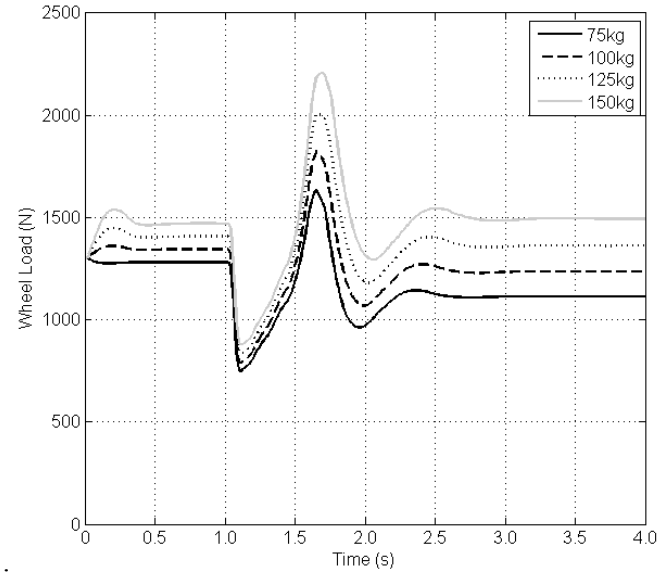

Figure 8.5: Left (inside) wheel load during ramp steer manoeuvre at varying payloads in SDTC mode.

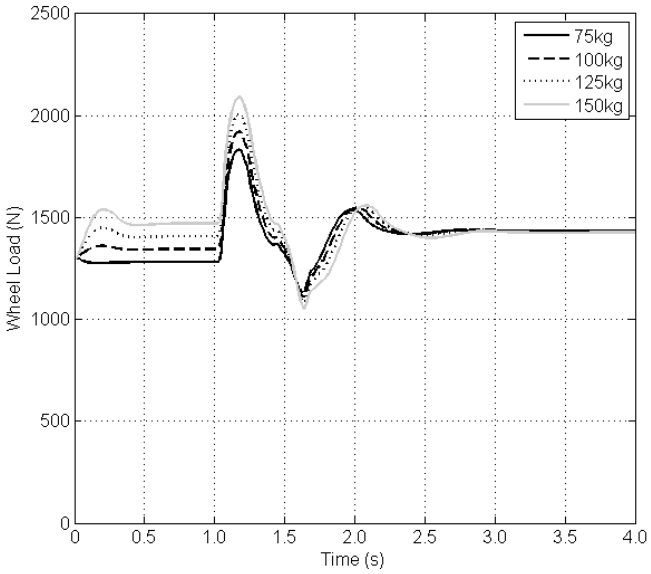

Figure 8.6: Right (outside) wheel load during ramp steer manoeuvre at varying payloads in SDTC mode.

The tilt responses shown in Figure 8.4 are all but indistinguishable from one another. Equally, the minimum inside wheel loads shown in Figure 8.5 are similar in magnitude. The higher inside (left hand) wheel loads observed at around t=1.7s lead to only a small corresponding reduction in the outside (right hand) wheel load (Figure 8.6). The outside wheel load remains above 1100N at all times and thus this characteristic is not considered detrimental to the vehicle's roll stability.

As was the case when using a DTC strategy, payload is found to have limited impact upon the transient vehicle stability when using a SDTC strategy. There remains some limited scope for a controller that varies the over-lean factor in response to payload in order to optimise the steady state wheel loads and reduce the actuator moment in transient situations, but only small benefits are anticipated. If such a controller were developed, the payload could be estimated from the suspension position sensors. In the absence of suspension position sensors, a crude estimate could be obtained from either a rear seat occupancy sensor or a rear seat seatbelt buckled sensor.

8.1.3. Rear Module Centre of Gravity Height

Along with the tilting moment produced by the DTC actuators, the roll moment generated by the lateral acceleration of the rear module mass contributes to the load variation that occurs across the rear axle of the CLEVER Vehicle. By setting the height of the rear module centre of gravity (CG_r) to ground level in the simulation model, it is possible to quantify the contribution of the rear module to the wheel load variation. Again, the simple ramp steer input of -7º over 0.3s and at a speed of 10m/s is used (Figure 8.1).

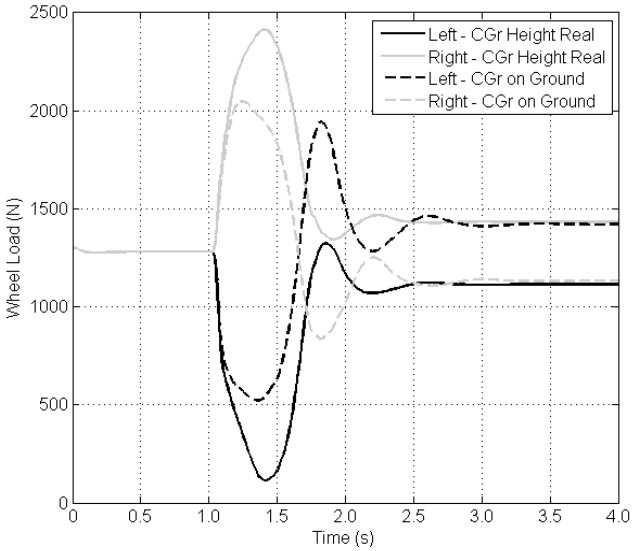

Figure 8.7: Wheel loads at varying CG_r heights

Figure 8.7 shows the wheel loads during the simulated ramp steer manoeuvre with the height of the CG_r at both its true value, and with it set at ground level. By eliminating the roll moment generated by the rear module mass, the minimum wheel load is increased from 114N to 521N and the load variation from the nominal static value of 1280N is reduced by 34.9% during the transient phase of the manoeuvre.

The steady state inside wheel load is also increased by the reduction in CG_r height. If a NTV with a significantly lower CG_r were designed, a lower 'over-lean factor' could safely be used in the controller, this would further increase transient stability by decreasing the DTC actuator moment.

8.2. Low Friction Road Surfaces

Changes in the road surface friction co-efficient are likely to affect the tilting performance of the CLEVER Vehicle's SDTC system, not least because the controller's estimation of the optimum tilt angle is based upon assumptions about the lateral acceleration which results from steer inputs. In this section, the performance of the CLEVER Vehicle controller in differing surface conditions will be assessed in order to ascertain whether a control strategy which adapts to the road surface conditions should be implemented on a future NTV.

The coefficient of friction between the tyre and road surface can vary widely, typically on a wet road surface it is 20 to 30% lower than that on an equivalent dry road surface [60]. If the wet road surface is also contaminated by dirt and oil, this creates a highly viscous lubricant and can halve the coefficient of friction from the dry value [60]. Whilst the coefficient of friction between the road surface and the tyre dictates the peak force that a tyre can generate, at modest slip angles its influence is much smaller and the cornering stiffness of the tyre dominates. Implementing wet road surface conditions in simulation is therefore not simply a case of multiplying the lateral force produced by the tyre by a scaling factor.

Chapter 5 detailed the implementation of Pacejka's 'Magic Formula' tyre models in the CLEVER Vehicle simulation. The Magic Formula models contains a 'road surface factor' (μ_y) term which typically has a value of 1. This surface factor value not only influences the magnitude of the 'peak factor' (D_{y0}), but also the 'stiffness factor' (B_{y0}) which dictates the slope of the lateral force / slip angle graph close to the origin. Thus, when alterations are made to the road surface friction coefficient, the slope of the tyre force / slip curve close to the origin remains constant.

8.2.1. Stability on Wet Road Surfaces

In this study, the CLEVER Vehicle simulation model is used to examine the influence of road surface conditions on the vehicle's roll stability. Three values of the surface factor are considered, 1 (dry), 0.75 (wet) and 0.5 (wet + dirty). Corresponding front and rear wheel tyre force / slip relationships are shown in Figure 8.8 & Figure 8.9. A 75kg driver mass is used throughout.

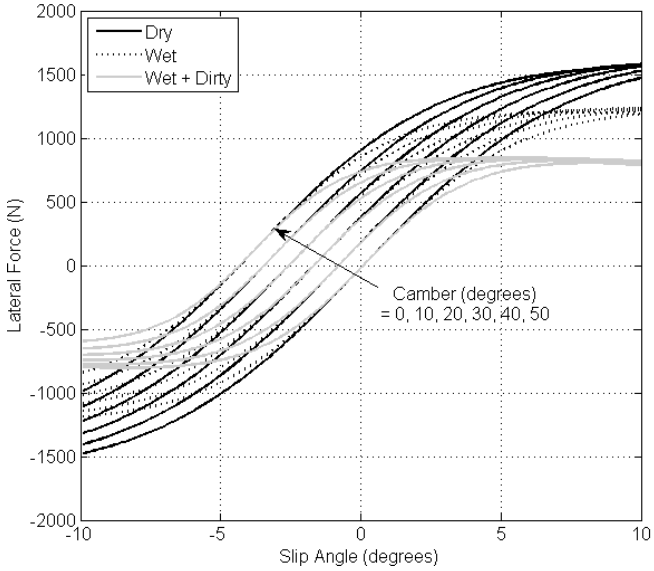

Figure 8.8: Front wheel lateral forces in dry, wet and wet + dirty road conditions.

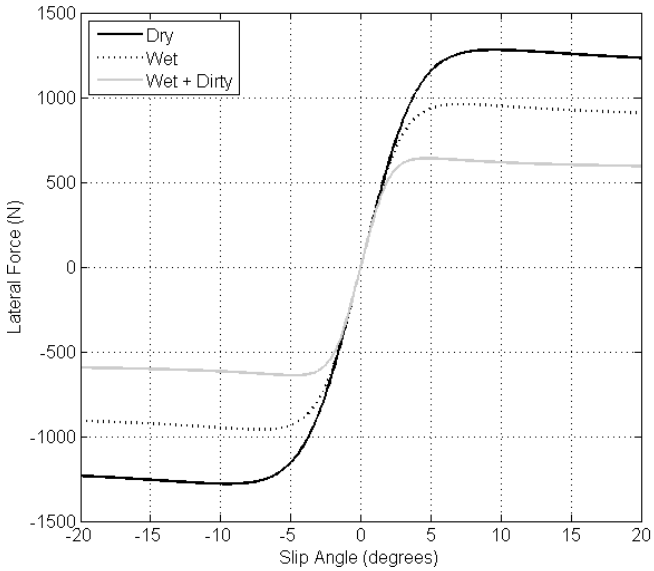

Figure 8.9: Rear wheel lateral forces in dry, wet and wet + dirty road conditions.

The steady state lateral acceleration response was simulated using a constant front wheel steer angle of 15º and by increasing the vehicle forward speed in 1m/s increments from 1 to 9m/s to generate the lateral acceleration demand. Figure 8.10 shows the lateral acceleration response of the CLEVER Vehicle on the three road surfaces. At lateral acceleration demands of up to 4m/s^2, the response of the CLEVER Vehicle remains consistent regardless of the road surface conditions. This occurs because the tyres are operating in their linear range (Figure 8.8 & Figure 8.9) and the lateral force output is dictated by the tyre cornering stiffness rather than the coefficient of friction. The lateral tyre force in the wet + dirty road case saturates at around 4.2m/s^2, and very large slip angles are generated Figure 8.11.

In the wet + dirty case, saturation of the lateral tyre forces occurs before saturation of the CLEVER Vehicle's ±45º tilt limits. Beyond the saturation point, increases in the lateral acceleration demand result in increases in tilt angle (up to the 45° maximum), but no additional lateral acceleration. Given that, thanks to the limited 'over-lean factor' (Chapter 4), the CLEVER Vehicle does not usually tilt enough for perfect wheel load distribution, roll stability in the wet + dirty case at lateral acceleration demands above 4m/s^2 is excellent, Figure 8.12. However, the rapid rise in the slip angles does suggest a catastrophic loss of yaw stability. By contrast, in the highest grip 'dry' case, the lateral acceleration continues to build after the maximum 45º tilt limit has been reached and large wheel load variations occur and the vehicle's roll stability is reduced.

In the wet case, the lateral acceleration saturates at a value of approximately 6.3m/s^2, this is roughly the same value as the saturation of the tilt angle limits (Chapter 3). The minimum steady state inside wheel load is approximately 550N in this case.

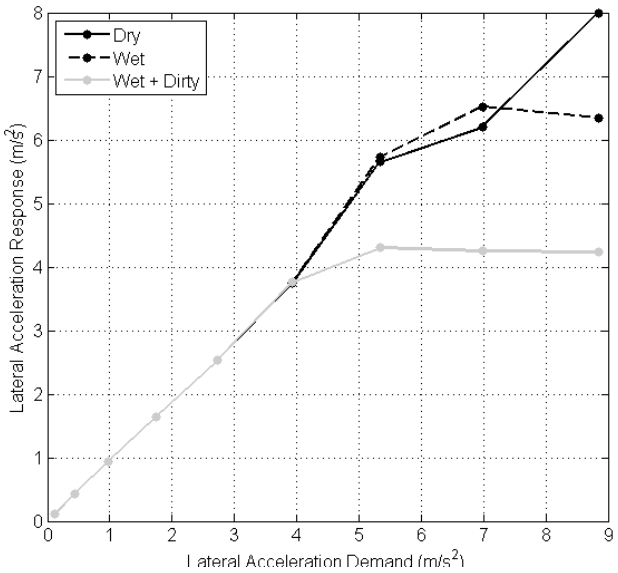

Figure 8.10: Steady state lateral acceleration response in dry, wet and wet + dirty road conditions.

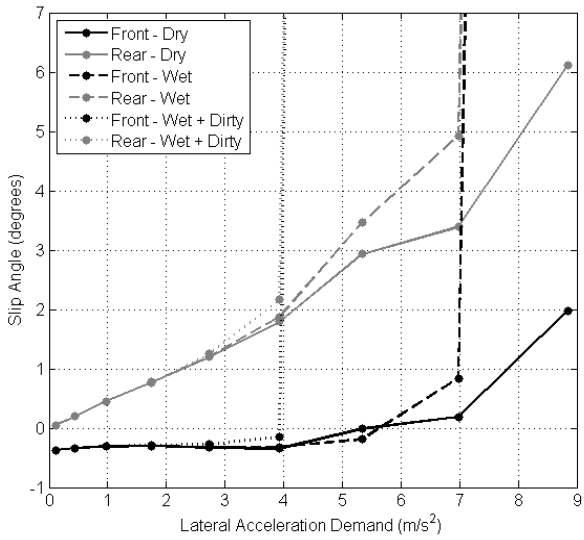

Figure 8.11: Steady state front and rear axle slip angles in dry, wet and wet + dirty road conditions.

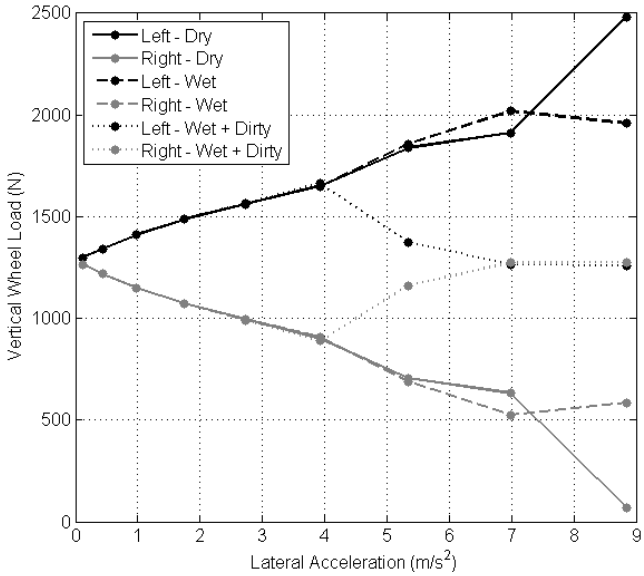

Figure 8.12: Steady state wheel loads in dry, wet and wet + dirty road conditions.

Having established acceptable roll stability on wet surfaces in steady state conditions, stability in transient conditions was assessed using a ramp steer input of -7º over 0.3s occurring at t=1s, and then reversed at t=4s, and a constant speed of 10m/s. Figure 8.13 shows that the lateral acceleration response on the wet road surface is almost indistinguishable from the response on a dry road surface. Again the tyres remain largely within the linear region where the lateral force is a function of the tyre slip stiffness rather than the road surface friction coefficient. Given the small lateral acceleration differences, it follows that the wheel loads are also similar in the two cases Figure 8.14.

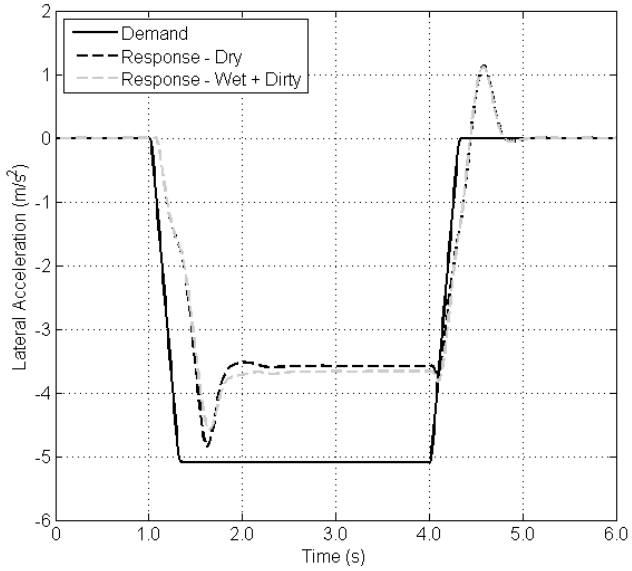

Figure 8.13: Lateral acceleration demand and response on dry and wet + dirty road surfaces.

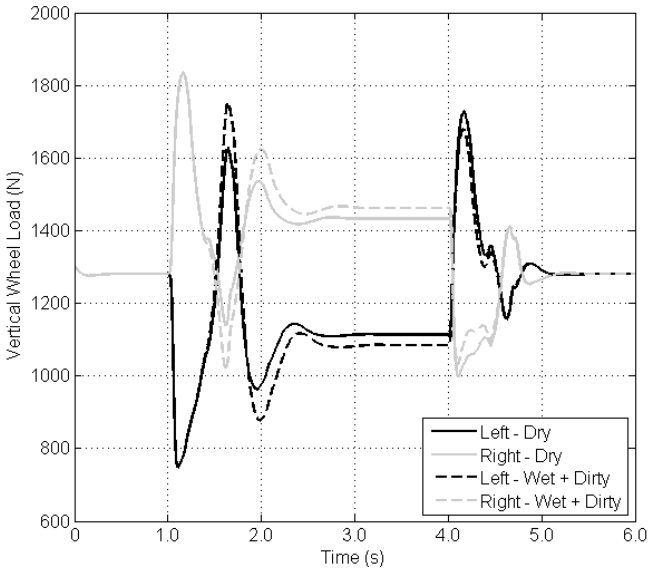

Figure 8.14: Wheel loads on dry and wet + dirty road surfaces.

8.2.2. Stability on Ice

In conditions of extremely low grip, the CLEVER Vehicle may tilt too much to remain balanced in the absence of the anticipated lateral acceleration. Both steady state and transient simulations were performed to asses the likelihood of 'over-tilting' leading to roll-over towards the turn centre. It is thought likely that, in transient conditions, the outside wheel load may be lowered further by DTC actuator moments, particularly on corner-exit.

In this section, a road surface factor of 0.1 is used in the Magic Formula tyre models, Figure 8.15. Whilst this may not replicate the true slip / force characteristics of a tyre on ice, it is considered a suitable worst case approximation for the purposes of assessing roll stability in extremely low grip situations. The true coefficient of friction between rubber and ice has been shown to be highly temperature and velocity dependent [61], with the heat produced by friction creating a lubricating film of water at higher speeds and/or temperatures only slightly below 0ºC.

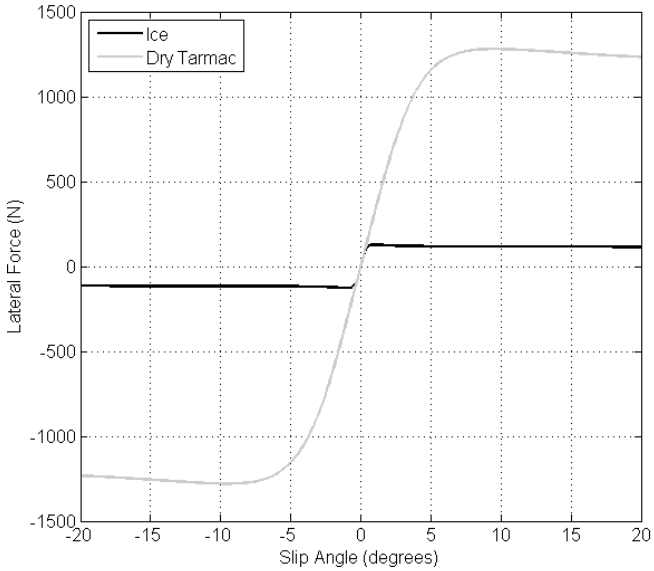

Figure 8.15: Magic Formula tyre force model on ice with dry tarmac shown for comparison.

Again, steady state simulations were performed with a constant steer angle of 15º and speed inputs varying from 1 to 9m/s. Since roll instability caused by over-tilting on very low friction surfaces will be exacerbated by higher payloads, a 150kg case will be examined in addition to the 75kg case.

The lateral acceleration response of the CLEVER Vehicle on ice is shown in Figure 8.16. The lateral acceleration saturates at approximately 1m/s^2 with subsequent increases in the lateral acceleration demand producing larger tilt angles buy only very slight increases in lateral acceleration response (caused by the increased front wheel camber angle). In the 150kg payload case, lateral acceleration demands over 5.5m/s^2, and the associated tilt angles, unload the outside wheel and cause capsize of the vehicle in the direction of the turn centre, Figure 8.17. In the 75kg payload case, the outside wheel load is a modest 350N after saturation of the lateral acceleration response. Whilst roll stability on ice appears to be poor at large lateral acceleration demands, it is worth noting that yaw stability will have been lost long before.

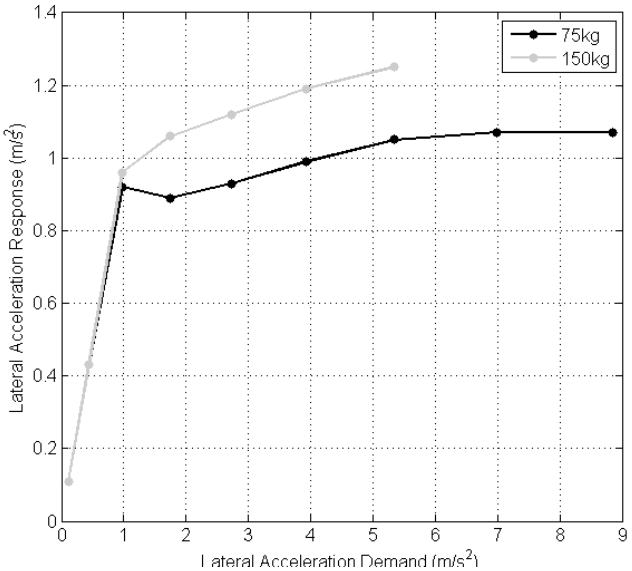

Figure 8.16: Steady state lateral acceleration response on an icy surface with 75kg and 150kg payloads.

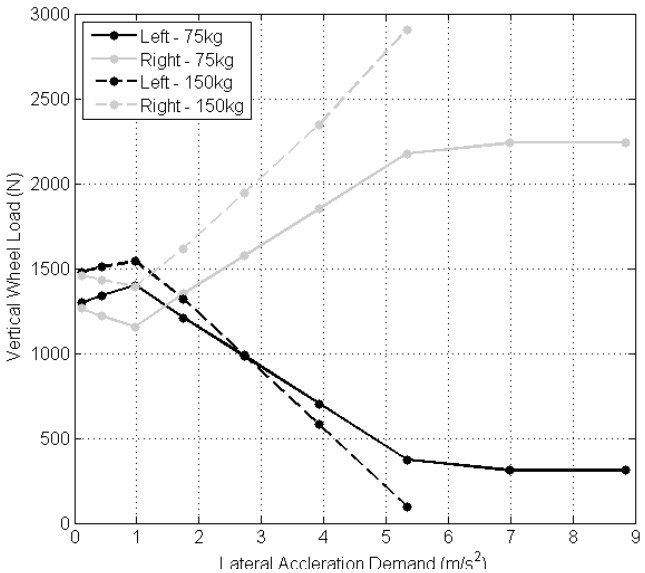

Figure 8.17: Steady state wheel loads on an icy surface with 75kg and 150kg payloads.

The same transient ramp steer manoeuvre used to assess stability in wet conditions was applied to the icy road case. The lateral acceleration response is shown in Figure 8.18 and the wheel loads in Figure 8.19. The lateral acceleration response in the 75kg payload case reaches saturation at approximately 1m/s^2, and does not return to zero when the reverse steer input occurs at t=4s. The reason for the continued lateral acceleration beyond 4s is that, again, yaw stability had been lost long before and the vehicle is in a spin. In the 75kg payload case, wheel lift-off occurred for a short duration at t≈1.7s, whilst in the 150kg case the load transfer was sufficient to lead to roll-over.

As was observed under the quasi-steady-state conditions, the roll-stability of the CLEVER Vehicle cannot be guaranteed in transient conditions on a very low friction surface. However, any manoeuvre likely to lead to roll-over will have lead to a loss of yaw-stability long before.

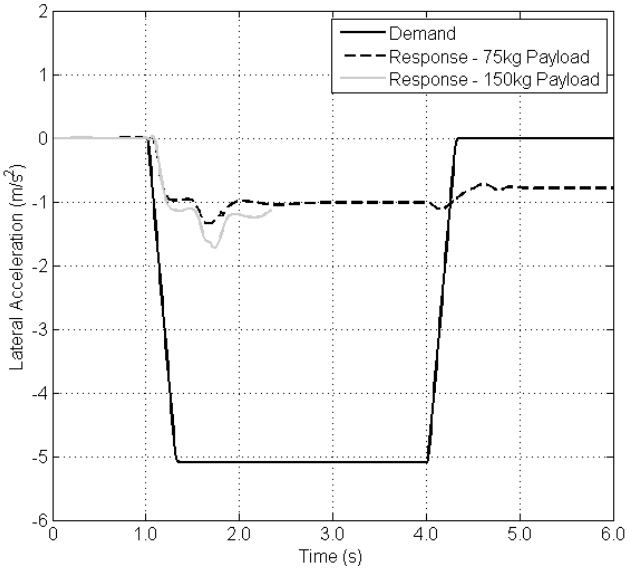

Figure 8.18: Lateral acceleration demand during a transient manoeuvre on an extremely low friction surface, and response with both 75kg and 150kg payloads.

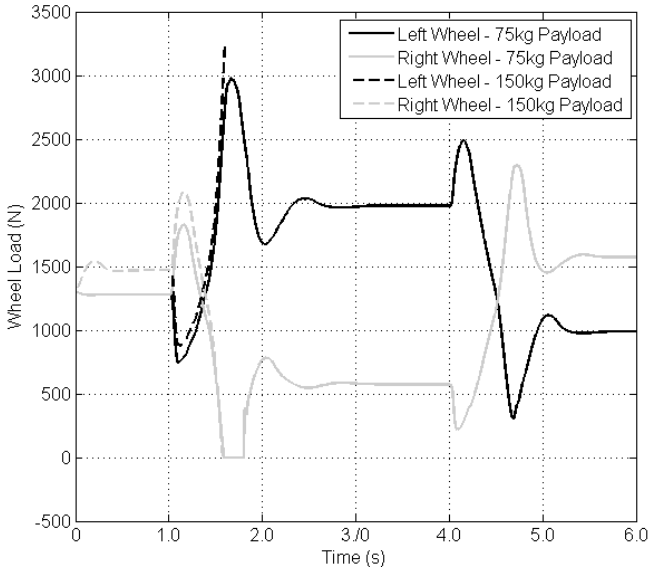

Figure 8.19: Rear wheel loads during the transient manoeuvre in both 75 and 150kg cases.

8.2.3. Low Friction Surfaces Summary

Roll stability in wet road conditions does not present an obstacle to the adoption of a SDTC system on future narrow tilting vehicles. The reduced maximum lateral accelerations achievable on road surfaces with a low coefficient of friction help to maintain good stability once the tilting limits are saturated. On icy roads, the roll stability of the CLEVER Vehicle cannot be guaranteed. However, since yaw stability is lost at lower lateral accelerations than roll stability, it is unlikely that a lateral acceleration demand high enough to cause roll-over will be generated.

A control strategy could be developed that continuously estimates the road surface conditions by comparing the lateral acceleration demand to a lateral acceleration measurement from an accelerometer. Such a control strategy would eliminate the 'over-tilting' that occurs in very low grip conditions and could be used to optimise the tilting performance and energy consumption under a wide range of road conditions. Such an approach may however be difficult to implement. It is difficult to estimate the tyre/road friction conditions from the lateral acceleration response, as at low to moderate slip, the tyre cornering stiffness dominates [62]. A more pragmatic approach may be to develop a controller that assumes dry road friction conditions in all but extreme circumstances. If a very large disparity did occur between the demand and measured lateral acceleration signals, the controller could then switch into a second mode. The second mode could either demand that the cabin remain upright, or could generate only modest tilt demand angles which are stable even in the absence of any lateral acceleration.

8.3. Feed-Forward Control

In [37], Edelmann *et al*. propose a switching SDTC system for a narrow tilting vehicle in which a feed-forward strategy is used to improve the response of the front wheel steer-by-wire system. In this section, the simulation model of the CLEVER Vehicle will be used to investigate the feasibility of such a control strategy.

Clarification of Front Wheel Steer Angle Values

Reference is made in this section to multiple variants of the front wheel steer angle (δ). In the interests of clarity the different front wheel steer angle parameters, and their meaning, are listed in Table 8.2.

Table 8.2: Front wheel steer angle parameters.

Symbol	Description
δ_d	Steer demand angle – The demand front wheel steer angle generated by the driver's steer inputs.
δ_{dff}	Steer demand angle with feed-forward – The steer demand angle after the addition of a feed-forward element.
δ_{as}	Active steering angle – The alteration to the front wheel steer angle produced by the active steering system.
δ_f	Front wheel steer angle – The front wheel steer angle resulting from a combination of the driver's steer demand angle and the active steering angle.

8.3.1. Feed-Forward of Steer Demand Rate to SDTC Controller

The existing SDTC controller was modified to include feed-forward of the steer angle rate to provide some estimation of the future steer angle. The steer angle rate was multiplied by a feed-forward gain (K_{ff}), and added to the steer angle to form a revised demand steer angle. This revised steer demand angle was then fed into the lateral acceleration and tilt angle calculations.

So as not to mask the full potential of the feed-forward control strategy, the ±5.6° active steering limits were removed from the simulation model used in this section.

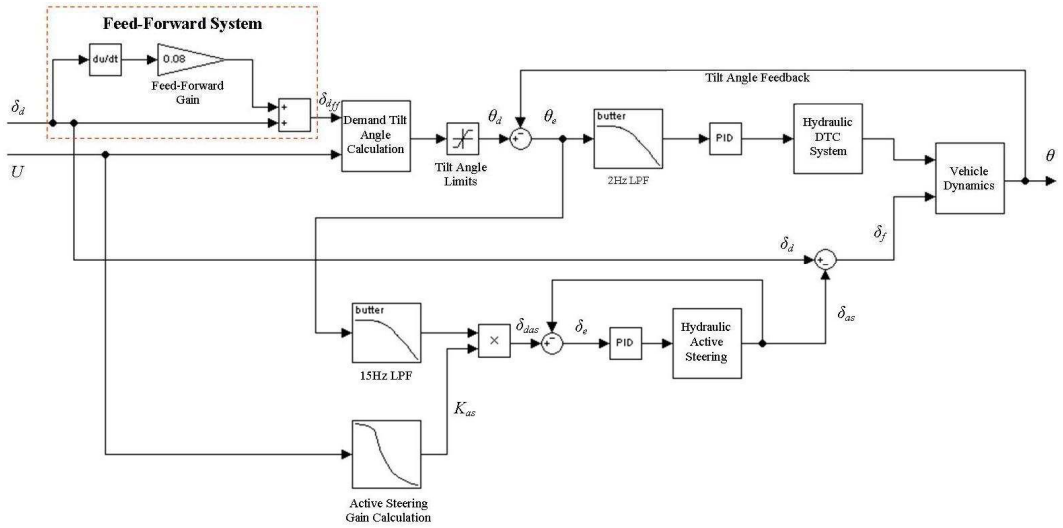

Figure 8.20: Block diagram of control system with feed-forward of the steering rate to the tilt angle calculation as used by both DTC and active steering systems.

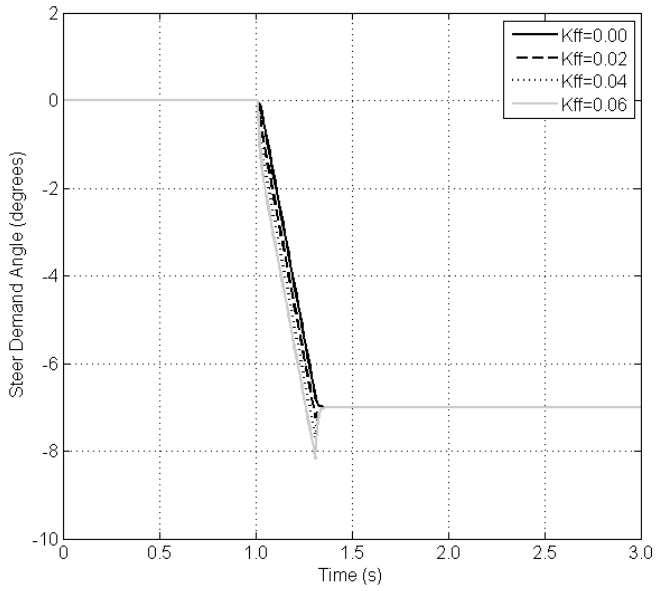

Figure 8.21: Steer demand angle including feed-forward element (δ_{dff}) at varying feed-forward gain values.

The SDTC with feed-forward controller was tested at 10m/s using a ramp steer input of -7° (at the road wheel) over a time period of 0.3s; this is of a similar magnitude and speed to steer inputs recorded during experimental testing of the prototype CLEVER Vehicle. A low pass filter was used to smooth the transitions slightly. The steer demand both before (δ_d) and after (δ_{dff}) the addition of the feed-forward element are shown in Figure 8.21.

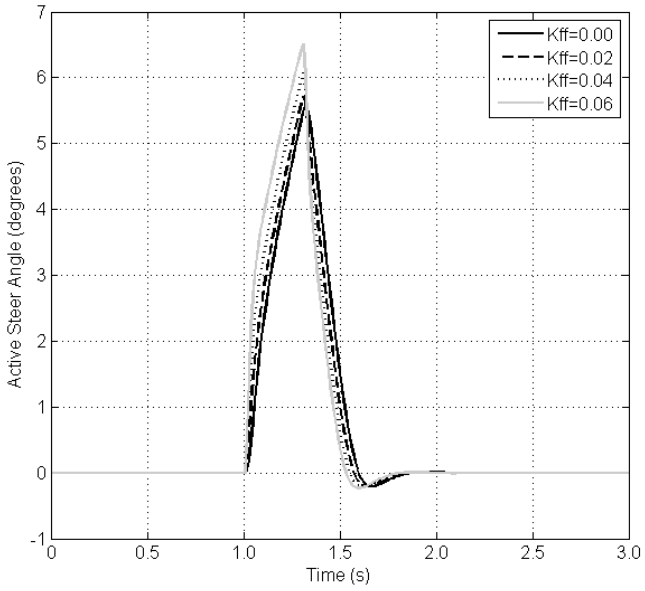

Figure 8.22: Active steering angles (δ_{as}) at varying feed-forward gain values.

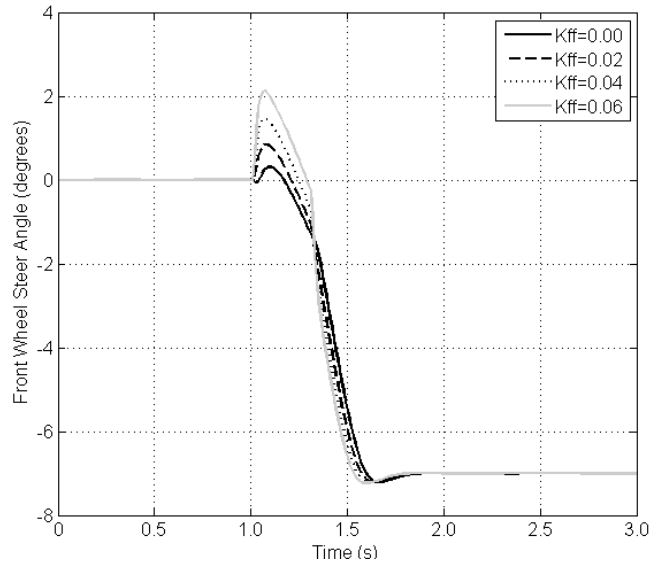

Figure 8.23: Front wheel steer angle response (δ_f) at varying feed-forward gains.

At higher feed-forward gain values the steer demand angle is generated more rapidly, this leads to larger tilt angles demands, tilt errors and therefore active steering angles, Figure 8.22.

The larger, earlier active steering angles result in a significant increase in the amount of countersteering action generated at the front wheel, Figure 8.23. A faster maximum front wheel steer angle rate is also evident.

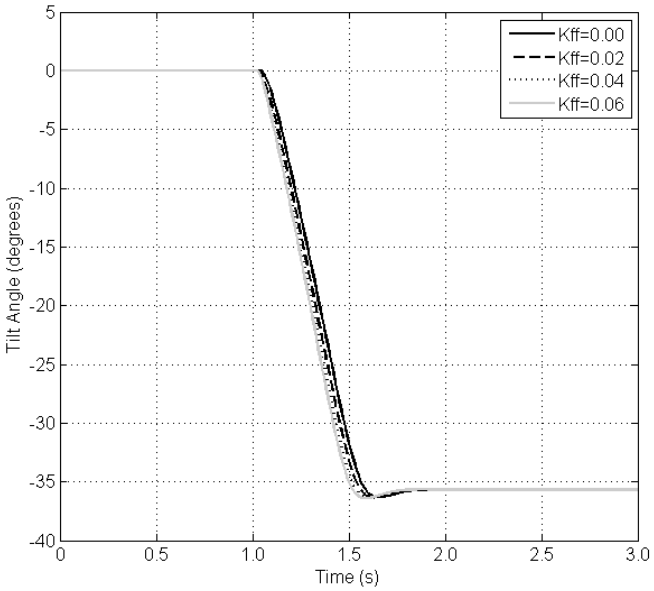

Figure 8.24: Tilt response at varying feed-forward gains.

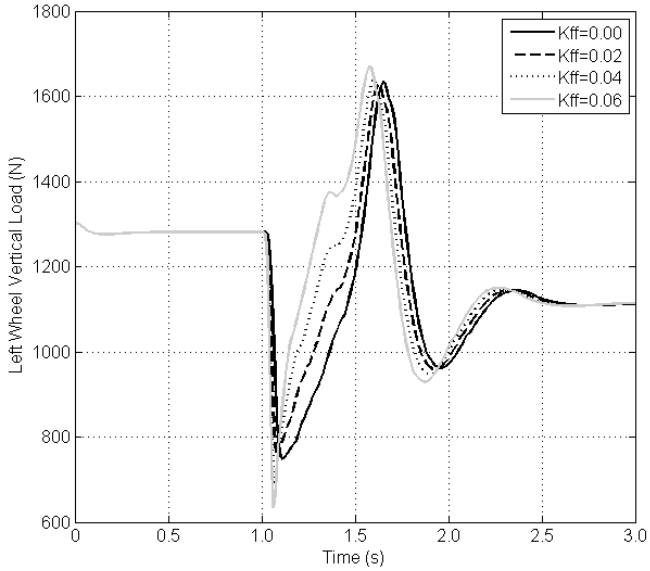

Figure 8.25: Left wheel vertical load at varying feed-forward gains.

Despite the larger, faster countersteering actions generated through the use of feed-forward in the controller, the stability of the CLEVER Vehicle is not improved. The left (inside) wheel vertical loads plotted in Figure 8.25 show that at the minimum load supported by the inside wheel during the ramp input manoeuvre is lowest in the highest gain case.

Since the feed-forward of the steering rate is used to calculate the demand tilt angle, it not only increases the active steering action, but it also increases the moment produced by the Direct Tilt Control actuators. It has been established previously that the DTC actuator moment can have a significant detrimental affect on the vehicle stability.

8.3.2. Feed-Forward of Steer Angle Rate to Active Steering System Only

It is evident from the results presented so far that feed-forward can lead to a faster active steering response. If this could be achieved without an accompanying increase in the DTC moment then an improvement in stability may be realised.

The controller was modified to remove the feed-forward of the steer rate to the DTC component of the control system; the tilt angle calculation with feed-forward was retained for the active steering system, Figure 8.26.

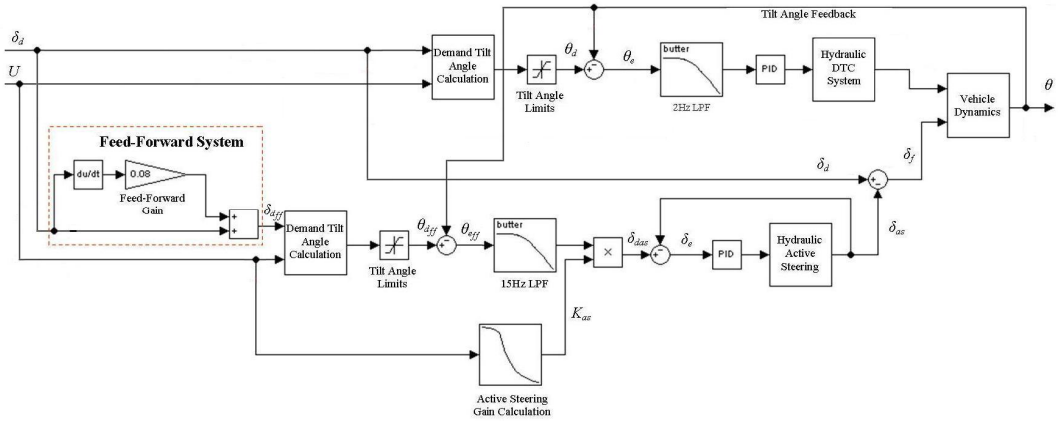

Figure 8.26: Block diagram of control system with feed-forward of steering rate to the active steering only.

This modified control system offered a faster active steer response without the increased DTC moments seen previously. The resulting minimum inside wheel loads during the ramp steer manoeuvre showed a considerable improvement over the previous feed-forward strategy but this revised strategy had its own limitations. Because the active steer angle was a function of not only the tilt error, but also the steer rate, when the tilting motion was underway and the tilt error began to fall, the active steer angle could remain large. Under some circumstances this lead to an excessive active steer angle and an unacceptable reduction in the outside wheel load. Results are not presented in this thesis as this control strategy was superseded by the use of feed-forward of the tilt angle error to the active steering system.

8.3.3. Feed-Forward of Tilt Error to Active Steering System

If the tilt angle error rate is fed-forward to the active steering system, it is possible to achieve a fast active steering response without the active steer angle persisting for too long, as was the case when the steer rate was fed-forward.

The controller was modified to remove all feed-forward of the steer angle rate, and replace it with feed-forward of the tilt angle error signal (θ_e). Again, the feed-forward element is applied only to the active steering system so as not to generate a larger DTC actuator moment. The revised block diagram is shown in Figure 8.27.

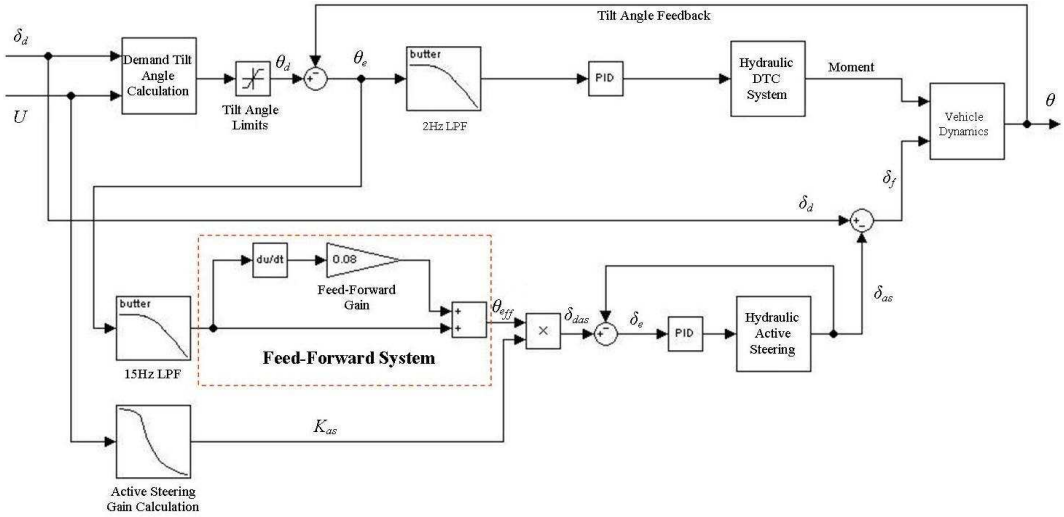

Figure 8.27: Block diagram of feed-forward of tilt error to the active steering system only.

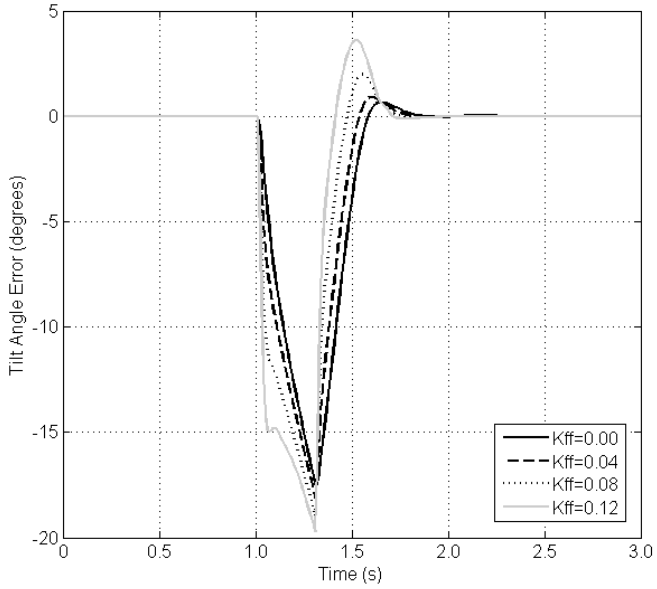

Figure 8.28: Tilt angle error signals fed to active steer system (θ_{eff}).

The tilt angle error feed to the active steering system is shown in Figure 8.28. Whilst the maximum tilt angle error only increases a small amount, it is generated more quickly as the value of K_{ff} rises. This in turn leads to a faster active steering response Figure 8.29.

Whilst the maximum value of the active steering angle only grows modestly with increasing feed-forward gain, the faster active steering response is critical to the countersteering action generated. This faster response to the driver's steer input means the initial countersteer rises from only approximately 0.25° when K_{ff}=0 to nearly 4° when K_{ff}=0.12, Figure 8.30.

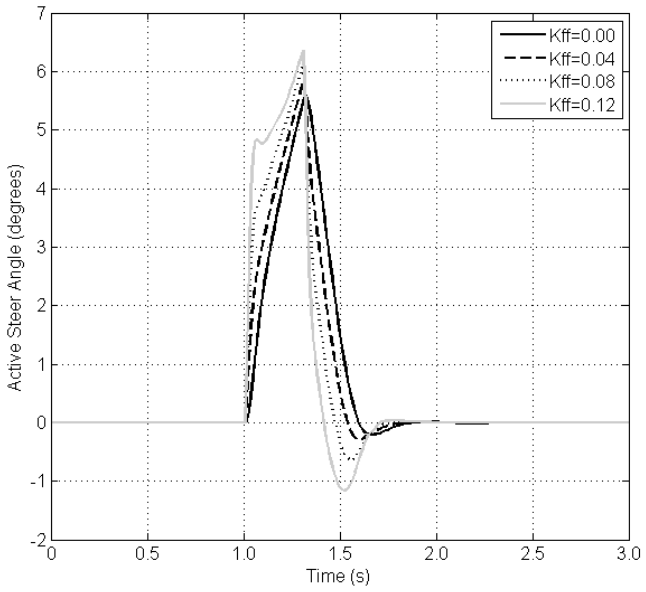

Figure 8.29: Active steering angles with various feed-forward gain values.

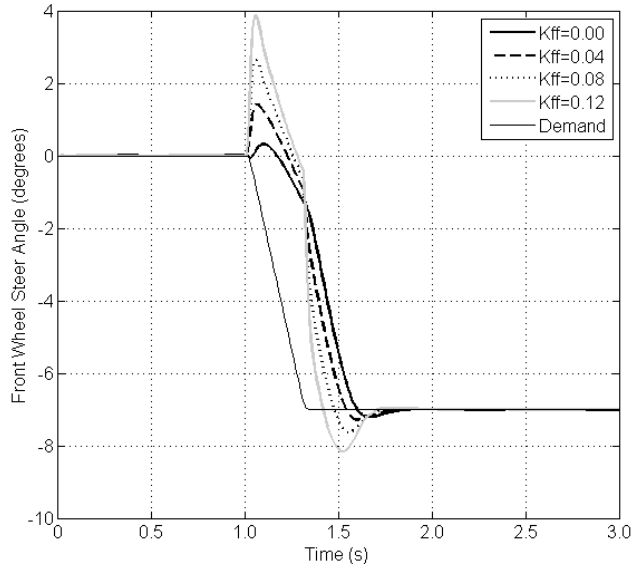

Figure 8.30: Front wheel steer angles with various feed-forward gain values.

Given the larger, faster countersteering actions, it may be expected that a faster tilt angle response would be achieved. However, this is observed not to be the case, Figure 8.31. The tilting response is limited not by the maximum moment the DTC system can generate, but by the flow rate through the DTC hydraulic valve and the 2Hz filtering of the tilt angle error feed to the DTC control loop. Note that the maximum tilt valve opening is deliberately restricted in the controller software to slow the tilt response to a comfortable level and limit the DTC actuator moment output.

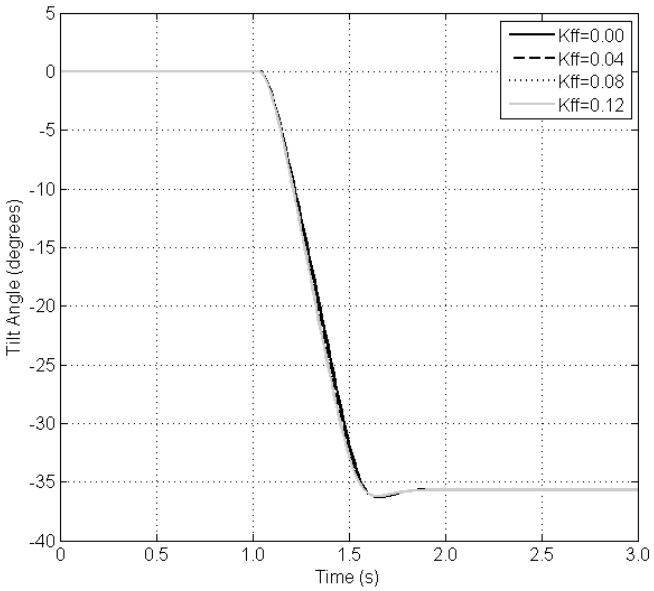

Figure 8.31: Tilt angle response at varying values of feed-forward gain.

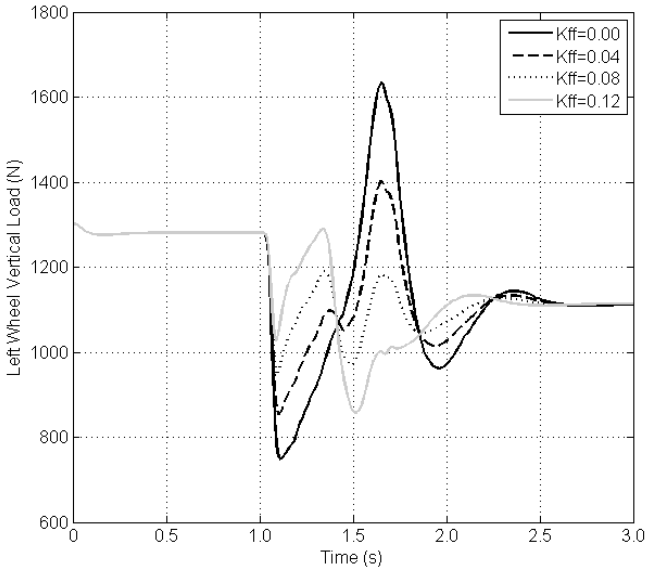

Figure 8.32: Left wheel vertical load at varying feed-forward gains.

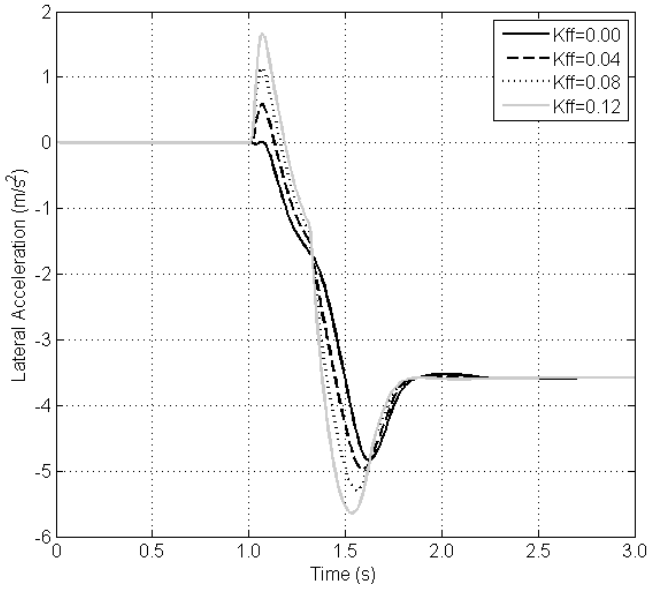

Figure 8.33: Lateral acceleration response at varying feed-forward gain values.

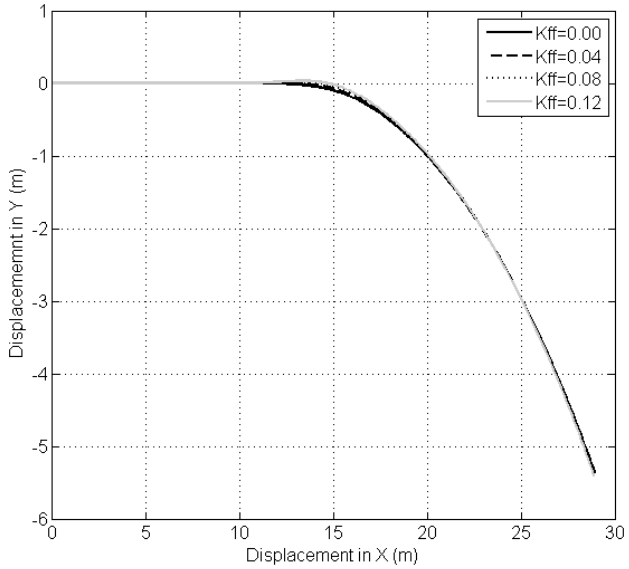

Figure 8.34: Vehicle trajectory at varying feed-forward gains.

Despite having little impact upon the tilting response, the larger countersteering actions seen at higher values of feed-forward gain do have a significant impact upon the vehicle's roll stability during the ramp steer manoeuvre. The minimum load supported by the left (inside) wheel increases from 750N without feed-forward to 950N at K_{ff}=0.08 (Figure 8.32); subsequent increases in gain lead to excessive countersteer at t≈1.5 (shortly after the steer angle reaches steady state) and a reduction in the left wheel load.

As well as improving stability, the larger countersteering actions produced by the feed-forward strategy are likely to impact upon the path followed by the CLEVER Vehicle in response to the driver's steer inputs. Figure 8.33 shows that higher feed-forward gains

produce significantly larger inverse lateral accelerations upon turn-in, and larger over-shoots before settling at steady state. The impact of the lateral accelerations on the path followed is illustrated in Figure 8.34, and is in fact very small. Whilst initially the feed-forward does increase the understeering tendency, the more rapid front wheel steer angle rate that then occurs, and the increased overshoot, mean that by t=3s feed-forward has resulted in a slightly tighter turn.

8.3.4. Feed-Forward Using Real Steer Inputs

So far the feed-forward simulations have been conducted using a synthetic ramp steer input and a constant forward speed of 10m/s. Fundamental to the operation of the feed-forward controller is the differentiation of the steer angle or tilt error signal to find the rate of change. In practise the differentiation of real signals presents a difficulty; real signals are subject to noise which is amplified significantly by differentiation.

In order to test whether implementation of a feed-forward controller on the CLEVER Vehicle is feasible, it is necessary to simulate the system's performance in response to real steer and speed inputs. The steer input shown in Figure 8.35 was generated as quickly as possible by a human driver whilst driving the prototype CLEVER Vehicle. As has been noted in previous chapters, the steering system of the prototype has a significant degree of back-lash which introduces the oscillations visible in the steer signal.

The following simulations were conducted using the control strategy detailed in Section 8.3.3 where by the tilt angle error rate is fed forward to the active steering system only.

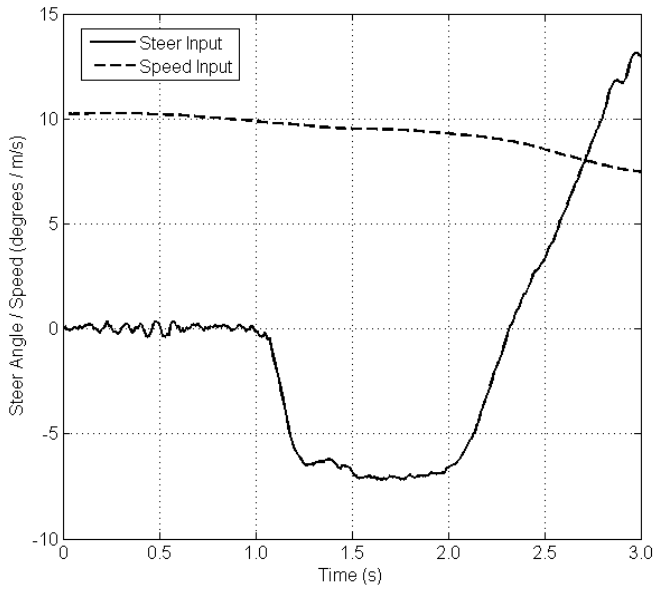

Figure 8.35: Logged steer and speed inputs.

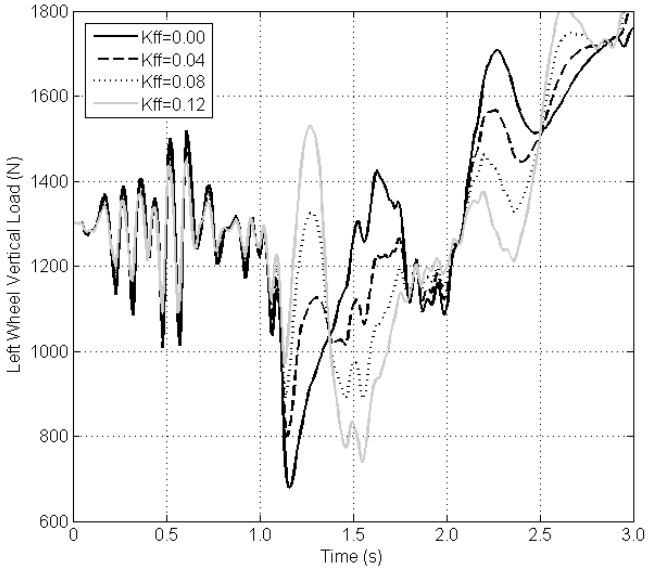

Figure 8.36: Left wheel vertical load at varying feed-forward gains (K_{ff}) when using logged steer and speed inputs.

The left wheel vertical loads during the steer input manoeuvre are shown in Figure 8.36. As the gain is increased the minimum wheel load at t≈1.2s also increases. At the highest gain value, the wheel load as the steer input reaches steady state (t≈1.5s) falls below the value at t≈1.2s; thus this gain is judged to be too high. At a gain value of K_{ff}=0.08 the minimum inside wheel load does not fall below 890N, an increase of some 210N (or 30%) on the case without feed-forward.

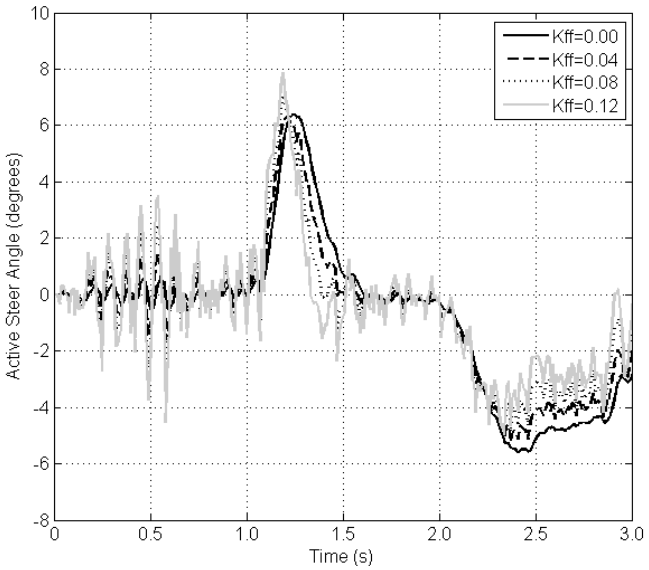

Figure 8.37: Active steering angles at various feed-forward gain (K_{ff}) values when using logged steer and speed inputs.

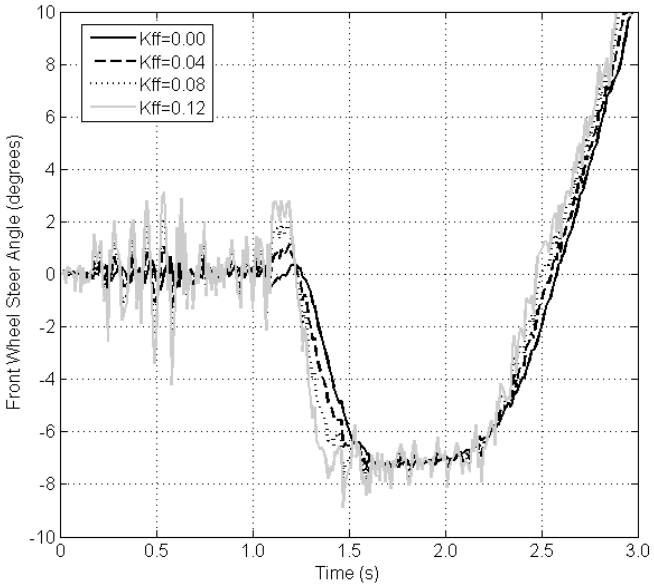

Figure 8.38: Front wheel steer angles (δ_f) at varying feed-forward gains (K_{ff}) when using logged steer and speed data as inputs.

Unfortunately the small oscillations in the logged steer demand angle data (Figure 8.35) percolate into the tilt angle error signal. These oscillations are amplified by the differentiation stage in the feed-forward controller and thus cause large disturbances to the active steering angle (Figure 8.37 and Figure 8.38). At the highest gain value of K_{ff}=0.12, the front wheel oscillations exceed ±3° and at K_{ff}=0.08 they exceed ±2°. Experimental testing of the CLEVER Vehicle has shown that oscillations as small as ±0.5° cause discomfort to the driver through both the steering wheel torque and the vehicle's subsequent tilt angle response.

Additional filtering and lower feed-forwards gain can be used to reduce the influence of noisy signals. Whilst results are not presented in the interests of succinctness, these measures have been found to impact upon the system performance to the extent that any advantage of the feed-forward control strategy is lost. However, if the backlash in the steering system could be reduced significantly, and a cleaner steer signal produced, a feed-forward control strategy has the potential to generate a significant stability improvement.

8.3.5. Feed-Forward Control Summary

The performance of feed-forward control strategies has been explored using simulations of the CLEVER Vehicle. Using a 'clean' synthetically generated steer demand signal, feed-forward has been shown to improve the speed of the active steering system with a subsequent increase in counter-steer. Feed-forward to the DTC system was found to be

undesirable as it results in increased tilting moments and reduced inside wheel loads on turn-in.

Applying a feed-forward control strategy to only the active steering system overcame the problem of increased DTC moment and resulted in considerably improved vehicle roll stability. Using feed-forward of the tilt angle error rate was found to offer better vehicle roll stability than feed-forward of the steering angle rate. Increases in inside wheel load of 30% were recorded. The vehicle's trajectory was found to be all but un-affected by the use of a feed-forward control strategy.

Steer angle and speed data logged during the testing of the prototype CLEVER Vehicle were introduced into the simulation. Differentiation of this data to obtain the rate of change amplified noise and lead to un-acceptably large oscillations of the front wheel steer angle. Reducing the feed-forward gain and increasing filtering undermined the system performance to such an extent that all advantage of the feed-forward strategy was lost.

Whilst the use of a feed-forward control strategy is not feasible on the current CLEVER Vehicle hardware, it may be possible to create a successful installation by making small hardware changes. If backlash in the steering system could be reduced a cleaner steer angle signal would result. A worthwhile reduction in the load transfer during transient manoeuvres is possible.

8.4. Concluding Remarks

The effectiveness of the Steering Direct Tilt Control (SDTC) strategy in variable operating conditions was examined in simulation with a view to developing further refinements to improve performance. A more advanced controller strategy with a feed-forward element was then introduced and assessed.

Increases in the payload carried by the vehicle were found to have very little effect on transient stability, the greater static vertical wheel load off-setting any additional load transfer. There is some limited scope to develop a controller which reduces the tilt angle at high payloads to realise a small improvement in both transient and steady state stability. The height of the rear module's centre of gravity was found to contribute significantly to the total roll moment; lowering it brought benefits to both transient and steady state roll stability.

Simulations of the SDTC control system's performance on wet road surfaces with a reduced coefficient of friction showed greater stability than when operating on dry roads. In contrast, the performance of the control system on ice was found to be poor. At high lateral acceleration demands, but low actual lateral accelerations (resulting from the low friction coefficient), the moment produced by the tilted cabin mass was sufficient to cause the vehicle to roll into the centre of the turn. A control strategy using an accelerometer to detect low friction surfaces, and therefore generate smaller tilt angle demands, was proposed but not developed.

Finally, simulations were used to show that a SDTC control strategy incorporating a feed-forward element could be used to achieve a fast active steering response and a 30% reduction in the load transfer in transient conditions. Introducing a measured steer signal, complete with noise, caused excessive oscillation of the active steer angle. Reducing the feed-forward gains and increasing filtering to reduce the oscillation removed the benefit of the feed-forward strategy. If backlash in the steering linkages of the prototype CLEVER Vehicle was reduced, the resulting cleaner steer signal may allow some benefit to be derived from a feed-forward control strategy.

Chapter 9. Conclusions and Further Work

9.1. Thesis Summary

Narrow Tilting Vehicles (NTVs) could form part of the solution to the problems of urban traffic congestion and carbon emissions, but first their inherent dynamic limitations must be overcome. A number of previous works have shown that both Direct Tilt Control (DTC) and Steering Tilt Control (STC) systems have significant disadvantages that prevent their successful implementation on a production NTV. In transient situations DTC systems generate very large tilting moments which lead to large variations in wheel loads. As well as influencing the yaw behaviour, if the wheel load variations are large enough, they can cause vehicle roll-over. Equally, STC systems are ineffective at low speeds and whilst stationary, and the automated steer inputs cause the vehicle to deviate from the driver's desired trajectory. They may also be unable to generate sufficient tilting moments to ensure stability on low friction road surfaces.

A number of combined Steering Direct Tilt Control (SDTC) strategies have been proposed in literature; these attempt to combine the best aspects of DTC and STC systems. Whilst a number of simulation models have been developed to test their effectiveness, very little experimental verification of SDTC systems has been published, and those experiments that have been published tend to be limited to low lateral accelerations and relatively gentle steer inputs. One possible explanation for the lack of experimental verification may be the availability of a suitable prototype vehicle; fortunately, the University of Bath possesses a functioning prototype NTV.

The Compact Low Emission VEhicle for uRban transport, or CLEVER Vehicle, was developed in 2006 in collaboration with a number of other industrial and academic institutions in a project funded by the EU. Originally constructed with a DTC system, the CLEVER Vehicle was found to offer good steady state roll stability, but poor transient performance and a lack of roll stability feedback to the driver. Subsequent research on the dynamics of the CLEVER Vehicle conducted at the University of Bath saw the development of a comprehensive non-linear simulation model of the lateral dynamics, and the proposal of a SDTC system.

This thesis presents the implementation of a SDTC system on the prototype CLEVER Vehicle. A hydraulic 'in-series' active steering system was developed in order to allow the tilt control system to alter the front wheel steer angle by ±5.6°, whilst retaining conventional steering feel when idle. The more complex tilt control strategy required the

development of new software, and the installation of a more powerful electronic controller on the prototype CLEVER Vehicle. The simulation model of the CLEVER Vehicle was modified to reflect the installation of the new control hardware, and validated using severe manoeuvres generating high lateral accelerations.

Having detailed its installation, this thesis presents experimental verification of the SDTC system's roll stability performance at high lateral accelerations and in highly transient manoeuvres. Also presented is a study of the SDTC system's influence on the vehicle's trajectory, and the driver's ability to modify their steer inputs to follow their chosen path. It was demonstrated that by altering the gain value applied to the active steering system, stability can be further enhanced at the expense of the yaw response and path following. The robustness of the control strategy is considered by examining its performance in a range of road surface friction and payload conditions. Finally, the use of a feed-forward type control strategy is considered with the intention of providing a faster active steering response and better transient stability.

9.2. Concluding Remarks

By recording data when operating the prototype CLEVER Vehicle in both DTC and SDTC modes, the stability enhancement provided by the more advanced control strategy has been quantified. The experiments were conducted at high lateral accelerations and in highly transient manoeuvres; as such this data represents new information not previously published. It was found that the SDTC system lead to an increase of 40% in the inside wheel load during a severe ramp steer input made whilst travelling at 10m/s. At lower speeds, and in less severe manoeuvres, a lesser stability enhancement was produced. The chosen active steering gain values were not sufficient to produce a significant countersteering action during any of the steer input tests conducted. Rather, the active steering system contributed to the vehicle's stability by delaying the onset of lateral acceleration and providing the tilt actuators with an element of lead.

When performing the above mentioned step input manoeuvres in SDTC mode, the human driver perceived a modest increase in transient understeer. However, this sensation did not occur when performing gentler manoeuvres and it did not have a significant adverse effect on the driving experience. Also noted was the reduced steering torque requirement in SDTC mode, this, combined with increased confidence in the vehicle's roll stability, lead to a tendency to generate larger and more aggressive steer inputs.

Both simulations and experiments showed that the SDTC strategy did have some influence on the path that a NTV would follow in response to a series of open loop steer inputs. However, the human driver was able to quickly adapt their steer inputs such that the ability to follow a path was retained. The revised steer inputs were shown to occur slightly earlier, and be larger in magnitude, in order to compensate for the lag introduced into the front wheel steer angle response. The human driver reported that generating the revised steer inputs felt natural after a short period of acclimatisation. Whilst it had been noted in literature that a SDTC strategy will lead to some deviation in the path, the nature of the revised steer inputs, and a human driver's ability to generate them, had not been investigated and therefore constitute new information.

It was demonstrated that higher active steering gain values promote improved roll stability whilst lower gain values provide a faster yaw response. Gain values should therefore be selected to provide an acceptable compromise between the two characteristics. Given the subjective nature of the selection criteria, the gain values for any future NTV will require tuning once a prototype has been developed.

Simulations of the CLEVER Vehicle operating on a wet road surface showed stability to be extremely good, principally because the maximum lateral acceleration value was limited. However, on an icy surface, the controller's lateral acceleration calculation was a gross over-estimate and could lead to the vehicle rolling over in the direction of the turn centre. It was noted that, on ice, yaw stability was lost at a far lower lateral acceleration demand than roll stability, thus roll over is unlikely to occur in practise. A control strategy using an accelerometer to detect low friction surfaces, and therefore generate smaller tilt angle demands, was proposed but not developed.

Increases in the payload carried by the vehicle were found to have very little effect on transient stability, the greater static vertical wheel load off-setting any additional load transfer. There is some limited scope to develop a controller which reduces the tilt angle at high payloads to realise a small improvement in both transient and steady state stability. The height of the rear module's centre of gravity was found to contribute significantly to the total roll moment; lowering it brought benefits to both transient and steady state roll stability.

Finally, simulations were used to show that a SDTC control strategy incorporating a feed-forward element could be used to achieve a fast active steering response and a 30% reduction in the load transfer in transient conditions. However, realising this stability improvement would require a steer signal with low noise as differentiation of a noisy

steer signal has been shown to lead to unacceptably large oscillations of the front wheel steer angle.

Whilst transient stability has been greatly enhanced by the adoption of a SDTC strategy, and it has been demonstrated that a human driver can maintain the ability follow a chosen path, there remain aspects of the CLEVER Vehicle's dynamics, and its control system, which require further investigation and development before roll stability can be assured in all driving scenarios. Even if an infallible tilting system were developed, the recent emergence of small electric commuter vehicles does bring into question whether there is a case for developing NTVs in future. With a low centre of gravity, high suspension roll stiffness and low friction tyres, the Renault Twizzy demonstrates that it is possible to create a stable non-tilting vehicle that is just 1237mm wide. Despite a 237mm width advantage, the extra expense and complexity of both the tilting and active steering systems may mean that a CLEVER-like NTV would struggle to find a place in the market.

9.3. Conclusions

The findings of the research presented in this thesis can be summarised as follows:

- Experimental verification of the performance of a Steering Direct Tilt Control (SDTC) strategy at high lateral accelerations and under transient conditions has been presented. This data represents new information not previously published.
- Using a SDTC strategy, rather than a DTC strategy, lead to a 40% reduction in the load transfer during a harsh ramp steer manoeuvre conducted at 10m/s.
- The SDTC strategy was found to produce a larger stability improvement at higher speeds.
- The human driver perceived the influence of the SDTC system on the front wheel steer angle as mild transient understeer. The driver was able to adapt the steer inputs so as to retain control of the vehicle's trajectory.
- Using an additional feed-forward element to produce a faster response from the active steering system could generate a further 30% reduction in the load transfer in transient conditions but only if the steer signal is sufficiently clean.

These findings meet the research objectives defined in Chapter 1 of this thesis.

9.4. Further Work

Should the case for continuing development of narrow tilting vehicles be successfully made, there are several areas which would benefit from further investigation.

The high centre of gravity and large mass of the CLEVER Vehicle's rear engine module has been shown to have a significant detrimental effect on both steady state and transient stability. Alternative vehicle packaging should be considered, perhaps using electric propulsion and batteries mounted low in the chassis to minimise the height of the centre of gravity.

The longitudinal dynamics of the CLEVER Vehicle have not been thoroughly investigated. It is likely that under heavy braking, as load is transferred forwards onto the single front wheel, the maximum safe DTC actuator moment will be reduced. Thus, a combination of simultaneous braking and steering inputs may lead to vehicle roll-over. The simulation model as it stands cannot replicate braking or driving forces and would require developing into a full multi-body model before combined longitudinal and lateral dynamics could be investigated.

Whilst the active steering system implemented on the CLEVER Vehicle has been successful in showing that significant stability improvements can be gained through the use of a SDTC strategy, it does have some limitations. Principally, the ±5.6º stroke limits have been shown to saturate during some manoeuvres reducing the effectiveness. Greater functionality may be realised by developing a full steer-by-wire system. In addition, the active steering gains have not been fully optimised; a further roll stability improvement whilst retaining acceptable yaw response may be possible.

Implementation of a feed-forward control strategy may realise a significant improvement in transient roll stability, and a controller with road surface friction detection could optimise the tilt response on low friction surfaces. Whilst it has been demonstrated that the CLEVER Vehicle can remain stable at steady state lateral accelerations of somewhere between 8 and 9m/s^2, on high grip surfaces the tyres are capable of generating even greater lateral accelerations. The active steering control system could be modified to limit the steer angle once the ±45° tilting limits are saturated, thus limiting the maximum steady state lateral acceleration to a safe level.

Finally, although not presented in this thesis, it was noted that when conducting transient simulations at high vehicle speeds (100km/h), yaw stability performance was very poor.

The rear wheel steering angle, which is linked to the cabin tilt angle, may be responsible. At high speeds, lateral acceleration demands large enough to produce a tilting response of 45° can be generated with front wheel steer inputs of less than 1°. Since the rear wheel steer angle is a function of the tilt angle, it will reach its maximum value of approximately 3°. This is far in excess of the driver's original steer input and the rear wheel steer angle that can safely be applied at this speed. Some form of active rear wheel steering, and an ESP-like yaw stability system, may be required.

References

[1] Karnopp, D. 2004. *Vehicle Stability*. New York, USA: Marcel Dekker.

[2] Heisler, H., 2002. *Advanced Vehicle Technology*. 2nd ed. Oxford, UK: Butterworth-Heinemann.

[3] Hollmotz, L., Sohr, S., Johannsen, H., 2005. CLEVER – A Three Wheel Vehicle With a Passive Safety Comparable to Conventional Cars. *Proceedings of the 19th International Technical Conference on the Enhanced Safety of Vehicles*, June 6-9, 2005, Washington, D.C., USA.

[4] Karnopp, D., Fang, C., 1992. A Simple Model of Steering Controlled Banking Vehicles. *ASME Dynamic Systems and Control*, 44(Transportation Systems), pp.15-28.

[5] Drew, B., Edge, K., Barker, M., Darling, J., Owen, G., 2005. System Development for Hydraulic Tilt Actuation of a Tilting Narrow Vehicle. *9th Scandinavian International Conference on Fluid Power, SICFP '05*, June 1-3, 2005, Linköping, Sweden.

[6] Wallis, G.L., 1965. *Improvements in or Relating to Pedal or Power-Driven Tricycles*. GB Patent 1146351.

[7] Anonymous, *Motor Scooter Guide* [online]. Available from: http://www.motorscooterguide.net/Honda/Gyro/Gyro.html [Accessed 07/10/2013].

[8] Anonymous, 2013, *Honda.co.jp* [online]. Available from: www.honda.co.jp/motor-lineup/category/ [Accessed 07/10/2013]

[9] Payne, E., *3-wheelers.com* [online]. Available from: www.3wheelers.com/gmlean.html [Accessed 15/12/2010].

[10] Drew, B.W., 2006. *Development of Active Tilt Control for a Three-Wheeled Vehicle*. Thesis (Ph.D.). University of Bath, Bath, UK.

[11] Anonymous, *Mercedes Benz UK* [online]. Available from: http://www2.mercedes-benz.co.uk/content/unitedkingdom/mpc/mpc_unitedkingdom_website/en/home_mpc/passengercars/home/passenger_cars_world/innovation_new/concept_cars.0004.html [Accessed 16/12/2010].

[12] Anonymous, 2002. *Carfolio.com* [online]. Available from: www.carfolio.com/specifications/models/car/?car=98153 [Accessed 09/10/2013].

[13] Anonymous. Uk.Piaggio.com [online]. Available from: http://www.uk.piaggio.com/piaggio/UK/en/news/history.html [Accessed 14/10/2013].

[14] Anonymous. Wide Magazine [online]. Available from: http://wide.piaggiogroup.com/scooter/index_en.html#/Product [Accessed 14/10/2013].

[15] Anonymous. *Lumeno.fr* [online]. Available from: http://www.lumeneo.fr/smera_technical_specifications_eng.php [Accessed 07/10/2013].

[16] Nunn, P., Stevens, D., 2009. *Autocar.co.uk* [online]. Haymarket Consumer Media. Available from: www.autocar.co.uk/News/NewsArticle/AllCars/243857 [Accessed 10/01/2013].

[17] van den Brink, C.R., Kroonen, H.M., van den Brink, P., van den Brink A., 2004. Slender Comfort Vehicles: Offering the Best of Both Worlds. *ATZ Auto Technology*, 1/2004, pp. 56-58.

[18] Blezard, P., 2009. *Evo.co.uk* [online]. Dennis Publishing Limited. Available from: www.evo.co.uk/front_website/gallery.php?id=344536 [Accessed 07/10/2013].

[19] Anonymous, 2012. *Autocar.co.uk* [online]. Haymarket Consumer Media. Available from: www.autocar.co.uk/car-review/renault/twizy/ride [Accessed 07/10/2013].

[20] Hibbard, R., Karnopp, D., 1992. Optimum Roll Angle Behaviour for Tilting Ground Vehicles. *ASME Dynamic Systems and Control*, 44(Transportation Systems), pp. 29-37.

[21] Hibbard, R., Karnopp, D., 1993. The Dynamics of Small, Relatively Tall and Narrow Tilting Ground Vehicles. *ASME Dynamic Systems and Control*, 52(Advanced Automotive Technologies), pp. 397-417.

[22] Barker, M.I., 2006. *Chassis Design and Dynamics of a Tilting Three-Wheeled Vehicle*. Thesis (Ph.D.). University of Bath, Bath, UK.

[23] Gohl, J., Rajamani, R., Alexander, L., Starr, P., 2004. Active Roll Mode Control Implementation on a Narrow Tilting Vehicle. *Vehicle System Dynamics*, 42(5), pp. 347-372.

[24] Mourad, L., Claveau, F., Chevrel, Ph., 2011. A Lateral Control Strategy for Narrow Tilting Commuter Vehicle[s] Based on the Perceived Lateral Acceleration. *Reprints of the 18th IFAC World Congress,* 28/08/2011-02/09/2011, Milano, Italy. Pp. 6254-6259.

[25] Mourad, L., Claveau, F., Chevrel, Ph., 2012. Design of a two DOF gain scheduled frequency shaped LQ controller for Narrow Tilting Vehicles. *Proceedings of the 2012 American Control Conference,* 27/06/2012-29/06/2012, Fairmount Queen Elizabeth, Montreal, Canada. Pp. 6739-6744.

[26] So, S.G., Karnopp, D., 1997. Active Dual Mode Tilt Control for Narrow Ground Vehicles. *Vehicle System Dynamics*, 27, pp. 19-36.

[27] So, S.G., Karnopp, D., 1997. Switching Strategies for Narrow Ground Vehicles with Dual Mode Automatic Tilt Control. *International Journal of Vehicle Design*, 18(5), pp. 518-532.

[28] Snell, S.A., 1998. An Active Roll Moment Control Strategy for Narrow Tilting Commuter Vehicles. *Vehicle System Dynamics*, 29(5), pp. 277-307.

[29] Pacejka, H.B., 2006. *Tyre and Vehicle Dynamics*. 2nd ed. Oxford, UK: Butterworth-Heinemann.

[30] Kidane, S., Alexander, L., Rajamani, R., Starr, P., Donath, M., 2005. Control System Design for Full Range Operation of a Narrow Commuter Vehicle. *Proceedings of the 2005 ASME International Mechanical Engineering Congress and Exposition*, 05/11/2005-11/11/2005, Orlando, Florida, USA. pp. 473-482.

[31] Kidane, S., Alexander, L., Rajamani, R., Starr, P., Donath, M., 2008. A fundamental Investigation of Tilt Control Systems for Narrow Commuter Vehicles. *Vehicle System Dynamics*, 46(4), pp. 295-322.

[32] Kidane, S., Alexander, L., Rajamani, R., Starr, P., Donath, M., 2007. Experimental Investigation of a Narrow Leaning Tilt Stability Control System. *Proceedings of the 2007 American Control Conference*. 11/11/2007-13/11/2007, New York, USA. pp. 1612-1617.

[33] Kidane, S., Rajamani, R., Alexander, L., Starr, P., Donath, M., 2009. Development and Experimental Evaluation of a Tilt Stability Control System for Narrow Commuter Vehicles. *IEEE Transactions on Control Systems Technology*, 18(6) pp. 1266-1279.

[34] Berote, J., Darling, J., Plummer, A., 2011. Lateral Dynamics Simulation of a Three-Wheeled Tilting Vehicle using a Multi-Body Chassis Model. Unpublished.

[35] Berote, J., 2010. *Dynamics and Control of a Tilting Three Wheeled Vehicle.* Ph.D. Thesis, University of Bath. Bath, UK.

[36] Berote, J., Darling, J., Plummer, A., 2011. Development of a Tilt Control Method for a Narrow Track Three Wheeled Vehicle. *Proceedings of the Institution of Mechanical Engineers, Part D, Journal of Automobile Engineering*, 226(1), pp. 48-69.

[37] Edelmann, J., Plöchl, M., & Lugner, P., 2011. Modelling and analysis of the dynamics of a tilting three-wheeled vehicle. *Multibody System Dynamics*, 26(4), pp. 469-487.

[38] Edelmann, J., Plöchl, M., 2011. Electronic Stability Control of a Narrow Tilting Vehicle. *SAE International Journal of Materials and Manufacturing,* 4(1) pp. 1006-1013.

[39] Furuichi, H., Huang, J., Matsuno, T., Fukuda, T., 2012. Dynamic Modelling of Three Wheeled Narrow Tilting Vehicle and Corresponding Experiment Verification. *IEEE/RSJ International Conference on Intelligent Robots and Systems,* 07/12/2012, Vilamoura, Portugal.

[40] Furuichi, H., Huang, J., Matsuno, T., Fukuda, T., 2012. Dynamic Model of Three Wheeled Narrow Tilting Vehicle and Optimal Tilt Controller Design. *IEEE International Symposium on Micro-NanoMechatronics and Human Science (MHS) 2012.* 04/11/2012-07/11/2012, Nagoya, Japan.

[41] van den Brink, C.R., 1997. Dynamic Vehicle Control for Enclosed Narrow Vehicles. *EAEC 6th European Automotive Congress*. 02/07/1997-04/07/1997, Cernobbio, Italy.

[42] van den Brink, C.R., 1999. Realization of High Performance Man Wide Vehicles (MWVs) with an Automatic Active Tilting Mechanism. *EAEC 7th European Automotive Congress*. 30/06/1999-02/07/1999. Barcelona, Spain.

[43] Pauwelussen, J.P., 1999. The Dynamic Behaviour of Man-Wide Vehicles with an Automatic Tilting Mechanism. *EAEC 7th European Automotive Congress*. 30/06/1999-02/07/1999, Barcelona, Spain.

[44] Pauwelussen, J.P., 2000. The Dynamic Performance of Narrow Actively Tilting Vehicles. *AVEC 5th International Symposium on Advanced Vehicle Control*. 22/08/2000-24/08/2000, Ann Arbor, Michigan, USA.

[45] van den Brink, C.R., Kroonen, H.M., 2004. DVC – The Banking Technology Driving the Carver Vehicle Class. *AVEC 7th International Symposium on Advanced Vehicle Control*. 23/08/2004 - 27/08/2004, Arnhem, Netherlands.

[46] UN Regulation 79 - Revision 2: 2005. *Uniform Provisions Concerning the Approval of Vehicles with Regard to Steering Equipment.* United Nations.

[47] Koehn, P., Eckrich, M., 2004. Active Steering – The BMW Approach Towards Modern Steering Technology. *SAE World Congress and Exhibition,* 08/03/2004 – 11/03/2004, Detroit, Michigan, USA.

[48] Ackermann, J., Bünte, T., Odenthal, D., 1999. Advantages of Active Steering for Vehicle Dynamics Control. *Proceedings of 32nd ISATA, Automotive Mechatronics Design and Engineering,* pp. 263-270.

[49] Cossalter, V., 2006. *Motorcycle Dynamics*. 2nd ed. Self Published.

[50] Cossalter, V., Ruffo, N., Biral, F., Berritta, R., 2000. Development of a Novel Three-Wheeled Vehicle. *Proceedings of the International Motorcycle Conference 2000*. 11/09/2000-12/09/2000. Munich, Germany.

[51] Barker, M., Drew, B., Darling, J., Edge, K.A., Owen, G.W., 2009. Steady-State Steering of a Tilting Three Wheeled Vehicle. *Vehicle System Dynamics*, 48(7) pp. 815-830.

[52] Maurice, J.P., Pacejka, H.B., 1997. Relaxation Length Behaviour of Tyres. *Vehicle System Dynamics*, 27(1) pp. 339-342.

[53] Darling, J., 2012. *ME30067 Vehicle Dynamics - Tyre Characteristics*. Lecture Notes. University of Bath, Bath, UK.

[54] Fox, S., 2010. *Cockpit Control Forces – or How Robust do Driver Controls Really Need to be?* [online]. Society of Automotive Engineers International. Available from: http://www.sae.org/students/cockpit_control_forces.pdf [Accessed 22/11/2013].

[55] Anonymous, 2010. *FP2, Component Selection for Hydraulic Systems*. University of Bath, Bath, United Kingdom. [Lecture Notes].

[56] Bosch Rexroth AG, Industrial Hydraulics, 2003. *4/2 and 4/3 proportional directional control valves direct operated, with electrical position feedback. Types 4WRE and 4WREE. RE 29 061/02.03*. [Component data sheet].

[57] Robertson, J. W., Darling, J., Plummer, A. R., 2014. Combined steering–direct tilt control for the enhancement of narrow tilting vehicle stability. *Proceedings of the Institution of Mechanical Engineers, Part D: Journal of Automobile Engineering*, [Published online before print] DOI: 10.1177/0954407014522445.

[58] Robertson, J. W., Darling, J., Plummer, A. R., 2012. Path following performance of narrow tilting vehicles equipped with active steering. *ASME 2012 11th Biennial Conference on Engineering Systems Design and Analysis,* pp. 679-686.

[59] BS ISO 3888-2:2002. *Passenger cars – Test Track for a Severe Lane-change Manoeuvre*. British Standards Institute.

[60] Persson, B. N. J., Tartaglino, U., Albohr, O., Tosatti, E., 2005. Rubber Friction on Wet and Dry Road Surfaces: The Sealing Effect. *Physical Review B,* 71(3), 035428.

[61] Higgins, D. D., Marmo, B. A., Jeffree, C. E., Koutsos, V., & Blackford, J. R., 2008. Morphology of ice wear from rubber–ice friction tests and its dependence on temperature and sliding velocity. *Wear*, 265(5), pp. 634-644.

[62] Müller, S., Uchanski, M., Hedrick, K., 2003. Estimation of the Maximum Tire-Road Friction Coefficient, *ASME Journal of Dynamic Systems, Measurement and Control*, 125, pp. 607-617.